Size Control and Uniformity in Animal Cells

Size Control and Uniformity in Animal Cells

A dissertation presented

by

Miriam Bracha Ginzberg

to

The Committee on Higher Degrees in Chemical Biology

in partial fulfillment of the requirements

for the degree of

Doctor of Philosophy

in the subject of

Chemical Biology

Harvard University

Cambridge, Massachusetts

December 2014

Dissertation Advisor: Marc Kirschner Miriam Bracha Ginzberg

Size Control and Uniformity in Animal Cells

Abstract

The homogeneity in cell size observed in many normal tissues, and the contrasting size disparities characteristic of some cancers, suggest that control mechanisms coordinate growth and cell cycle progression, but the existence of such mechanisms has not been firmly established. To address this problem, we used quantitative fluorescence microscopy to measure cell cycle position, total protein content, and the level of cell growth regulators such as phosphorylated ribosomal protein S6, in tandem in single cells. Measurements were made on large numbers of cells drawn from proliferating populations of both non-transformed and cancerous cells. Analysis of the joint distribution of cell size and cell cycle position revealed a control mechanism that restricts cells to a specified size range at several points in the cell cycle. Combining our measurements with live-cell imaging showed that this restriction is the result of a negative correlation between cell size and subsequent growth rate, indicating that cells can sense their own size and modulate their growth accordingly. We also observed cell-size-dependent adjustments of cell cycle length, which further reduced size variability. We then identified drugs that change the mean cell size without disrupting the cell-autonomous control mechanism, as well as drugs that weaken the size-dependence of either growth rate or cell cycle progression and increase cell-to-cell size variability. In particular, long- and short-term drug treatments revealed that mTORC1 inhibition decouples the rate of cell growth from cell size, impairing the efficiency of cell size specification and increasing size variability. Our measurements of mTORC1 activity as a function of size and cell cycle position suggest that mTORC1 assumes its role in growth

control following S-phase entry. Although mTORC1 activity, assayed by levels of mTORC1-target phosphorylation, increases abruptly during G1, it becomes correlated with cell size only upon G1 exit. The mTORC1 inhibitor rapamycin preferentially inhibits growth in S-phase cells. Taken together, these results indicate that the mTOR pathway maintains size homogeneity by stimulating growth in a cell-size-dependent manner after G1 exit. The screening and analysis methods developed here will be used to further elucidate the cellular size-control mechanism.

Table of Contents

Acknowledgements

I want to thank the people who have helped me in this research, and throughout my PhD. Firstly, I want to express my heartfelt gratitude to my advisor, Marc Kirschner, for generously welcoming me into his lab and for his continued mentorship. It was only in the process of writing this thesis that I fully realized how much I have learned and gained from my years in his lab. I owe a lot of that to Ran Kafri, a great collaborator, mentor, and friend. Most of this work was done in collaboration with him, and he has taught me a lot. I also want to thank the Chemical Biology program directors, particularly Jon Clardy and Suzanne Walker, and the coordinator, Samantha Reed, for their advice. Lastly, I want to thank my dissertation committee members, Alfred Goldberg, Andrew Murray, and David Sabatini for generously giving their time to advise me, even outside of committee meetings.

The drug screen discussed here was done in collaboration with Marc Hild and Jeremy Jenkins at Novartis. Much of the imaging was done at the Nikon Imaging Center at Harvard Medical School, with the expert support of Jennifer Waters, Wendy Salmon, and Lara Petrak. The cytoskeleton work described in Appendix II was done in Timothy Mitchison's lab at Harvard Medical School, and I am grateful to all of the lab members for their support. In particular, I want to thank Sophie Dumont for her kind and wise mentorship.

I would also like to take this opportunity to thank my parents, my entire family, and my dear friends who have supported and encouraged me all along the way. This thesis is dedicated to my incredible siblings- Binyomin, Chani, Altea, Chaya Baila, Suri, and Yitzi- with gratitude and love.

Chapter 1

Introduction: Do animal cells measure their own size?

This work explores a fundamental, yet controversial, question in cell biology: what determines the appropriate size for a given cell type, and how do cells of each type maintain their characteristic sizes? Do individual cells sense their size in relation to a predetermined target size, and if so, how do they use this information to achieve the target size? Despite the fact that these questions have puzzled biologists for decades, the quest for a complete understanding of cell size control has been hampered by many experimental challenges. Measuring the sizes of individual cells can be difficult, particularly for live cells, making measurement of their growth rates even more difficult. Furthermore, since size in a proliferating population has only a two-fold dynamic range, precise measurements are necessary to make meaningful comparisons of individual cellular growth rates. Additionally, cell size is the outcome of many interconnected processes, making it hard to isolate the effects of particular factors.

The review article below, which I wrote together with Ran Kafri and Marc Kirschner, outlines the major questions and hypotheses that motivated the work described in this thesis. It summarizes the observations which led many to believe that cell size is not actively specified and is simply a byproduct of the relative rates of cell division and growth dictated by extracellular signals. It then presents several studies that contradicted this view, suggesting that individual cells might autonomously sense and specify their own size. Since this review was written recently, this section also includes results from the early stages of our work (specifically the insights gained from the Ergodic Rate Analysis discussed in detail in subsequent chapters)

that strengthened the case for active cell size specification. We end with a discussion of the physiological implications of cell size abnormalities and review relevant literature to assess the importance of precise size specification.

In chapter two, I describe our efforts to conclusively determine whether individual cells sense and regulate their own size. I begin with experiments that tested whether cells regulate G1-exit and the length of the cell cycle to adjust their total growth prior to division. I then describe experiments designed to test whether cells regulate their rates of growth to maintain a specific cell size. These investigations yielded the surprising result that cells adjust both their cell cycle and growth rate in a size-dependent manner to maintain uniformity in a population. In chapters three and four, I describe multiple lines of effort to identify the molecular mechanisms and signaling pathways responsible for these behaviors.

Throughout this thesis I highlight the fundamental difficulties that have classically limited progress in this field. I describe our approaches to circumvent these challenges, as well as the limitations of these approaches. I conclude with where my investigation has left our understanding of this complex problem, and a discussion of additional approaches and experiments that may complete our understanding in the near future.

On being the right (cell) size

Miriam B. Ginzberg*, Ran Kafri*, Marc Kirschner*

*Authors contributed equally.

Abstract

Different animal cell types have distinctive and characteristic sizes. How a particular cell size is specified by differentiation programs and physiology remains one of the fundamental unknowns in cell biology. In this review we explore the evidence that individual cells autonomously sense and specify their own size. We discuss possible mechanisms by which size sensing and size specification may take place. Finally, we explore the physiological implications of size control. Why is it important that particular cell types maintain a particular size? We develop these questions by examination of current literature and pose the questions that we anticipate will guide this field in the upcoming years.

Introduction

Early cytologists found that, within a species, it is the number of cells, rather than the size of the cells that makes one individual larger than another; cell size is relatively constant (*1*). While this seems to downgrade the question of cell size in favor of proliferative potential, it raises the curious question of how cells of a common cell type achieve such a uniform size, yet

are capable of changing their size by orders of magnitude during differentiation or in response to physiological stimuli. For example, pancreatic beta cells are surrounded by acinar cells that are roughly twice their size, and chondrocytes increase their volume by 10 to 20 fold during hypertrophic bone growth (*2*). These examples, among others (figure 1), demonstrate that a cell's size is not the result of physical constraints, but rather it is adaptively regulated. What, then, specifies a particular cell's size?

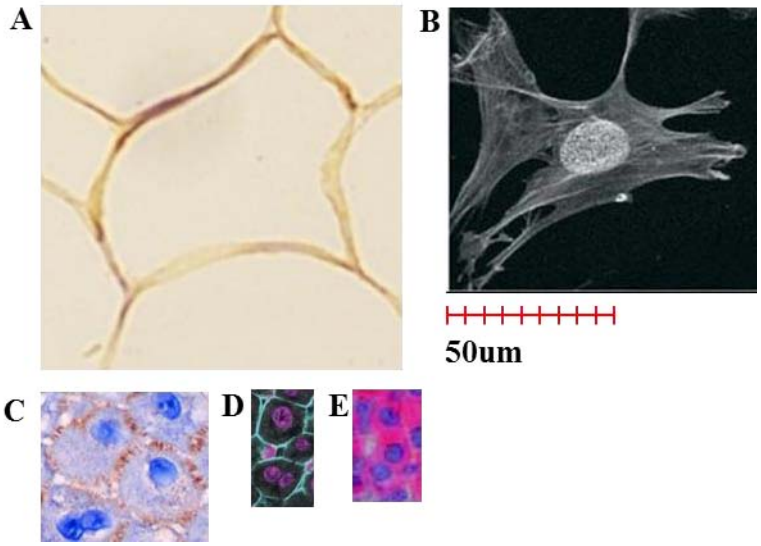

Figure 1.1: Sizes of different human cell types. Cells are shown to scale. (A) Adipocytes from subcutaneous tissue (*76*) (B) Fibroblasts, cultured (*77*) (C) Keratinocytes from oral tissue (*78*) (D) Hepatocytes from liver sections, stained for β-catenin and DNA (*79*) (E) Pancreatic beta cells, stained for insulin (*80*)

Much work on this subject has focused on identifying extracellular factors (and their intracellular responsive pathways) that elicit changes in cell size. These studies found that the size of a cell of is largely controlled by its cell surface receptors and the combinations of growth factors, mitogens and cytokines in its environment. In the 1980s (*3, 4*), Zetterberg and coworkers distinguished between factors, such as insulin-like growth factor 1 (IGF-1) and insulin, that primarily initiate cell growth and factors such as epidermal growth factor (EGF) that primarily drive cell cycle progression even in the absence of growth. In Schwann cells, for example, IGF-1

functions primarily as a growth factor increasing cell mass, while glial growth factor (GGF) acts as a mitogen inducing proliferation (*5, 6*) . Consequently, Schwann cell size can be manipulated by adjustment of the relative concentrations of IGF-1 and GGF in their environment. These findings caused some to conclude that, in proliferating animal cells, growth and cell cycle progression are independent processes, each governed by extracellular cues. According to this view, size itself is not actively controlled, but merely results from the independent control of the rates of cell growth and cell division.

Although it is clear that extracellular growth factors and mitogens can trigger changes in cell size, such cues do not account for how cell size variance is constrained, to achieve the uniformity in cell size typically seen in tissues. These extracellular signals can dictate the mean size of cells, but individual cells will still deviate from that mean. Variability in cell size can arise from variability in growth rate and cell cycle length, or asymmetry in cell division. These sources of inevitable variation raise the question of whether there are cellular mechanisms that might act to increase size homogeneity. Size variation can only be reduced with processes that differentially affect cells of different sizes, despite the fact that they share the same environment. Such a process could reduce heterogeneity by eliminating cells that deviate widely from the mean, through cell death or differentiation. Alternatively, a size-discriminatory process could force large cells to accumulate less mass than small ones, in response to identical extracellular signals. This kind of control requires a mechanism whereby individual cells measure their own size and adjust their cell cycle length, growth rate, or both, as necessary to achieve a common target size. In this review, we will discuss a growing body of evidence that such mechanisms exist and address the following questions:

1. Do animal cells have mechanisms to autonomously measure and adjust their individual sizes?
2. Does the presence of such mechanisms indicate that there is an optimal cell size for a particular cell's function?

Our discussion of cell size control will focus on proliferating populations of cells, which have been more extensively studied in this context, although many of the issues raised are relevant in non-proliferating tissues as well.

Ways to limit heterogeneity in cell size

In proliferating cells, size variability can be constrained if cells progress through the cell cycle in a size-dependent manner (figure 2A). Cells that are born small would have more time to grow before their next division, as compared to oversized cells which would divide more quickly. Several groups have suggested that mammalian cells have a size threshold for exit from G1 phase of the cell cycle (*7-9*), as has been observed in budding yeast (*10*). In order for a size threshold to work, cell size must be reported to the processes regulating the cell cycle. The "signal" could be the amount of a particular protein or protein modification, the distance between cytoskeletal features, or even the number or size of the cell's neighbors.

Instead of (or in addition to) changing their cell-cycle length in a size-dependent manner, cells could also reach their target size by adjusting their growth rate, so that small cells grow quickly, while large cells grow slowly (figure 2B). This growth rate adjustment could be modulated by the sort of signals described above. Alternatively, the growth rate, and the final

cell size, could be determined by a "balance point" of synthesis and degradation. If, for example, cells synthesize proteins at a fixed rate but degrade them at a rate that is proportional to their total cell size, net growth would slow as cell size increases. Note that this is not a trivial condition, because it requires that degradation depend on the total amount of protein in the cell, rather than the protein concentration.

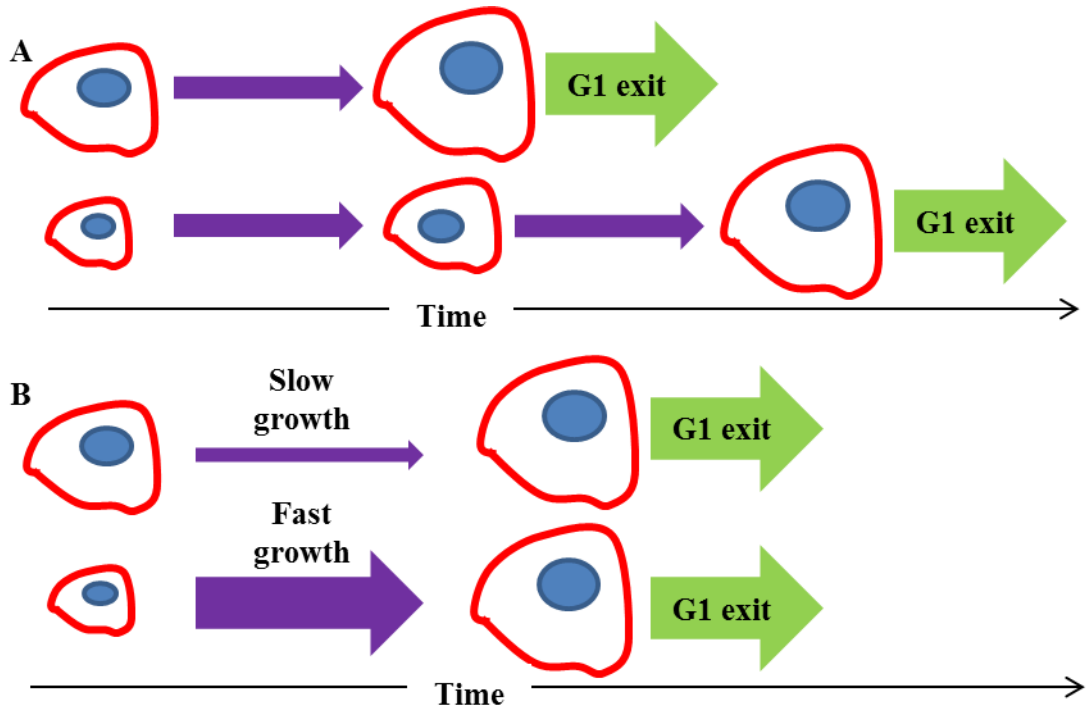

Figure 1.2: Strategies of size regulation. To exit G1 with the appropriate size, cells can either adjust the amount of time spent in G1 (A) or the rate at which they grow (B).

Evidence for cell autonomous size measurement

There is increasing evidence that cells autonomously regulate their size to reduce cell size variation. In 1965, Killander and Zetterberg used interferometric microscopy to measure the dry mass of individual fibroblasts as a function of time since division. They reported that cells that had recently entered S-phase were less variable in size than those in early G1 (*8*). S-phase entry appeared to be more heavily dependent on a cell's size than its age, as cells entered S-phase at

similar sizes, whereas their age at S-phase entry varied widely. These results suggested that there might be a cell-size threshold gating G1-exit in animal cells. Killander et al. also showed that cells split into separate culture dishes often displayed slight difference in phenotypes, including cell size (*7*). When comparing cell size and cell cycle distributions of different cultures, they noticed that populations with smaller average birth sizes had longer average G1 lengths, such that cells exited G1 at a similar size in all populations. They concluded that a critical cell mass is required for S-phase entry.

A dependence of G1 length on cell size was also observed by Dolznig, et al. (*9*). They engineered avian erythroblasts to proliferate in the absence of cytokines, under control of a viral constitutively active EGF-R1, v-ErbB. When v-ErbB signaling was blocked with an EGF-R inhibitor, and the cells were supplied with the appropriate cytokines, they proliferated under the control of their physiological receptors, c-Kit and EpoR. Cells were significantly larger when driven by v-ErbB than they were during c-Kit/EpoR-driven proliferation. Dolznig et al. monitored the cell cycle distribution after switching cells from v-ErbB- to c-Kit/EpoR-driven proliferation. They reasoned that if there is a size threshold which is lowered in c-Kit/EpoR-driven proliferation, the first cell cycle following the switch should be shorter than subsequent cycles. This expectation was fulfilled, suggesting that there is a size threshold at G1 exit that is influenced by extracellular conditions. While the results of Killander and Zetterberg can be explained by a correlation between G1 length and size at any point in G1, Dolznig's work suggests that a true size threshold restricts G1 exit. Notably, Echave et al. (*11*) transferred Schwann cells from 3% serum (in which they maintain a large size) to serum-free medium (in which they are small) and failed to see a shortening of the first cell cycle. This discrepancy may be attributable to differences in experimental conditions or cell type.

Kafri et al. provided evidence of a size-discriminatory process that reduces variability in cell mass (assayed by protein staining) at G1-exit in several normal and transformed cell lines (*12*) . To reveal the coordination of growth and cell cycle progression, using fixed unsynchronized cell preparations, they applied a fundamental statistical principle: In an unsynchronized population of cells, the proportion of cells characterized by a certain property or phenotype is a function of the duration of the events during the cell cycle where that phenotype is expressed. Specifically, if cells of a given size and cell cycle position are underrepresented in the population, those cells must either grow or progress through that stage of the cell cycle more rapidly. Based on this "ergodic rate analysis" (ERA) of large populations captured in a single image, they detected a prominent fingerprint of feedback regulation. In late G1, large cells are distinguished from small cells in a process that causes large cells to accumulate less mass than smaller ones, thereby decreasing size heterogeneity in the population. Their conclusions were consistent with either of two possibilities: a faster growth rate or a longer duration of G1 for smaller cells.

A major source of variation in size is variation in the rates at which individual cells grow. Growth rates of individual cells are very hard to measure, requiring methods for resolving small differences in mass (a fraction of the mass of a single cell). To address this problem, Scott Manalis and colleagues developed a microfluidic resonator that measures the buoyant mass of single cells with exquisite accuracy, enabling measurement of the instantaneous growth rate of a cell with a resolution of about 3 minutes (*13*). Their experiments on mouse lymphocyte precursors provided the first highly accurate, direct measurements of growth curves of single cells (*14*). They observed a convergence of the variable growth rates of individual cells, as they approach the end of G1. At birth there are large disparities in growth rate among individual cells

in the population, and, as cells progress through the cell cycle, their growth rates continuously increase, creating more disparity. However, in these cells, G1 length is inversely proportional to a cell's initial *rate of growth,* not *size.* Slower-growing cells are held in G1, allowing them more time to accelerate their growth, so that all cells exit G1 with similar growth rates. These results suggest that a growth rate threshold gates G1 exit. Such a mechanism would reduce the rate at which variation builds up during cell growth, by both allowing slower-growing cells more time to grow between divisions and reducing growth rate disparities. An alternative possibility consistent with these observations is that cells measure not their rate of growth, but the amount of mass accumulated since birth.

For many investigators in the past few decades, the question of whether cells regulate their own size was tied to another, more abstract question: do cells grow with linear or exponential kinetics (*15-19*)? At first glance, the latter question may seem to have little biological relevance. But, upon closer examination, a distinction between these models carries significant implications. With exponential growth, larger cells grow faster than smaller cells, amplifying any existing size disparities in proliferating populations. Therefore, evidence that cells grow exponentially, and are expected to diverge in size, would suggest that regulatory mechanisms exist to counterbalance this effect and maintain size homeostasis.

Despite the elegance of this claim, to actually distinguish exponential from linear kinetics requires measurements of cell size with an error smaller than 6% (*20*), a resolution that was technologically unavailable until recently. Ingeniously circumventing this challenge, in 1963 Collins and Richmond (*21*) published a method to calculate growth kinetics from three static size distributions: a distribution of newborn cells, dividing cells, and an unsynchronized population. Intuitively, if one observes very few cells in the unsynchronized population with a particular

size, this might be because (i) cells of this size grow very quickly (and spend very little time at this volume), (ii) most newborn cells are larger than this, or (iii) most cells divide before reaching this size. By comparing the three size distributions in the Collins-Richmond relation, the effects of (ii) and (iii) can be estimated, and one can infer the average growth rate for cells of any given size. The most difficult aspect of applying the Collins-Richmond method is measuring the sizes of newborn and dividing cells. This challenge was overcome in 2009 (*20*), by culturing mouse lymphoblasts that were loosely attached to a membrane, such that one daughter cell from every mitosis was released, and the volumes of these newborn cells were measured via Coulter counter. The size distribution of dividing cells was inferred, by assuming that the volume of a cell just before division is the same as the total volume of the two resulting newborns.

Applying the Collins-Richmond equation to the measured cell volume distributions revealed that growth kinetics are more complex than either the linear or the exponential models. Overall, lymphoblast growth rates do increase with cell size, upholding the exponential growth model, although this trend is reversed in the very largest of cells. Additionally, during early G1, the growth of all cells accelerates faster than predicted by either model. The extent of this complexity was further revealed by the newly-developed methods described above (*12, 14*), which detailed how growth kinetics vary over the course of the cell cycle.

The finding that growth is size-dependent during much of the cell cycle suggested that lymphoblasts must have a robust size-control mechanism. To investigate this possibility, the authors tracked the size distribution of a synchronized population of cells over several cycles. They found that for cells of equal age, the larger is more likely to divide. Similarly, for two cells of equal size, the older cell is more likely to divide. This implies that lymphoblast division is regulated by both cell size and age—that both a “sizer” and a “timer” are involved.

How can a cell measure its own size?

While changes in cell size are easily induced by extracellular conditions, such as growth factor levels, cells of different types in a common environment display characteristic and distinctive sizes. It is clear that different cell types respond to the same signals in different ways, such that their size distinction is preserved. The combination of a cell's differentiation state and the composition of its environment specify the particular target size it will maintain. The uniformity in cell size of most cell types suggests that single cells sense their individual size in relation to this target size. Perhaps the most intriguing aspect of such a regulatory mechanism is that both the cell's target size and its actual size must be evaluated on absolute rather than relative scales. This type of absolute size measurement has been proposed to occur in keratinocytes, which differentiate only at a diameters between 12 and 14 um (*22*) .

How can individual cells assess their size on an absolute, rather than a relative, scale? Researchers studying size control in the fission yeast, Schizosaccharomyces pombe, proposed that a physical basis for size sensing is an intracellular gradient of the mitotic inhibitor Pom1, whose concentration is high at the cell ends and decreases towards the cell center (*23-25*). As the S. pombe cell grows by elongation, a Pom1-depleted region is established at its center and plays a role in triggering mitosis. The concentration profile of intracellular Pom1 was proposed to serve as a ruler marking the distance between the cell tips. More recent work, showing that cells maintain size homeostasis even in the absence of Pom1, led others to conclude that the Pom1 gradient is not the direct size sensor responsible for the negative correlation between cell size at birth and cell cycle length (*26*). However, Pom1 does modulate the absolute size for mitotic entry, possibly by preventing mitosis near cell ends, thereby ensuring a minimum cell length. In

this example, the link between cell cycle progression and cell size is thought to be the kinetics of a reaction-diffusion system. Despite the fact that most cells lack the morphological simplicity of the rod-shaped S. pombe, it is possible that such intracellular gradients serve as cellular "rulers" in many contexts.

The observation that growth rates of lymphocyte precursors converge at G1-exit raises the possibility that a target growth rate, and not a target size, is required for cell cycle progression, and that individual cells measure their own rates of growth. There is evidence that this type of mechanism is active in the budding yeast Saccharomyces cerevisiae, where cells must achieve a threshold protein synthesis rate before progressing through G1 to S-phase. There is a well-established link between growth and G1/S progression in S. cerevisiae (see (*27*) for a comprehensive review), which is reflected in the negative correlation between cell size at birth and G1 duration (*28*). Di Talia et al. showed that size control is imposed during the earlier part of G1 and depends on the G1 cyclin Cln3, while the late events of G1 are size-independent (*28*). In small cells, G1 is lengthened, allowing cells to approach a "size threshold" before passing *Start* and subsequently exiting G1. In S. cerevisiae cells, growth rate is proportional to size (*28*), so a growth rate threshold gating G1 exit would give the appearance of a size threshold.

Cln3 has been implicated as a sensor of the rate of protein synthesis (*29, 30*). Cln3 is a rate-limiting determinant of G1 exit; mutants with highly abundant Cln3 have a shorter G1 and smaller size than wild-type cells (*31*) . The link between cell growth and G1 exit may lie in the CLN3 5' untranslated region, where an open reading frame allows appreciable Cln3 synthesis only when there are sufficient ribosomes to bypass the block. Because this leaky scanning mechanism is inefficient, Cln3 synthesis requires a minimium rate of protein translation (*29*). As Cln3 is highly unstable (*31*), its abundance at any given time is indicative of the current

translation rate. This work suggests that, in budding yeast, cell cycle entry is regulated by a threshold on the overall rate of protein synthesis. A similar threshold has been proposed to regulate mitotic entry. Both cdc25 (a dosage dependent activator of mitosis) and the G2/M cyclin cdc13 mRNAs have long 5' untranslated regions containing open reading frames, rendering their levels particularly sensitive to the rate of translation initiation (*32*).

Cln3 promotes cell cycle progression by relieving inhibition of the transcription factor SBF, activating the transcription of many cell cycle genes, including downstream G1 cyclins Cln1 and Cln2. These cyclins further activate SBF, triggering a positive feedback loop which ensures an irreversible commitment to the cell cycle ("Start") (*33-35*). Among its other modes of action, Cln3 localizes to SBF binding sites in the CLN2 promoter, where it releases SBF inhibitor Whi5 (*30*). Titration of Cln3 against the fixed number of SBF binding sites in the genome may be the means by which the cell senses the total amount of Cln3, despite the increasing volume of the cell that is expected to stabilize Cln3 concentration (*30*).

In vertebrate systems, cyclin E is functionally homologous to the yeast Cln3. Expression of human cyclin E can compensate for loss of Cln3 in yeast lacking all G1 cyclins (Keyomarsi K. personal communication). Active cyclin E activates CDK2, thereby promoting G1 exit and the onset of the cell division cycle. In line with is roles in cell cycle, cyclin E overexpression shortens G1 resulting in a decreased cell size (*36, 37*).

The idea that cyclin E might serve as sensor of protein translation rate, analogous to Cln3, was first proposed by Edgar and Nuefeld (*37*), in their work on growth of the drosophila wing disc. Like Cln3, the drosophila cyclin E contains several open reading frames in its 5'

untranslated region (*38*). Ras activation, which increases cell size and growth rates, was found to cause a posttranscriptional increase in cyclin E levels, promoting G1/S progression (*39*).

Similarly, in mammalian hepatocytes, cyclin E abundance correlates more strongly with cell growth than with cell cycle progression (*40-42*). Transfecting hepatocytes with cyclin D causes proliferation one day after treatment. Six days later, hepatocytes show little proliferation but increased growth. Though the amount of cyclin E mRNA is highly increased during the earlier proliferative phase, a large increase in the cyclin E protein abundance occurs only later, with cell growth. The fact that translation, but not transcription, of cyclin E is correlated with cell growth suggests that it might serve as a translation rate sensor. However, due to the correlative nature of these findings, further investigation is still needed to determine whether cyclin E truly links cell growth to cell cycle progression. Another potential translation rate sensor is the E2F1 transcription factor. E2F1 drives endocycles in drosophila salivary cells, by promoting cyclin E expression and S-phase entry, and translational control of E2F1 was found to couple rates of endocycle progression to cellular growth rates (*43*).

Physiological consequences of cell size

Why would cells need a mechanism to specify and fine-tune their individual sizes? For certain cells, there is an obvious association between a cell's function and its physical dimensions. Neurons, for example, must span the distance across which they relay information. Yet, for the majority of cell types, whether epithelial or mesenchymal, the advantage of a specific size is not obvious. A famous 1945 study by Gerhard Fankhauser documents the effects of the increased cell size in polyploid salamander larvae on the formation of various multicellular

structures, such as pronephric tubules (*44*). In many organs, the shape and dimensions of these structures are unchanged, with a decrease in cell number compensating for the increase in cell size. In pentaploid larvae, this compensation meant that the circumference of pronephric tubules and ducts was often spanned by just a single cell! The fact that normal structures could be formed even with large alterations in cell size suggested that, for many cell types, a cell's size is not imposed by its role as the structural unit of the organism. Notable exceptions to this trend include the observation that cell size influences the size and morphological complexity of the brain (*45*).

There is some indication that a cell's size is commonly related to its physiology, since some cells change their size in response to external cues. For example, kidney epithelial cells modulate their size in response to rates of fluid flow in the nephron ducts, sensed by mechanical shear on the primary cilium (*46*). Cell size also often changes during differentiation. Lymphocytes, for instance, rapidly grow to a larger size after exposure to cytokines or TLR stimulation (*47*). However, in these cases, it is not clear whether size is the target of regulation or a by-product of some other adaptation.

A change in organ size, when demanded by physiology, can be accomplished through a change in cell number, a change in cell size, or both. The choice of modulating organ growth through cell growth or proliferation is often context-dependent. Pancreatic beta cells, for example, increase their size by over 25% during pregnancy, in response to increased insulin demand (*48*). However, the insulin demand resulting from beta cell death leads to increased proliferation of beta cells, without changing their size (*48*). Similarly, liver size increases during pregnancy through hepatocyte hypertrophy, whereas liver regeneration after surgical resection occurs by increased hepatocyte proliferation. These examples suggest that, under particular

physiological conditions, it might be advantageous for a specific cell to have a specific size. This raises the question: do cells function most efficiently when at the 'right' size?

Because cells have multiple roles, a cell's "function" is hard to define and its functional efficiency hard to quantify. Another difficulty is, for most cell types, size has not been a primary focus of investigation. Consequently, literature that systematically quantifies cell size and relates it to cell behavior is sparse. An exception to this rule is the case of the pancreatic beta cell. Insulin secretion is associated with beta cell mass, so the size of beta cells has been the subject of much research. To a simple approximation, a beta cell may be described as a device that performs one main function- secretion of insulin in response to increases in blood glucose- and this process can be measured quantitatively. For these reasons, we will examine the evidence of a size-function relationship in beta cells, with the hope that this discussion will stimulate similar investigations of other cell types.

Giordano et al. found that the rate of insulin production of individual rat beta cells is more strongly correlated with cell size than with metabolic activity as assayed by NAD(P)H fluorescence (*49*) . In fact, in cultured rat beta cells, insulin secretion, metabolic activity, and global rates of protein production are all correlated with cell size. These correlations are further reinforced in transgenic mice harboring mutations that affect cell size. For example, beta cells of mice lacking S6K1 are reduced in size (*50, 51*). These small beta cells secrete less insulin per cell than normal beta cells, possibly due to the reduction in membrane surface available, leading to hypoinsulinemia. By contrast, rapamycin treatment of wild-type beta cells, which reduces S6K1 activity but does not change beta cell size, does not affect insulin secretion, indicating that the reduced insulin secretion results from a size defect rather the absence of S6K1 (*50*).

Additional studies suggest that there is an optimal size for maximum efficiency of insulin secretion. Like S6K1 knockouts, mice expressing only a mutant, non-phosphorylatable ribosomal protein S6 have small beta cells (*52-54*). However, in these mutants, the cell size defect is compensated by increased cell number so that their total beta cell mass is similar to that of wild-type mice. Despite this rough conservation of bulk mass, these mutants are still hypoinsulinemic, suggesting that small cells are disproportionately less efficient insulin producers than normal-sized cells. Furthermore, mice expressing constitutively active protein kinase Akt1 have larger beta cells than wild-type mice and an increased rate of insulin secretion (*55*). However, insulin secretory capacity per unit of beta cell mass is lower. A persistent hyperinsulinemia in these transgenic mice may indicate inefficiency in hormone secretion. These results suggest that beta cell function may be impaired in cells that are either larger or smaller than their target size. A caveat to this interpretation comes from the pleiotrophic effects of pathways like mTOR, MAPK and PI3K, pathways which, in addition to affecting cell size, can also regulate many other functions. Hence, it is hard to know whether a change in size actually causes a change in function or is simply correlated with it.

Another case where evidence may suggest an optimal cell size criterion is that of mammalian adipocytes. Clear differences in gene expression between large and small adipocytes suggest that cell size influences adipocyte biology (*56, 57*). One explanation for this effect is that cellular enlargement, by increasing cell surface area and modifying interactions between the cell and its extracellular matrix, activates the β_1-integrin/ERK signaling pathway that modulates several transcription factors (*57*). Large adipocytes display a marked increase in the activity of fatty acid synthase and lipoprotein lipase. These changes are further manifested in the altered metabolic activity of large adipocytes. For example, Smith et. al. compared large and small

adipocytes isolated from the same specimen of human adipose tissue (*58, 59*) and found that large adipocytes have higher rates of lipid synthesis. This increase in lipogenesis rate is still evident when measurements are normalized to cell size, meaning that large cells are disproportionally more productive than small cells. Changes in cell size have also been linked to transcriptional and metabolic changes in other cell types, including hepatocytes and erythrocytes (*60-63*).

However, the increased metabolic efficiency of large adipocytes comes at a price. Larger cells are less sensitive to the stimulating effects of insulin on glucose uptake, the oxidation of glucose to CO2 (*64*), and the uptake of triglyceride fatty acids (*65*). These defects may result from the stress of adipocyte enlargement against the physical constraints imposed by collagen and the extracellular matrix (*66*). The balance between metabolic capacity that scales positively with adipocyte size and insulin sensitivity that scales negatively with size implies an optimal adipocyte size. Supporting this idea, increased adipocyte size, rather than total body fat, is associated with insulin resistance in obesity and is a risk factor for development of type II diabetes mellitus (*67*).

Several lines of research have suggested an interesting link between the regulation of cell size variability and the pathology of cancer, although the systematic studies needed to confirm this link are still lacking. While cancer is a disease of deregulated proliferation, in clinical histology it is the size of cancer cells that renders their appearance distinct from the surrounding tissue (*68*). Malignant tumor cells are both larger and more variable in size than normal cells. Pleomorphism, the increased variability in cell size and shape, is a histological characteristic of many malignant lesions (*69-71*) and is sometimes used as a criterion for the determination of histologic grade. The loss of cell size regularity in cancer cells also occurs when cell lines of

normal and neoplastic origin are grown in matching culture conditions, indicating that the increased size variability in cancer is cell-autonomous and not a product of the tumor microenvironment (*72*). Furthermore, when epidermoid carcinoma cell lines were classified based on cell size variability, only the highly heterogeneous lines initiated tumors upon heterotransplatation into mice (*72*). These experiments raise the question of whether aberrant regulation of cell size has a role in tumorigenesis, although increased cell size variability may also be a mere correlate of tumor biology (perhaps the result of aneuploidy), and further experiments are warranted to resolve this conflict.

Questions, challenges, suggestions

Early cell cycle research featured a debate over whether the cell cycle was the result of a linear cascade of interdependent events, with early events providing substrates essential for later ones, or whether there was an independent master regulator of cell cycle – a cell cycle clock (*73*). Investigations of cell size now face a similar dilemma. Is the size of a cell simply the byproduct of its rate of growth and frequency of division? Or is there a master regulator that independently specifies cell size on the basis of a cell's function and physiological needs? The evidence reviewed above, suggests that there is a separate and at least partially independent pathway for cell size regulation.

Almost exclusively, studies of size regulation have focused on the possibility of a size checkpoint, an event that regulates either G1 exit or cell division based on cell size. The checkpoint model posits that the size of a cell is specified by adjusting the *amount of time* during which it grows. Lengthening G1 would increase the amount of time in which a cell grows,

resulting in an increased cell size. This possibility is grounded in observations from yeast biology (*10*) . Yet, there is also an alternative class of mechanisms that can just as easily dictate cell size. Instead of regulating the amount of time during which they grow, cells may regulate the *rate* at which they accumulate mass. To limit size disparity, small cells could accelerate their growth rate, or large cells could decelerate it. This alternative has remained unexplored, largely because of the difficulty of making precise measurements of cell growth.

If individual cells were to specify their size by modulating their growth rates rather than their cell cycle length, a cell's overall synthetic machinery would have to be fine-tuned to reflect its size. In other words, there would have to be feedback linking a cell's physical dimensions to its anabolic control. The identification of such a mechanism would significantly alter the way we understand growth control. We would need to expand the simple and intuitive model of a discrete size checkpoint to include the continuous modulation of growth rates.

It has been over 150 years since Virchow wrote, "omnis cellula e cellula", giving us a very modern concept of the cell; since that time, the problem of how cell size is regulated has been staring us in the face. Today we have only achieved a partial phenomenological explanation of cell size homeostasis. Why has it been so difficult? Despite the simplicity of size as a phenotype, its study is inherently challenging. The specific size of a cell is an outcome of numerous and diverse processes. Accumulation of cell mass is directly related to a cell's metabolic and anabolic activity, as well as protein turnover and autophagy. In proliferating populations, cell size reflects a balance between growth and division. In some cases, size is also affected by a cell's state of differentiation and physiological conditions. For this reason, it is hard

to establish whether a mutation or chemical perturbation that affects cell size is associated with size control per se. In a screen for cell size mutants, Jorgenson et al pointed out this problem, stating that an increase in the mean cell size in a population could reflect a shift to later cell cycle stages, rather than abnormal growth (*74*) . Additionally, a change in rates of cell division could increase or decrease cell size, even if growth rates remain unchanged. In retrospect, anatomical structure has been easier to study than physiological process. Chemical composition yielded to biochemical investigation more readily than integrated mechanisms like growth, shape, motility, and behavior. Whereas genetics could point us to processes that affect size, it could not easily disentangle contributions from nutrition, biogenesis, differentiation, and cell division. But, most importantly, we had only the crudest quantitative measures for the very processes we wished to study at the single cell level: growth and size.

The advances in recent years, summarized above, have provided evidence that growth and cell cycle progression are coordinated in proliferating cells. Confident that we are not merely studying the wake behind the boat, but that real circuits exist to precisely specify cell size, we can confront the underlying molecular circuitry and explore its biological consequences. We have interesting questions to address. How is the mean cell size established for each lineage? How do cells adapt to external stimuli to change the set point for their size? How does each cell measure its size and assess its deviation from the mean? By what mechanism do proliferating cells alter their rates of growth or passage through the cell cycle to prevent the natural accumulation of size variability? How do size changes affect cell function and do certain cells function best at a given size? What role does cell size play in pathology and senescence? JBS Haldane reminded us of the importance of size at the organism level in his lively essay, " On being the right size." (*75*) Biologists who have reveled in the qualitative complexity of cells

might take new inspiration from the simple process of size control; it is certain to have deep consequences and fascinating explanations.

Acknowledgements

We would like to thank Dr. Bruce Spiegelman and Dr. Ulf Smith for their advice on size regulation in adipose cells, and Dr. Sophie Martin for her input on size regulation in fission yeast. Many thanks to Dr. Yuval Dor and Dr. Ravid Straussman for critical reading of the manuscript.

1. E. B. Wilson, *The cell in development and heredity*. (The Macmillan company, New York,, ed. 3d, 1925), pp. xxxvii p., 1 l.,.

2. K. L. Cooper *et al.*, Multiple phases of chondrocyte enlargement underlie differences in skeletal proportions. *Nature* **495**, 375 (Mar 21, 2013).

3. A. Zetterberg, W. Engstrom, E. Dafgard, The relative effects of different types of growth factors on DNA replication, mitosis, and cellular enlargement. *Cytometry* **5**, 368 (Jul, 1984).

4. A. Zetterberg, O. Larsson, Coordination between cell growth and cell cycle transit in animal cells. *Cold Spring Harbor symposia on quantitative biology* **56**, 137 (1991).

5. I. J. Conlon, G. A. Dunn, A. W. Mudge, M. C. Raff, Extracellular control of cell size. *Nature cell biology* **3**, 918 (Oct, 2001).

6. M. N. Hall, M. C. Raff, G. Thomas, *Cell growth : control of cell size*. Monograph (Cold Spring Harbor Laboratory Press, Cold Spring Harbor, N.Y., 2004), pp. xii, 652 p.

7. D. Killander, A. Zetterberg, A quantitative cytochemical investigation of the relationship between cell mass and initiation of DNA synthesis in mouse fibroblasts in vitro. *Experimental cell research* **40**, 12 (Oct, 1965).

8. D. Killander, A. Zetterberg, Quantitative Cytochemical Studies on Interphase Growth. I. Determination of DNA, Rna and Mass Content of Age Determined Mouse Fibroblasts in Vitro and of Intercellular Variation in Generation Time. *Experimental cell research* **38**, 272 (May, 1965).

9. H. Dolznig, F. Grebien, T. Sauer, H. Beug, E. W. Mullner, Evidence for a size-sensing mechanism in animal cells. *Nature cell biology* **6**, 899 (Sep, 2004).

10. G. C. Johnston, J. R. Pringle, L. H. Hartwell, Coordination of growth with cell division in the yeast Saccharomyces cerevisiae. *Experimental cell research* **105**, 79 (Mar 1, 1977).

11. P. Echave, I. J. Conlon, A. C. Lloyd, Cell size regulation in mammalian cells. *Cell cycle* **6**, 218 (Jan 15, 2007).

12. R. Kafri *et al.*, Dynamics extracted from fixed cells reveal feedback linking cell growth to cell cycle. *Nature* **494**, 480 (Feb 28, 2013).

13. T. P. Burg *et al.*, Weighing of biomolecules, single cells and single nanoparticles in fluid. *Nature* **446**, 1066 (Apr 26, 2007).

14. S. Son *et al.*, Direct observation of mammalian cell growth and size regulation. *Nature methods* **9**, 910 (Sep, 2012).

15. I. Conlon, M. Raff, Differences in the way a mammalian cell and yeast cells coordinate cell growth and cell-cycle progression. *Journal of biology* **2**, 7 (2003).

16. I. Conlon, M. Raff, Control and maintenance of mammalian cell size: response. *BMC cell biology* **5**, 36 (Sep 30, 2004).

17. S. Cooper, Control and maintenance of mammalian cell size. *BMC cell biology* **5**, 35 (Sep 29, 2004).

18. H. E. Kubitschek, K. B. Clay, A second growth state for Schizosaccharomyces pombe. *Experimental cell research* **165**, 243 (Jul, 1986).

19. E. C. Anderson, G. I. Bell, D. F. Petersen, R. A. Tobey, Cell growth and division. IV. Determination of volume growth rate and division probability. *Biophysical journal* **9**, 246 (Feb, 1969).

20. A. Tzur, R. Kafri, V. S. LeBleu, G. Lahav, M. W. Kirschner, Cell growth and size homeostasis in proliferating animal cells. *Science* **325**, 167 (Jul 10, 2009).

21. J. F. Collins, M. H. Richmond, Rate of growth of Bacillus cereus between divisions. *Journal of general microbiology* **28**, 15 (Apr, 1962).

22. Y. Barrandon, H. Green, Cell size as a determinant of the clone-forming ability of human keratinocytes. *Proceedings of the National Academy of Sciences of the United States of America* **82**, 5390 (Aug, 1985).

23. S. G. Martin, Geometric control of the cell cycle. *Cell cycle* **8**, 3643 (Nov 15, 2009).

24. S. G. Martin, M. Berthelot-Grosjean, Polar gradients of the DYRK-family kinase Pom1 couple cell length with the cell cycle. *Nature* **459**, 852 (Jun 11, 2009).

25. J. B. Moseley, A. Mayeux, A. Paoletti, P. Nurse, A spatial gradient coordinates cell size and mitotic entry in fission yeast. *Nature* **459**, 857 (Jun 11, 2009).

26. E. Wood, P. Nurse, Pom1 and cell size homeostasis in fission yeast. *Cell cycle* **12**, 3228 (Oct 1, 2013).

27. J. J. Turner, J. C. Ewald, J. M. Skotheim, Cell size control in yeast. *Current biology : CB* **22**, R350 (May 8, 2012).

28. S. Di Talia, J. M. Skotheim, J. M. Bean, E. D. Siggia, F. R. Cross, The effects of molecular noise and size control on variability in the budding yeast cell cycle. *Nature* **448**, 947 (Aug 23, 2007).

29. M. Polymenis, E. V. Schmidt, Coupling of cell division to cell growth by translational control of the G1 cyclin CLN3 in yeast. *Genes & development* **11**, 2522 (Oct 1, 1997).

30. H. Wang, L. B. Carey, Y. Cai, H. Wijnen, B. Futcher, Recruitment of Cln3 cyclin to promoters controls cell cycle entry via histone deacetylase and other targets. *PLoS biology* **7**, e1000189 (Sep, 2009).

31. M. Tyers, G. Tokiwa, R. Nash, B. Futcher, The Cln3-Cdc28 kinase complex of S. cerevisiae is regulated by proteolysis and phosphorylation. *The EMBO journal* **11**, 1773 (May, 1992).

32. R. R. Daga, J. Jimenez, Translational control of the cdc25 cell cycle phosphatase: a molecular mechanism coupling mitosis to cell growth. *Journal of cell science* **112 Pt 18**, 3137 (Sep, 1999).

33. G. Charvin, C. Oikonomou, E. D. Siggia, F. R. Cross, Origin of irreversibility of cell cycle start in budding yeast. *PLoS biology* **8**, e1000284 (Jan, 2010).

34. L. Dirick, K. Nasmyth, Positive feedback in the activation of G1 cyclins in yeast. *Nature* **351**, 754 (Jun 27, 1991).

35. J. M. Skotheim, S. Di Talia, E. D. Siggia, F. R. Cross, Positive feedback of G1 cyclins ensures coherent cell cycle entry. *Nature* **454**, 291 (Jul 17, 2008).

36. T. P. Neufeld, A. F. de la Cruz, L. A. Johnston, B. A. Edgar, Coordination of growth and cell division in the Drosophila wing. *Cell* **93**, 1183 (Jun 26, 1998).

37. T. P. Neufeld, B. A. Edgar, Connections between growth and the cell cycle. *Current opinion in cell biology* **10**, 784 (Dec, 1998).

38. H. E. Richardson, L. V. O'Keefe, S. I. Reed, R. Saint, A Drosophila G1-specific cyclin E homolog exhibits different modes of expression during embryogenesis. *Development* **119**, 673 (Nov, 1993).

39. D. A. Prober, B. A. Edgar, Ras1 promotes cellular growth in the Drosophila wing. *Cell* **100**, 435 (Feb 18, 2000).

40. L. K. Mullany *et al.*, Akt-mediated liver growth promotes induction of cyclin E through a novel translational mechanism and a p21-mediated cell cycle arrest. *The Journal of biological chemistry* **282**, 21244 (Jul 20, 2007).

41. C. J. Nelsen *et al.*, Induction of hepatocyte proliferation and liver hyperplasia by the targeted expression of cyclin E and skp2. *Oncogene* **20**, 1825 (Apr 5, 2001).

42. C. J. Nelsen, D. G. Rickheim, N. A. Timchenko, M. W. Stanley, J. H. Albrecht, Transient expression of cyclin D1 is sufficient to promote hepatocyte replication and liver growth in vivo. *Cancer research* **61**, 8564 (Dec 1, 2001).

43. N. Zielke *et al.*, Control of Drosophila endocycles by E2F and CRL4(CDT2). *Nature* **480**, 123 (Dec 1, 2011).

44. G. Fankhauser, Maintenance of normal structure in heteroploid salamander larvae, through compensation of changes in cell size by adjustment of cell number and cell shape. *The Journal of experimental zoology* **100**, 445 (Dec, 1945).

45. G. Roth, J. Blanke, D. B. Wake, Cell size predicts morphological complexity in the brains of frogs and salamanders. *Proceedings of the National Academy of Sciences of the United States of America* **91**, 4796 (May 24, 1994).

46. C. Boehlke *et al.*, Primary cilia regulate mTORC1 activity and cell size through Lkb1. *Nature cell biology* **12**, 1115 (Nov, 2010).

47. A. K. Abbas, A. H. Lichtman, S. Pillai, *Cellular and molecular immunology*. (Elsevier/Saunders, Philadelphia, ed. 7th, 2012), pp. x, 545 p.

48. S. Dhawan, S. Georgia, A. Bhushan, Formation and regeneration of the endocrine pancreas. *Current opinion in cell biology* **19**, 634 (Dec, 2007).

49. E. Giordano *et al.*, B-cell size influences glucose-stimulated insulin secretion. *The American journal of physiology* **265**, C358 (Aug, 1993).

50. M. Pende *et al.*, Hypoinsulinaemia, glucose intolerance and diminished beta-cell size in S6K1-deficient mice. *Nature* **408**, 994 (Dec 21-28, 2000).

51. M. C. Fabian, J. R. Lakey, R. V. Rajotte, N. M. Kneteman, The efficacy and toxicity of rapamycin in murine islet transplantation. In vitro and in vivo studies. *Transplantation* **56**, 1137 (Nov, 1993).

52. I. Ruvinsky *et al.*, Ribosomal protein S6 phosphorylation is a determinant of cell size and glucose homeostasis. *Genes & development* **19**, 2199 (Sep 15, 2005).

53. I. Ruvinsky *et al.*, Mice deficient in ribosomal protein S6 phosphorylation suffer from muscle weakness that reflects a growth defect and energy deficit. *PloS one* **4**, e5618 (2009).

54. I. Ruvinsky, O. Meyuhas, Ribosomal protein S6 phosphorylation: from protein synthesis to cell size. *Trends in biochemical sciences* **31**, 342 (Jun, 2006).

55. E. Bernal-Mizrachi, W. Wen, S. Stahlhut, C. M. Welling, M. A. Permutt, Islet beta cell expression of constitutively active Akt1/PKB alpha induces striking hypertrophy, hyperplasia, and hyperinsulinemia. *The Journal of clinical investigation* **108**, 1631 (Dec, 2001).

56. C. Farnier *et al.*, The signaling pathway for beta1-integrin/ERKs is involved in the adaptation of adipocyte functions to cell size. *Annals of the New York Academy of Sciences* **973**, 594 (Nov, 2002).

57. C. Farnier *et al.*, Adipocyte functions are modulated by cell size change: potential involvement of an integrin/ERK signalling pathway. *International journal of obesity and related metabolic disorders : journal of the International Association for the Study of Obesity* **27**, 1178 (Oct, 2003).

58. U. Smith, Effect of cell size on lipid synthesis by human adipose tissue in vitro. *Journal of lipid research* **12**, 65 (Jan, 1971).

59. U. Smith, B. Jacobsson, Studies of human adipose tissue in culture. II. Effects of insulin and of medium glucose on lipolysis and cell size. *The Anatomical record* **176**, 181 (Jun, 1973).

60. T. R. Gregory, A bird's-eye view of the C-value enigma: genome size, cell size, and metabolic rate in the class aves. *Evolution; international journal of organic evolution* **56**, 121 (Jan, 2002).

61. T. P. Miettinen *et al.*, Identification of transcriptional and metabolic programs related to Mammalian cell size. *Current biology : CB* **24**, 598 (Mar 17, 2014).

62. S. Maciak, E. Bonda-Ostaszewska, M. Czarnoleski, M. Konarzewski, J. Kozlowski, Mice divergently selected for high and low basal metabolic rates evolved different cell size and organ mass. *Journal of evolutionary biology*, (Jan 13, 2014).

63. M. A. Monnickendam, M. Balls, The long-term organ culture of tissues from adult Amphiuma, the Congo eel. *Journal of cell science* **11**, 799 (Nov, 1972).

64. L. B. Salans, J. L. Knittle, J. Hirsch, The role of adipose cell size and adipose tissue insulin sensitivity in the carbohydrate intolerance of human obesity. *The Journal of clinical investigation* **47**, 153 (Jan, 1968).

65. P. J. Nestel, W. Austin, C. Foxman, Lipoprotn lipase content and triglyceride fatty acid uptake in adipose tissue of rats of differing body weights. *Journal of lipid research* **10**, 383 (Jul, 1969).

66. T. Khan *et al.*, Metabolic dysregulation and adipose tissue fibrosis: role of collagen VI. *Molecular and cellular biology* **29**, 1575 (Mar, 2009).

67. A. Guilherme, J. V. Virbasius, V. Puri, M. P. Czech, Adipocyte dysfunctions linking obesity to insulin resistance and type 2 diabetes. *Nature reviews. Molecular cell biology* **9**, 367 (May, 2008).

68. D. W. Kufe, *Cancer medicine 6 review : a companion to Holland-Frei Cancer Medicine-6*. (B.C. Decker, Hamilton, Ont. ; London, 2003), pp. x, 178 p.

69. G. Majno, I. Joris, *Cells, tissues, and disease : principles of general pathology*. (Oxford University Press, New York, ed. 2nd, 2004), pp. xxviii, 1005 p.

70. F. Moinfar, *Essentials of diagnostic breast pathology : a practical approach*. (Springer, New York, ed. 1st, 2007).

71. E. Rubin, H. M. Reisner, *Essentials of Rubin's pathology*. (Wolters Kluwer Health/Lippincott Williams & Wilkins, Philadelphia, ed. 6th, 2014), pp. xii, 826 p.

72. T. Caspersson, G. E. Foley, D. Killander, G. Lomakka, Cytochemical Differences between Mammalian Cell Lines of Normal and Neoplastic Origins. Correlation with Heterotransplant- Ability in Syrian Hamsters. *Experimental cell research* **32**, 553 (Dec, 1963).

73. A. W. Murray, M. W. Kirschner, Dominoes and clocks: the union of two views of the cell cycle. *Science* **246**, 614 (Nov 3, 1989).

74. P. Jorgensen, J. L. Nishikawa, B. J. Breitkreutz, M. Tyers, Systematic identification of pathways that couple cell growth and division in yeast. *Science* **297**, 395 (Jul 19, 2002).

75. J. B. S. Haldane, *Possible worlds and other essays*. (Chatto & Windus, London,, 1927), pp. viii, 312 p.

76. L. S. Baptista *et al.*, Adipose tissue of control and ex-obese patients exhibit differences in blood vessel content and resident mesenchymal stem cell population. *Obesity surgery* **19**, 1304 (Sep, 2009).

77. H. Fidlerova *et al.*, Replication-coupled modulation of early replicating chromatin domains detected by anti-actin antibody. *Journal of Cellular Biochemistry* **94**, 899 (Apr 1, 2005)

78. N. M. Suliman, A. N. Astrom, R. W. Ali, H. Salman, A. C. Johannessen, Clinical and histological characterization of oral pemphigus lesions in patients with skin diseases: a cross sectional study from Sudan. *BMC oral health* **13**, 66 (Nov 21, 2013).

79. S.K. Pandit *et al.*, E2F8 is essential for polyploidization in mammalian cells. *Nature Cell Biology* **14**, 1181 (Nov, 2012)

80. J. Auffret *et al.*, Defective prolactin signaling impairs pancreatic beta-cell development during the perinatal period. *American journal of physiology. Endocrinology and metabolism* **305**, E1309 (Nov 15, 2013).

Chapter 2

Cell-autonomous adjustments of cell cycle length and growth rate ensure size uniformity in proliferating populations

Introduction

How do the different cell types maintain their distinctive and characteristic sizes? The precision with which size is controlled is demonstrated by the uniformity in cell size typically seen in tissues. Most epithelial tissues, for example, display a striking regularity in the size and morphology of cells, while size heterogeneity can be a sign of neoplastic growth[1,2]. Size variation can only be reduced with processes that differentially affect cells of different sizes, despite the fact that they share the same environment. This kind of control requires that individual cells measure their own size and adjust their behavior as necessary, to achieve a common target size.

The body of evidence supporting and contradicting the idea of cell-autonomous size control is reviewed in chapter one. Most of this work focuses on whether and how cell size and cell cycle are coordinated. To date, most of our knowledge concerning the coordination between cell growth and division comes from the study of single-cell fungal yeast, in which size-dependent thresholds have been suggested at G1/S transition and/or mitotic entry[3–8]. In animal cells, however, there is still no definite conclusion as to whether cell division is coordinated with cell growth[9–13].

Studies of proliferating Schwann cells have suggested that cell size is the passive outcome of cell growth and divisions, which are independently regulated processes[9,11–13]. These

studies, however, examined changes in mean size in response to extracellular signals, not size variability in a population. Several pieces of evidences support the existence of coordination between cell growth and division to correct deviations from the population mean[14–17].

As a measure of cell size, we considered the total cellular protein mass, which composes the majority macromolecular dry mass in a cell [18]. Previously, we developed ergodic rate analysis (ERA), a method to infer dynamic behavior of cells from single-timepoint measurements of an unsynchronized population. We applied this method to cellular protein content measurements, to investigate cell growth over the cell cycle. ERA detects the presence of regulatory mechanisms, by analyzing how the shape of the measured distribution (in this case, the distribution of cell size) changes as a function of the cell cycle. This study detected the presence of a mechanism that reduces variability in cell size at S-phase entry, providing further evidence of cell-autonomous size specification in proliferating animal cells.

While most studies have focused on possible links between cell size and cell-cycle transitions, variance in a population can also be constrained if cellular growth rates are regulated in a cell-size-dependent manner. This is a largely unexplored possibility, which may provide insight into how non-proliferating and differentiated cells maintain the correct size. Since ERA relies on cell cycle markers as a measure of time, it cannot conclusively determine whether size regulation is accomplished by cell cycle length adjustment or by changes in cellular growth rates.

In the work described below, we set out to conclusively determine whether individual cells sense and regulate their own size. We developed separate assays to assess control of cell-cycle length and control of growth rate on the single-cell level. Our results suggest that cell size plays a role in control of cell both cycle progression and cell growth.

Results

Investigating the coordination of growth and cell cycle progression

To measure the total protein content of single cells, we used amine-reactive fluorescent dye AlexaFluor 647-Succinimidyl Ester (SE-A647) to covalently label lysine residues, as described earlier [17]. The integrated fluorescence intensity of an SE-A647-stained cell reflects the amount of protein it contains and correlates well with its total dry mass measured by quantitative phase microscopy[19] (figure 2.1A). We demonstrated the sensitivity of this method by labeling S-phase cells with a 20 minute-long pulse of EdU and measuring the protein content of the EdU-positive cells at various time intervals after pulse-labeling. Figure 2.1B shows that our measurement is sensitive enough to detect the change in protein mass that occurs in less than three hours of growth, under 10% of the total mass accumulated during the average cell cycle. For the first six hours after labeling, the size distribution shifts to the right as the labelled cells grow. Nine hours after labeling, labeled cells have begun to divide, so the distribution is bimodal with its first peak (representing newborn cells) at approximately half the size of its second peak (representing older cells). Between twelve and twenty-four hours after labeling, all labeled cells have divided, and the size distribution gradually shifts to the right again as they continue to grow.

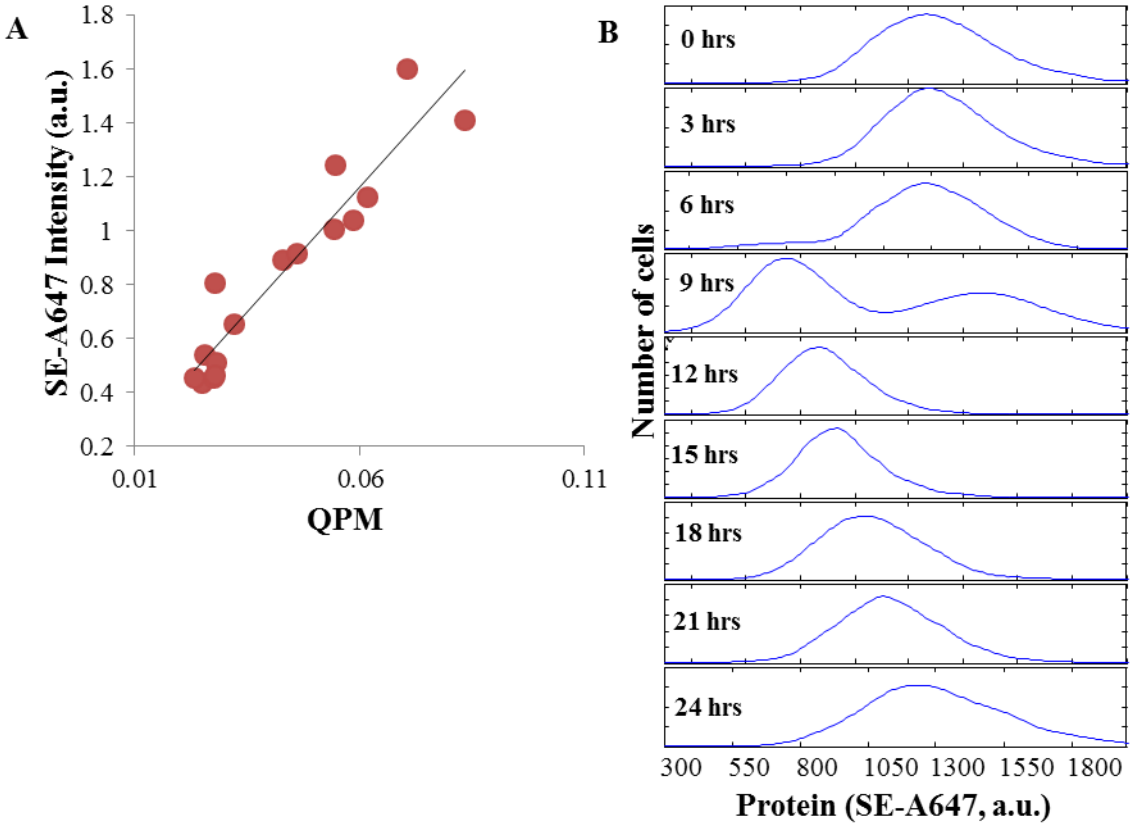

Figure 2.1: (A) Correlation between integrated SE-A647 intensity of single cells, measured by widefield microscopy, and dry mass (phase shift) measured by quantitative phase microscopy. (B) Series of protein (SE-A647) histograms of EdU-labeled cells measured at three-hour intervals following incubation with EdU.

To monitor cell growth over time, unsynchronized populations of live cells were imaged at 15 minute intervals for 1-3 days, via phase-contrast and fluorescence microscopy, followed by fixation and SE-A647 staining. We developed computational strategies (detailed in the methods section) to track thousands of individual cells over the course of the time-lapse movies and record the amount of time that elapsed between each cell's "birth" via mitosis and its fixation, which we will refer to as the cell's "age". Figure 2.2A and 2.2B show the average cell size (i.e. protein content) as a function of cell age for HeLa and Rpe1 cells. In both cases, the average size of the oldest cells is approximately double that of the youngest, further attesting to the reliability of our measurements. In addition, comparing the size distribution of the youngest cells (first 1.5 hours after birth) to that of mitotics (identified by their rounded shape) shows a doubling in cell

size over the course of the cell cycle (figure 2.2C). As expected, the size distribution of mitotics is identical to that of the oldest cells tracked. We also notice a transient slowing of cell growth about 10 hours after birth, which is the average age of S-phase entry. This is consistent with the behavior we previously reported, when we measure mean size as a function of cell cycle position rather than age [17]. With these confirmations of the method's reliability, we proceeded to use the combination of time-lapse microscopy and fixed-cell protein measurements to probe the coordination of cell growth and cell cycle progression.

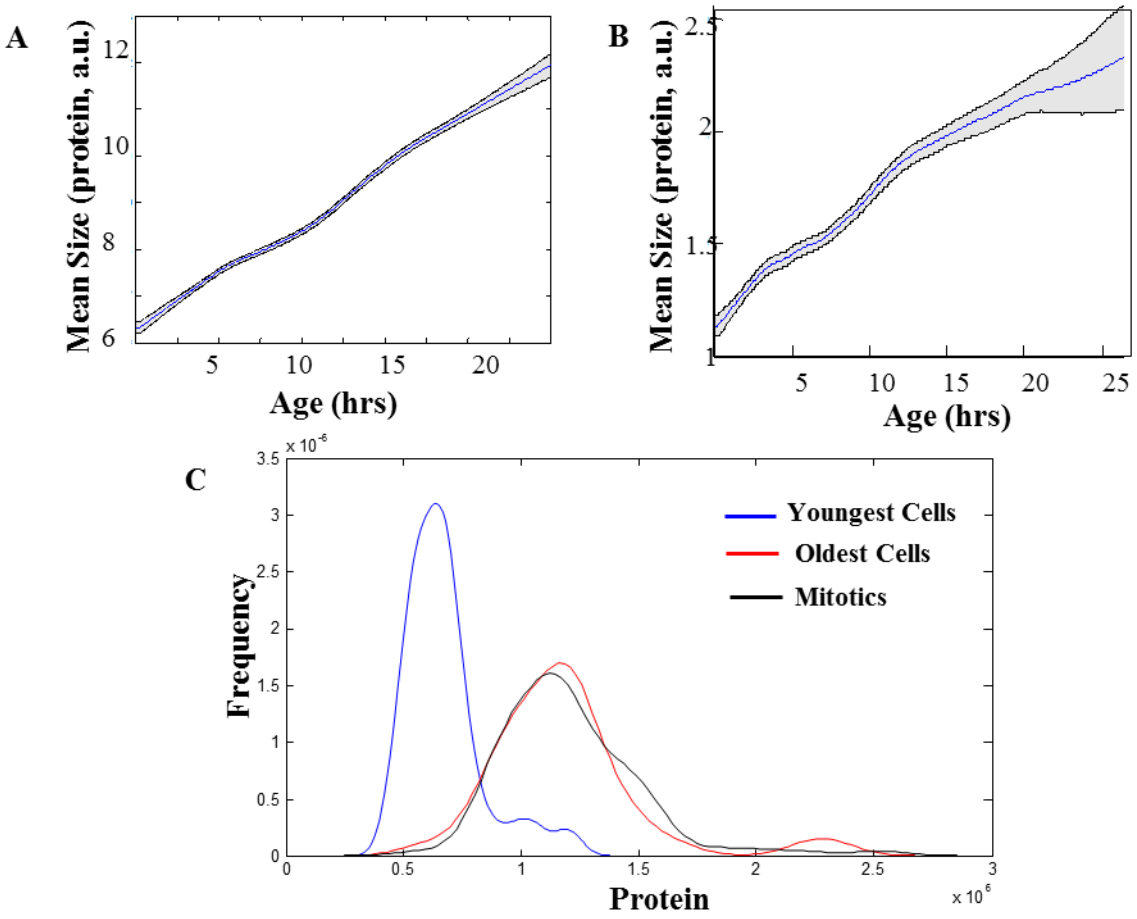

Figure 2.2: Mean cell size as a function of age in (A) HeLa and (B) Rpe1cells. Shaded region marks 20% and 80% bootstrapping confidence intervals. (C) Size distributions of the youngest (<1.5 hrs old), oldest, and mitotic cells.

S-phase cells are larger than G1 cells of the same age.

Previous studies have suggested that a cell-size checkpoint coordinates growth and cell cycle progression[3,6,8,14,16,17]. To determine whether there is a size threshold gating G1-exit, we used cells transfected with mAG-hGem, a reporter of the G1-S transition [20]. The mAG-hGem construct encodes a constitutively-expressed fluorescent protein fused to the geminin degron, so that it is continuously degraded by APC/C^{Cdh1} during G1 and accumulates in the cell following APC/C^{Cdh1} inactivation. To test that mAG-hGem expression precisely marks S-phase entry, we co-transfected cells with a DNA-ligase-dsRed fusion[21] and observed a nearly perfect correlation between the S-phase-entry times reported by the two markers (figure 2.3).

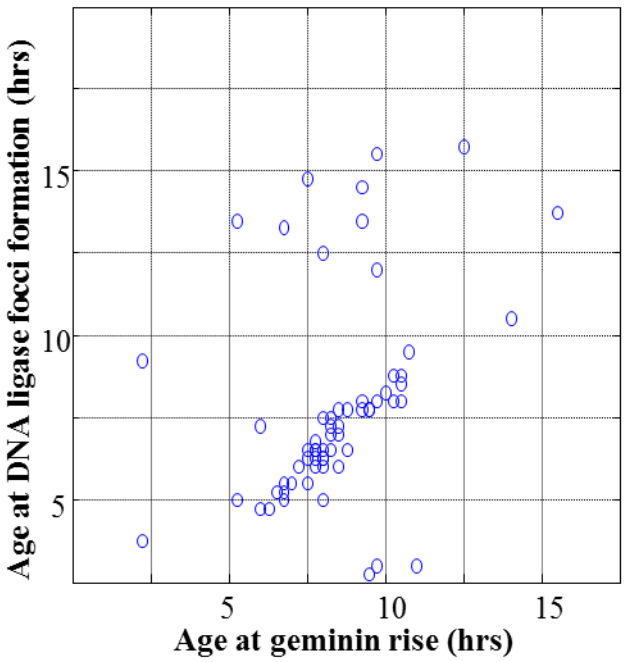

Figure 2.3: Reporters of S-phase entry. The age of HeLa cells at the time of DNA-ligase-dsRed focci formation is plotted vs. their age at the start of mAG-hGem accumulation.

Figure 2.4A shows the average cell size as a function of cell age, plotted separately for G1 and post-G1 HeLa cells. As expected, young cells (<6 hours post birth) are all still in G1 while cells over 15 hours old have all exited G1. Cells of intermediate ages are a mixture of G1

and post-G1 cells, enabling us to test for a size difference between G1 and post-G1 cells that is independent of cell age. For any given age, we find that post-G1 cells are larger than G1 cells of the same age, even though both have been growing for the same amount of time (figures 2.4A and 2.4B). This result suggests that cells exit G1 in a size-dependent manner. Furthermore, the mean size of G1 cells plateaus as cells begins to enter S-phase, consistent with a mechanism where cells enter S-phase upon reaching a particular size. (The size difference between the distributions of G1 and post-G1 cells of the same age is statistically significant (student's t-test $p< 3.92e-04$). Three independent replicates also showed significant differences ($p<0.009$, $p<5.80e-08$, $p<9.07e-15$).

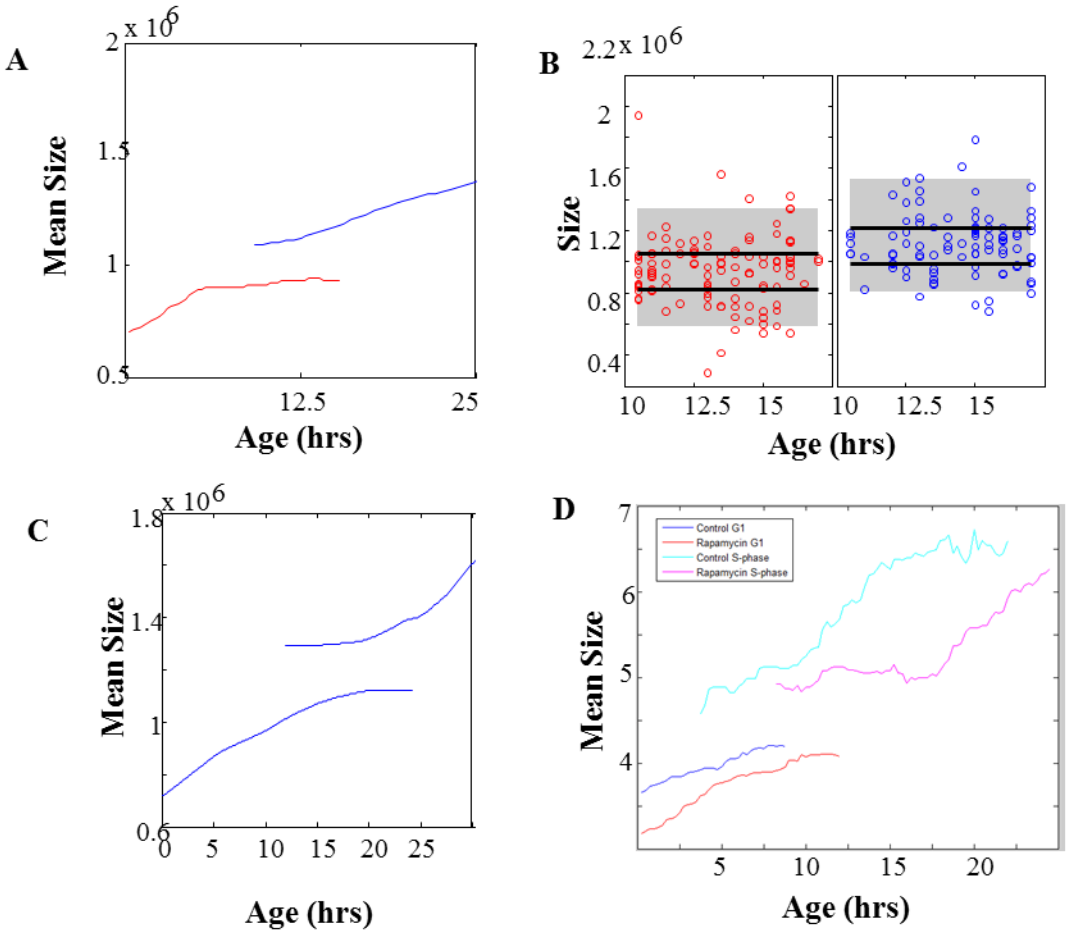

Figure 2.4: Post-G1 cells are larger than G1 cells of the same age. (A) Mean size of G1 (red) and post-G1 (blue) cells as a function of cell age. Post-G1 cells are identified by geminin level. (Legend continues on next page.)

Figure 2.4 (continued): (B) Size vs. age scatter plots for cells in the overlap region shows difference in size (student's t-test p< 3.92e-04). (C) Mean size of G1 and post-G1 cells as a function of cell age. Post-G1 cells are identified by DAPI level. (D) Control: Mean size of G1 (blue) and post-G1 (cyan) cells as a function of cell age. Rapamycin: Mean size of G1 (red) and post-G1 (magenta) cells as a function of cell age.

The mAG-hGem reporter is a sensitive detector of G1 exit, and is compatible with live-cell imaging, but its use raised the following concern. If large cells have a higher basal synthesis rate than smaller cells (a possible explanation for the weak correlation between size and "background" mAG-hGem fluorescence during G1), large cells might accumulate mAG-hGem more quickly right after APC/C^{Cdh1} inactivation. They would be immediately identified as post-G1 cells, while smaller cells could still be mistakenly classed as G1, creating an artificial size difference between G1 and post-G1 cells. To make sure that the "size threshold" shown in figure 2.4A is not artifactual, and validate this reporter for use in our further investigations of growth/cell cycle coordination, we repeated the analysis using DNA content (measured by DAPI staining) to differentiate between G1 and post-G1 cells. DNA was quantified by DAPI staining, and figure 2.4C shows the average cell size as a function of cell age, plotted separately for G1 (2N) and post-G1 (DNA content greater than 2N) cells. The behavior observed with the mAG-hGem reporter is preserved, confirming that that these results reflect a dependence of G1 exit on cell size.

We reasoned that if cells leave G1 only when a particular size has been reached, slowing down their growth rate would prolong G1, as cells would require more time to reach the threshold size. The mTOR inhibitor, rapamycin, is expected to slow down translation and cell growth. HeLa cells grown in 70 nM rapamycin continue to proliferate for several weeks, with no increase in cell death (figure 2.5A). They maintain a stable size distribution with a smaller mean size (measured by SE-A647 staining, figure 2.5B) and volume (measured by Coulter counter, figure 2.5C) than controls. Time-lapse microscopy of mAG-hGem-expressing cells reveals that

rapamycin does indeed cause an increase in G1 length, as predicted (figure 2.5D). Furthermore, plotting the mean size (measured by SE-A647 staining) of rapamycin-treated cells as a function of age shows that rapamycin-treated cells enter S-phase when they reach the same size at which untreated cells enter S-phase, consistent with a size-dependent G1 exit mechanism (figure 2.4D).

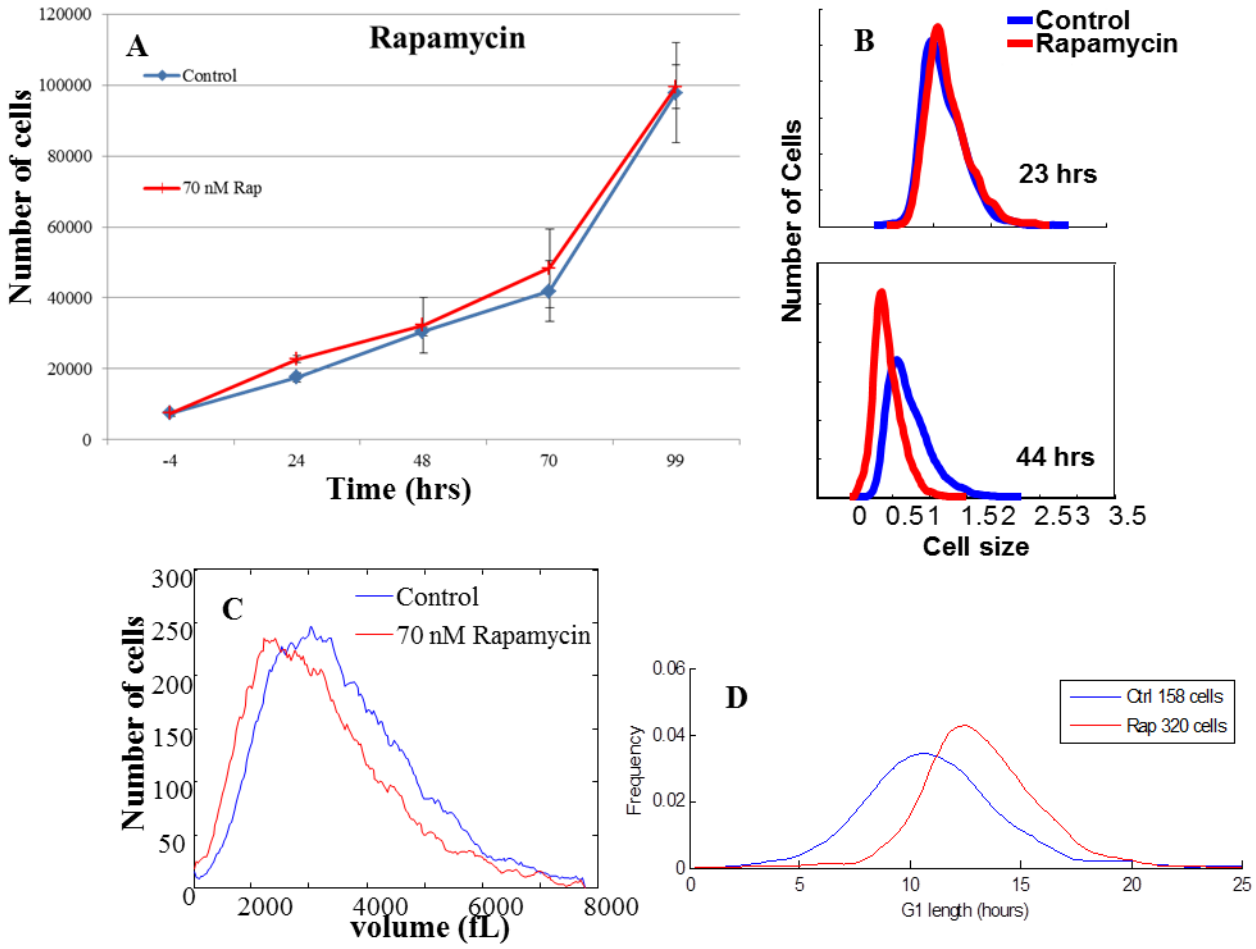

Figure 2.5: Stationary-state growth in rapamycin. (A) Growth curve of exponentially-proliferating HeLa cells in rapamycin (red) overlays control (blue). (B) Size distribution (protein content, SE-A647 stain) of cells after 23 hrs (top) and 44 hrs (bottom) of growth in rapamycin. (C) Volume distribution of cells after two days of growth in rapamycin. (D) Distribution of G1 lengths in control and rapamycin-treated cells.

To further test this conclusion, we exploited the natural variability in mean cell size observed among unperturbed cultures. We measured the average cell size (via 647-SE staining) of many cell populations, cultured in parallel wells of a multi-well plate. For each of these

populations, we also measured the proportion of cells in G1, to estimate G1 length as described previously[17]. Consistent with the cell-size checkpoint model, we observed a negative correlation between the average cell size in a well and the proportion of its cells in G1 (Figure 2.6A), indicating that an increases in cell size are accompanied by decreased G1 lengths. Rapamycin-treated populations followed the same trend, with extensions in G1 length proportional to decreases in mean size (Figure 2.6B). Taken together, these results suggest that a minimum size threshold for G1-exit ensures that small cells have more time to grow before their next division, increasing size uniformity in the population.

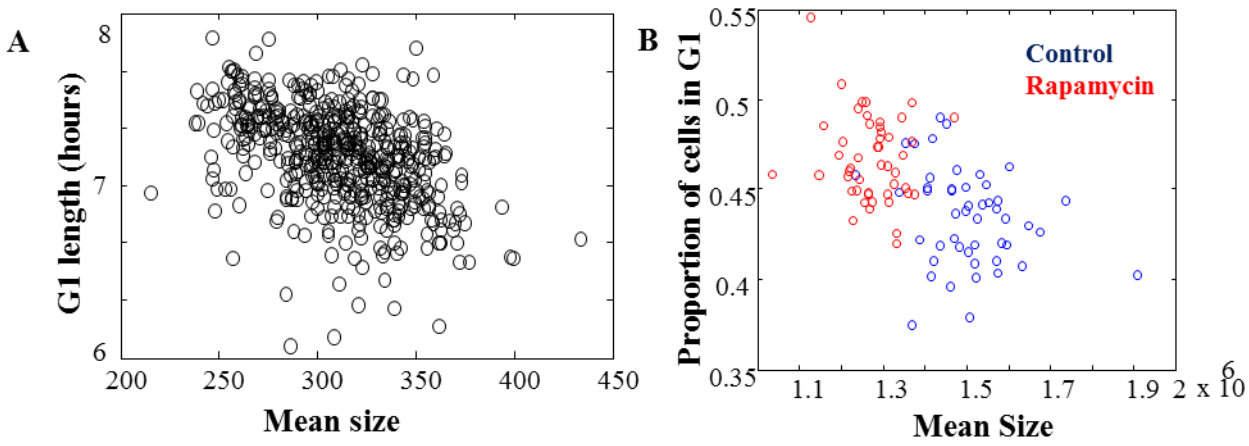

Figure 2.6: Populations with larger cells have short G1 lengths. (A) Proportion of cells in G1 vs. mean size, for unperturbed populations of HeLa cells. Each circle represents one well containing several thousand cells. (B) Proportion of cells in G1 vs. mean size, for control (blue) and rapamycin-treated (red) populations grown side by side in a multiwall plate.

A cell size threshold gating G1-exit may not be sufficient to account for the specification of cell size.

The results described above suggest that animal cell size is specified by a mechanism that reduces size variability by keeping small cells in G1 for longer periods of growth. A few observations, however, suggest that this is not the sole strategy by which uniformity is maintained. Firstly, terminally differentiated animal cells do not divide and yet, often undergo

precise adjustments of cell size[22] suggesting the presence of size specification mechanisms that are not dependent on regular cell division. Our experiments on proliferating cells also speak against the universality of a G1-exit threshold as a size control mechanism. Although size differences between G1 and S-phase HeLa cells of the same age are pronounced, these size differences are less dramatic for the Rpe1 cell line (figure 2.7A). Unperturbed populations of Rpe1 cells also do not show the negative correlation between mean cell size and proportion of cells in G1 that is seen in HeLa cells (figure 2.7B).

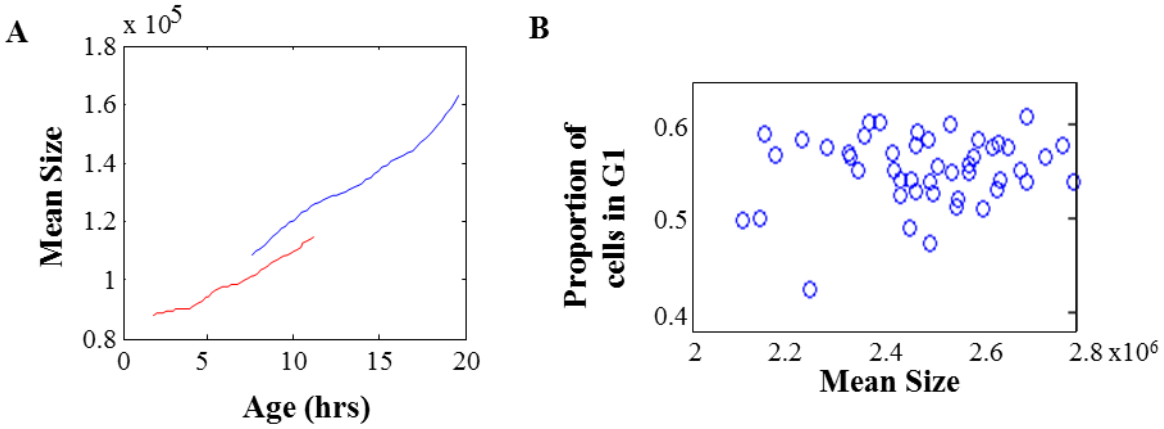

Figure 2.7: Reduced dependence of G1-exit on size in Rpe1 cells. (A) Mean cell size vs. age plotted for G1 (red) and post-G1 (blue) cells. (Student's t-test for size difference between G1 and post-G1cells in the overlap region in three independent replicate experiments: $p<0.033$, $p<1.14e-06$, $p<0.1078$.) (B) Proportion of cell in G1 vs. mean cell size plotted for unperturbed populations of Rpe1 cells.

Comparing the joint distributions of size and cell cycle position in proliferating Rpe1 and HeLa populations suggested a possible reason for this discrepancy. Cells were fixed and stained with SE-A647 and DAPI, and each cell was assigned a position on a continuous cell cycle axis based on its combination of mAG-hGem expression and DNA content, as reported previously[17] and illustrated in figure 2.8. The heat map in figure 2.9 shows the joint distribution of size and cell cycle position for Rpe1 (figure 2.9A) and Hela (figure 2.9B) populations, with color corresponding to the number of cells. To remove the bias introduced by sampling more cells at

some cell cycle positions than others, each column in the heat map is normalized, so that the plot illustrates how the shape of the size distribution changes over the course of the cell cycle. The HeLa population shows a disproportionate accumulation of small cells in late G1, consistent with the theory that small cells are prevented from exiting G1 until they reach a particular size threshold. However, the most noticeable feature of the Rpe1 distribution is a disproportionate accumulation of very *large* cells earlier in G1, which cannot be explained by a simple threshold model. The image in figure 2.9C features one of these aberrantly large cells, which are characteristic of Rpe1 cultures.

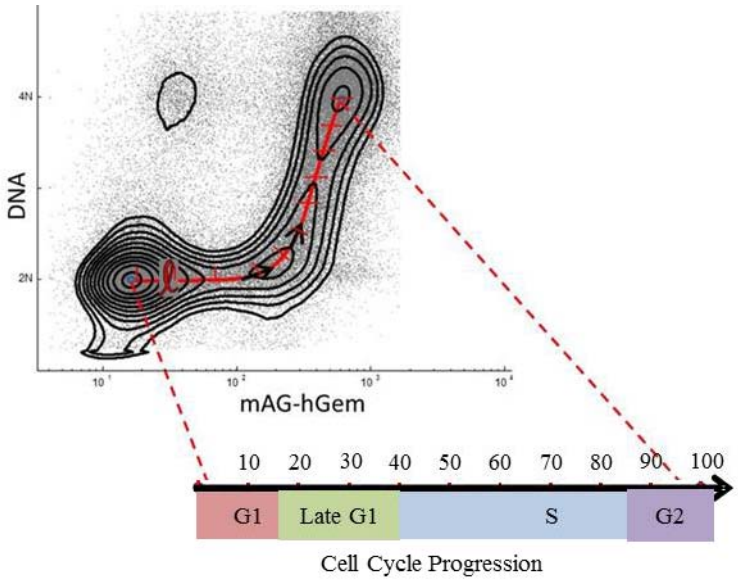

Figure 2.8: Continuous parametrization of a cell cycle axis. Cells are assigned a position on a continuous axis of cell cycle progression, based on their mAG-hGem and DNA levels. mAG-hGem level rises in late G1 (after APC inactivation. S-phase progression is monitored by DNA content.

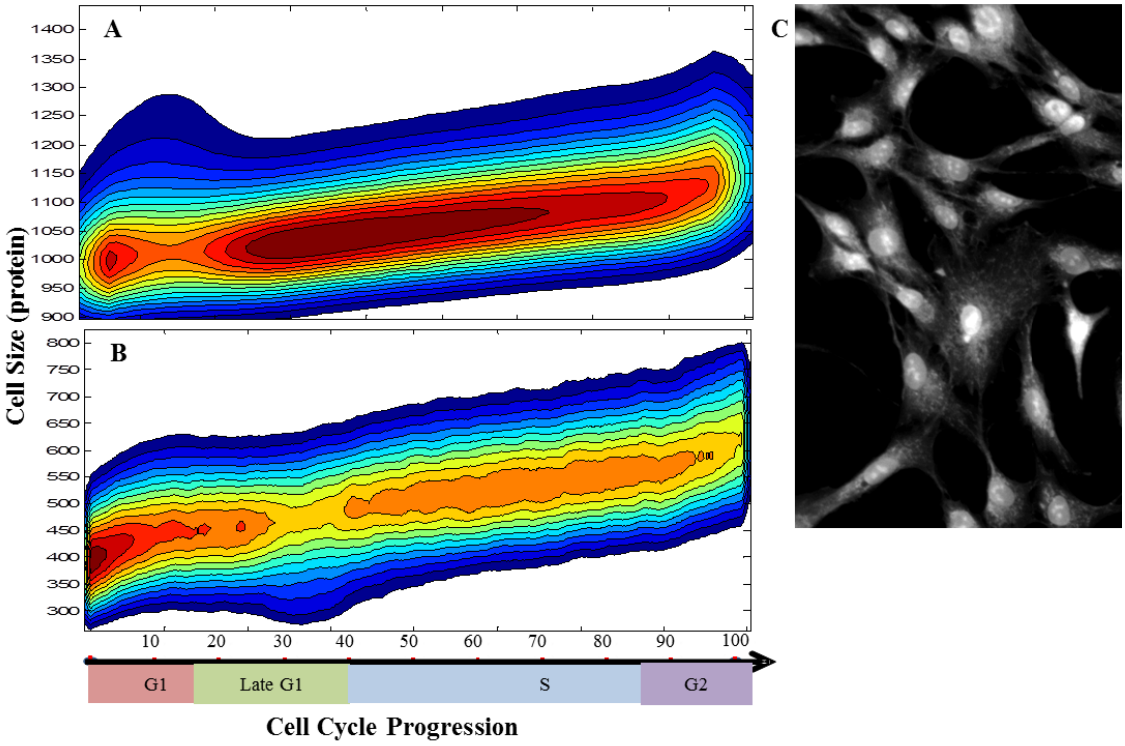

Figure 2.9: Size heterogeneity in G1 Rpe1 cells. (A,B) Joint distributions of size and cell cycle position for populations of (A) Rpe1 and (B) HeLa cells. (C) Rpe1 cells stained with SE-A647.

The presence of very large cells early in the cell cycle led us to consider a fundamental limitation of the size threshold model. A robust mechanism specifying cell size must function to reduce incidence of cells either smaller or larger than their target size. While the average cell doubles in size during the cell cycle, a size threshold can maintain uniformity by ensuring that small cells have enough time to grow more than twofold before dividing, thereby reducing the size deficit of their next generation. Similarly, large cells can be allowed to divide before doubling in size, but this correction is limited by the time required for other cell cycle events. If some cells grow fast enough to double in the minimal cell cycle time, the threshold alone cannot constrain size variability in the population.

To illustrate this limitation, we constructed a simple model wherein cells grow exponentially, a condition that is susceptible to "runaway" growth of large cells. We simulated a population of newborn cells, which are assigned initial sizes (s) and growth constants (k) from

normal distributions with means chosen such that the average cell doubles during its cell cycle. During each time increment, cells grow at a rate dependent on their size (s), so $ds/dt = ks$. During each time increment cells may exit G1, with the probability that a cell will exit G1 increasing with age (a). Similarly, during each time increment cells that have already exited G1 may divide symmetrically, with the probability of division increasing with age. To simulate a size threshold, we made the probability of a cell exiting G1 dependent on its size, so that a cell exits G1 if it meets either of the following conditions:

$$s > s_t \;\&\; p < p_s \;\&\; a > g_{min}$$

or

$$a > g \;\&\; p < (1 - p_s)$$

The variable s_t represents the threshold size required for G1-exit, chosen for each cell from a normal distribution whose mean is consistent with doubling in size over the cell cycle, and whose variance determines the precision of the size threshold. The variable g is chosen for each cell from a normal distribution of G1 lengths. The constant g_{min} represents the shortest possible G1 length. The variable p is chosen for each cell at each time from a uniform distribution ranging from 0 to 1. The dependence of G1-exit on size is set by p_s, which ranges from 0 (G1-exit is independent of size) to 1 (G1-exit is completely dependent on size).

We chose values for the variance of initial (birth) sizes, the mean and variance of g, and the constant g_{min}, based on our experimental observations (table 2.1). Under these conditions, the variance in size in the population is unbounded and continues to grow over time (figure 2.10A). Even the strongest G-exit size threshold ($p_s = 1$) could not cause the variance to converge, even if g_{min} was reduced, as long as any minimum G1 length was enforced. This occurs because large

cells can grow "out of range" of the size control mechanism (and could be avoided in a system with shorter S and G2 phases relative to G1, or very little noise in the growth constants).

Simulation Parameters

CV of birth sizes (initial values of s)	0.1
CV of threshold size (s_t)	0.2
Mean G1 length (g)	15*
CV of G1 length (g)	0.3
g_{min}	5
CV of growth constants (k)	0.3

*60% of the average cell cycle in our simulation (S/G2 length = 10)

Table 2.1: Values of fixed parameters used in exponential growth simulation.

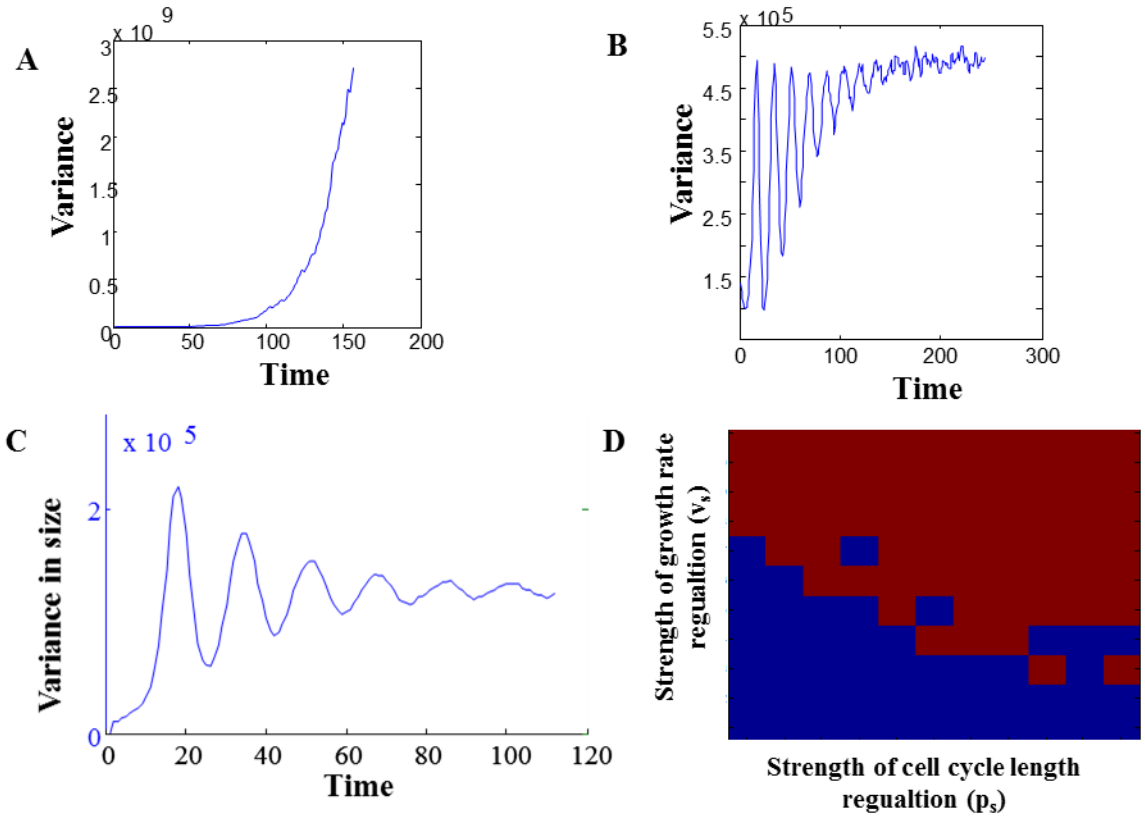

Figure 2.10: Behavior of size variance in population of cells under exponential growth model. (A) No size-control mechanism. (Legend continues on next page.)

Figure 2.10 (continued): (B) Negative correlation between size and growth rate in G1 cells under age 10. (C) Growth rate control period and size threshold for G1-exit. (D) Varying strength of growth rate correction and G1-exit size threshold. Red = variance converges. Blue = variance diverges.

Adjustment of cellular growth rates in a cell-mass-dependent manner reduces variability in cell size.

All of the considerations above raise the question of whether cells have a size-correction mechanism that isn't dependent on adjusting their cell cycle length. This would require that cells adjust their actual rate of growth, instead of just the duration of time in which they grow. To test this hypothesis, we searched for ways to examine the relationship between growth rate and cell size.

If a cell senses its own size and adjusts its rate of growth accordingly, just as a thermostat coordinates heat production with room temperature, we can expect that these corrections may be subtle and transient. We circumvented this experimental challenge by deriving an indirect inference method to assay whether growth rates of individual cells are dependent on cell size. Using the combination of live microscopy and SE-A647 staining, we sorted cells based on their ages and monitored how variance in cell size changes as cells grow and progress through the cell cycle. In the absence of any size-dependent growth rate regulation, we expect the variance in cell size to increase as cells grow, since individual cells in a population will have some variance in their growth rates. In any given time interval, fast-growing cells will accumulate more mass than slow-growing cells, thereby increasing disparities in cell size (figure 2.11A). Variance in size will only decrease if small cells grow faster than large cells (figure 2.11B).

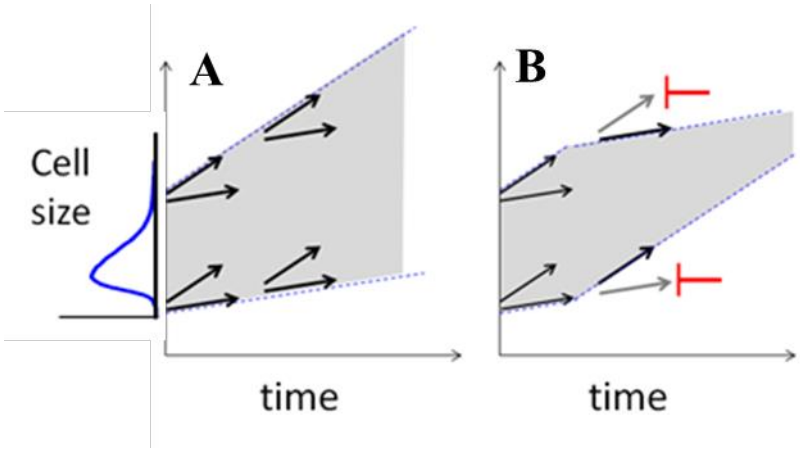

Figure 2.11: Only a per-cell coupling of cell growth and cell size can result in controlled cell size variability. Variation in growth rates drives a time-dependent increase in cell size variance(A, B). Regulation that limits cell size variance must function by a cross-talk between growth and cell size in individual cells.

Figure 2.12 shows the variance in size as a function of age for Rpe1 (fig. 2.12C) and HeLa (fig. 2.12D). The mean size as a function of age is plotted above (fig. 2.12D,E) for reference. It is immediately obvious that there are periods during which cells grow (mean size increases), but the variance in size is constant, or even decreases, which indicates that cells are growing in a size-dependent manner to increase uniformity in a population. The Rpe1 cells show a dramatic dip in variance. Comparing the full distributions of cells before, during, and after the dip shows that the distribution narrows from both ends- suggesting that small cells are growing, while large cells are actually shrinking (fig. 2.12.1).

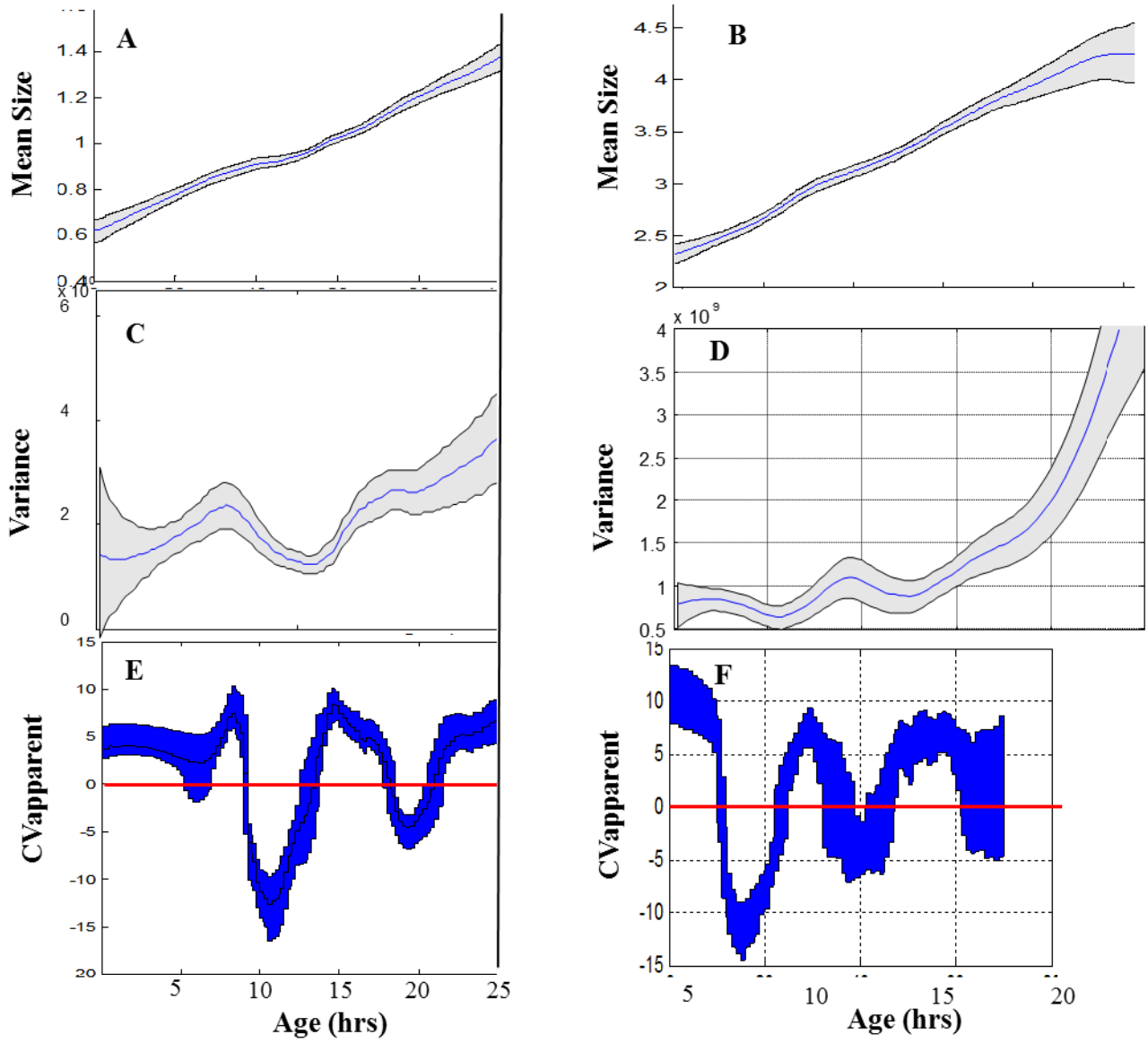

Figure 2.12: Mean size, variance, and $CV_{apparent}$ plotted as a function of age for HeLa (A,C,E) and Rpe1 (B,D,F). Shaded regions mark 20% and 80% bootstrapping confidence intervals.

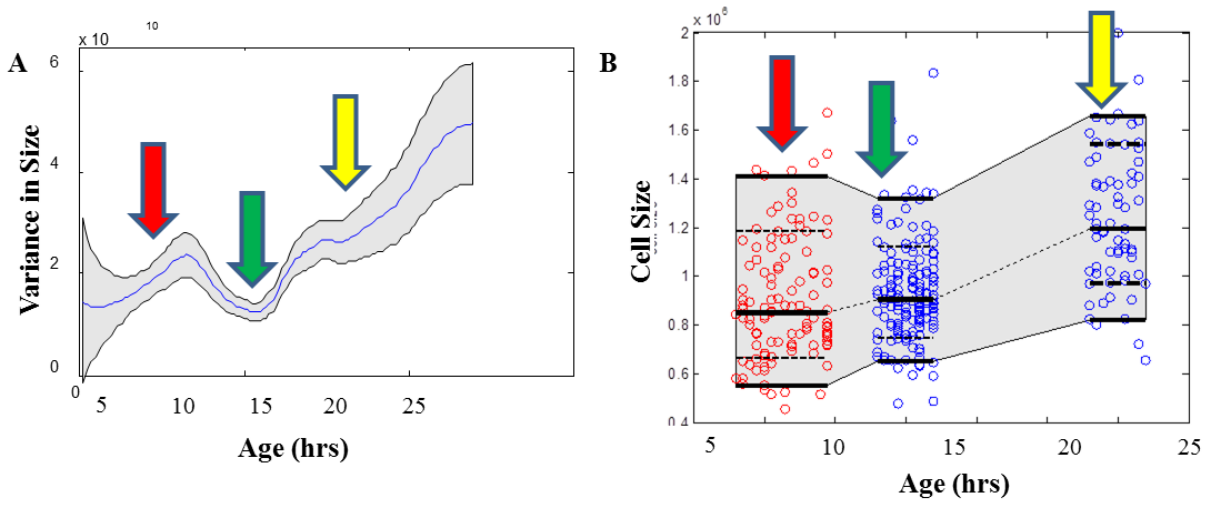

Figure 2.12.1: Decrease in size variance indicates growth rate regulation. Dip in variance in Rpe1 cell size marks narrowing of the size distribution from both ends.

To sensitively detect periods of growth rate regulation, we used the following relationships. Cell size variance, Var (S_2), at any given time t_2 is related to the cell size variance at any previous time t_1 by:

$$\text{Var}(S_2) = \text{Var}(S_1) + \text{Var}(\Delta S) + 2\text{Cov}(S_1, \Delta S) \quad (1)$$

where ΔS is the change in cell size accruing over a time period ($dt = t_2 - t_1$), i.e. the growth rate. If growth is independent of size, i.e. Cov(S_1, ΔS)=0, the increase in variance of the cell size distribution during a single increment of time is equal to the variance in growth rates:

$$\text{Var}(\Delta S) = \text{Var}(S_2) - \text{Var}(S_1) \quad (2)$$

To assess the change in size variance relative to the amount of growth that has occurred (i.e. the change in mean size,$\bar{S}$) we define the metric:

$$\text{CV}_{\text{apparent}} = \frac{\sqrt{\text{Var}(S_2) - \text{Var}(S_1)}}{\bar{S}_2 - \bar{S}_1}$$

for a time increment during which variance has increased (Var (S_2) - Var (S_1) > 0) and

$$CV_{apparent} = - \frac{\sqrt{|\mathrm{Var}\ (S_2) - \mathrm{Var}\ (S_1)|}}{\overline{S}_2 - \overline{S}_1}$$

for a time increment during which variance has decreased.

As long as the mean size is increasing over time, $CV_{apparent}$ can be interpreted as follows. If a cell's growth rate is independent of its size, $CV_{apparent}$ directly equals the coefficient of variation of cellular growth rates. This can be shown by substituting the relationship in eq. 2 into the formula for $CV_{apparent}$, noting that variance will increase if growth rates are size-independent:

$$CV_{apparent} = \frac{\sqrt{\mathrm{Var}\ (\Delta S)}}{\overline{S}_2 - \overline{S}_1}$$

Since variance is by definition positive, negative values of $CV_{apparent}$ (arising from dips in variance) imply that growth rate is actually not independent of size, and that cell size and subsequent growth rate are negatively correlated. We can also note that if $CV_{apparent}$ is much higher than is plausible for the CV of growth rates (which will equal 1 if growth is a Poisson process), it is likely that growth is positively correlated with size, as in the case of exponential growth.

Plotting $CV_{apparent}$ versus cell age (Fig. 1) consistently reveals two distinct periods during which growth rates and size are negatively correlated, in both HeLa and Rpe1 cells.
This result is striking, because it suggests a communication between cell size and cellular growth rate that is transiently established twice during the cell cycle, perhaps due to cell-cycle-dependent signaling linking size and growth rates.

Since the cells were sorted based on their age, irrespective of cell cycle stage, these results cannot be explained by size-dependent regulation of cell cycle progression and are

therefore evidence that cells sense their own size and regulate their growth accordingly. The only other possibility is that cells are removed from the distribution, by either dividing or dying in a size-dependent manner. This is very unlikely to be the case, since the dips occur earlier than cells start dividing. (This is true for at least the first dip in Rpe1 and both dips in HeLa, where the mean cell cycle length is 21 hrs, with a standard deviation of 1.6 hrs. See supplementary figure S2.3 for a sample cell cycle length distribution.) There was also a very low rate of apoptosis (<1% of cells imaged from birth died before dividing).

Growth rate and cell cycle length correction mechanisms can cooperate to maintain uniformity in a population

Even a transient period of growth rate correction has the potential to have a strong effect. This can be demonstrated with the exponential growth model we built above. We incorporated a period of size-dependent growth rate control into the model by switching the growth rate *of G1 cells younger than 10 only* from $ds/dt = ks$ to

$$ds/dt = (1- v_s)ks + v_s(b(s_{gt}-s) + c)$$

The constant s_{gt} is the "target size" that the average-sized newborn cell should reach during G1 if it is to double during the cell cycle. The cell measures its deviation from this target (s_{gt}-s) and uses this information to adjust its growth. The scaling factors b ($b=\sigma_{growth\ rates}/\sigma_{sizes}$) and c (adjusted to allow or prevent large cells from actually shrinking) control the magnitude of size-dependent adjustments to growth rate. The strength of this control mechanism is set by the value of v_s which ranges from 0 (no growth rate correction) to 1 (growth rate is anticorrelated with size). This is analogous to p_s above, which defines the strength of the G1-exit-threshold control mechanism.

Applying a transient period of strong growth rate correction ($v_s = 0.8$) to the exponential growth model, in the absence of any size-dependent control of cell cycle length ($p_s = 0$) causes the population's variance in size to converge over time, stabilizing the size distribution (fig. 2.10B) in a case where even the strictest size threshold for cell cycle progression failed. (The early oscillations in variance occur because cells are synchronized at the start of the simulation, so the size distribution switches between unimodal, when all cells are in middle of the cycle, and bimodal, when some cells are at the end while others have just divided, until synchronization is lost- just like the experimental result shown in fig. 2.1B.) Combining both control mechanisms (high values of v_s and p_s) yields a stable population with a lower variance than growth rate control alone can maintain (fig. 2.10C). Size-dependent control of cell cycle length can also stabilize at a lower value of v_s (weaker growth rate control) than is possible in its absence (fig. 2.10D).

Direct observation of size-dependent growth rate correction

Ideally, we would like to verify the presence of a growth-rate-correction mechanism by monitoring growth in live cells. Since we cannot use the protein staining technique in live cells, we measured the growth of the nucleus as a proxy for cell growth, using time-lapse microscopy. In yeast, the nucleus has been observed to grow along with the cell[23]. We quantified the 2-d projected area of the nucleus (i.e. the area of the image covered by the nucleus), which we found correlates to cellular protein content (fig. 2.13A). This correlation is strong enough that plotting the mean nuclear size vs. cell cycle progression reproduces the features of the mean protein vs. cell cycle curve, more accurately than plotting the total projected area of the cell (fig. 2.13B).

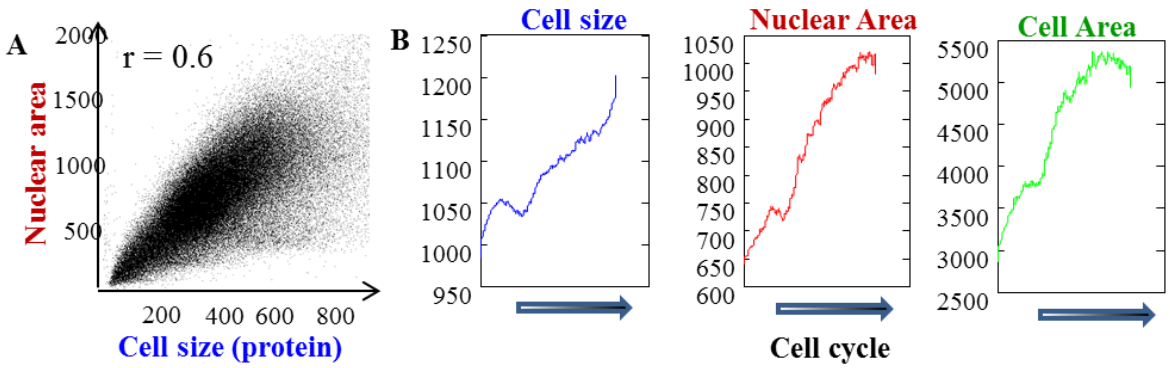

Figure 2.13: Projected nuclear area as a proxy measurement for cell size. (A) Nuclear size vs. protein content (SE-A647 stain) of HeLa cells. Pearson's r=0.6. (B) Comparison of cell cycle trends in mean cell size (SE-A647), projected area of the nucleus and projected area of the cell. Dip in mean size in late G1 reflects an accumulation of small cells (as shown in figure 2.9B).

To further verify that nuclear growth accompanies cellular growth, independent of cell cycle progression, we arrested the cell cycle with aphidicolin and still observed a dramatic increase in nuclear size as cells grow, using the DNA-ligase-dsRed reporter to confirm that cells did not enter S-phase (fig. 2.14). Because cell cycle progression is still likely to further influence nuclear size, in the experiments described below we generally make comparisons between cells at the same cell cycle stage, by synchronizing individual cell trajectories based on the time of cell birth.

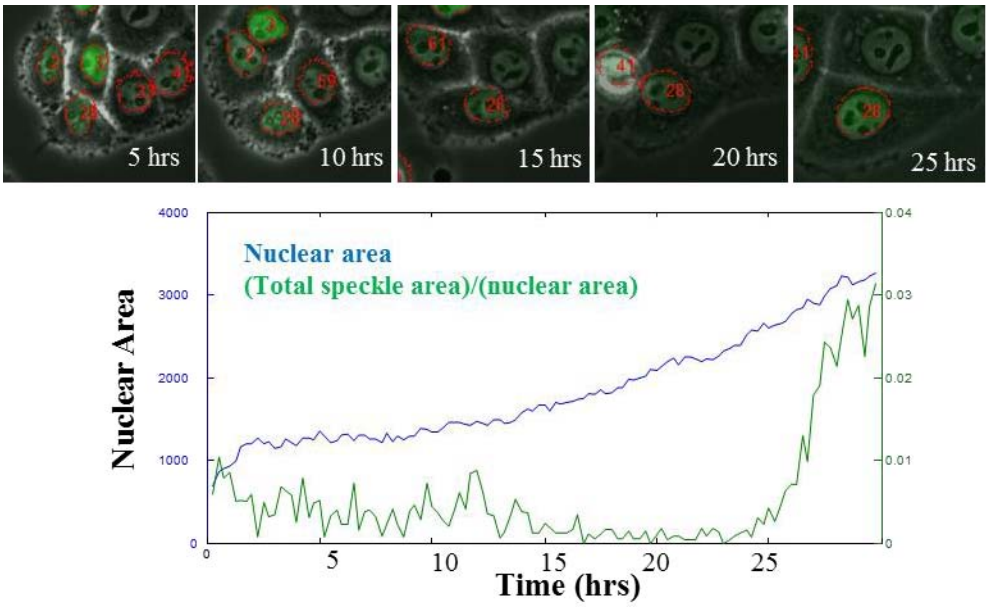

Figure 2.14: Nucleus grows with cell during aphidicolin arrest. Images show cells growing for 25 hrs after aphidicolin treatment. Nuclear size for cell labeled 28 is plotted below (blue). Green trace quantifies the density of DNA-ligase focci, showing that cell does not enter S-phase for 25 hrs.

As illustrated in figure 2.15, we tracked individual HeLa cells over time and monitored their cell cycle progression (with the FUCCI reporters[20]) and nuclear growth. Note that, in these cells, the nucleus tends to elongate as it grows, rather than expanding as a sphere. (This is significant because spherical expansion could yield a spurious correlation between size and growth of the 2-d projected area. We chose to monitor projected area so as not to make assumptions about nuclear shape in calculating volume, while bearing in mind the potential artifacts. We also trim the first 1.25 hrs of each trajectory, to avoid the effects of possible changes in nuclear shape as the cell flattens after mitosis. The fact that the correlations we report below show cell-cycle dependence and are sensitive to drug treatments support the conclusion that they are true physiological trends.)

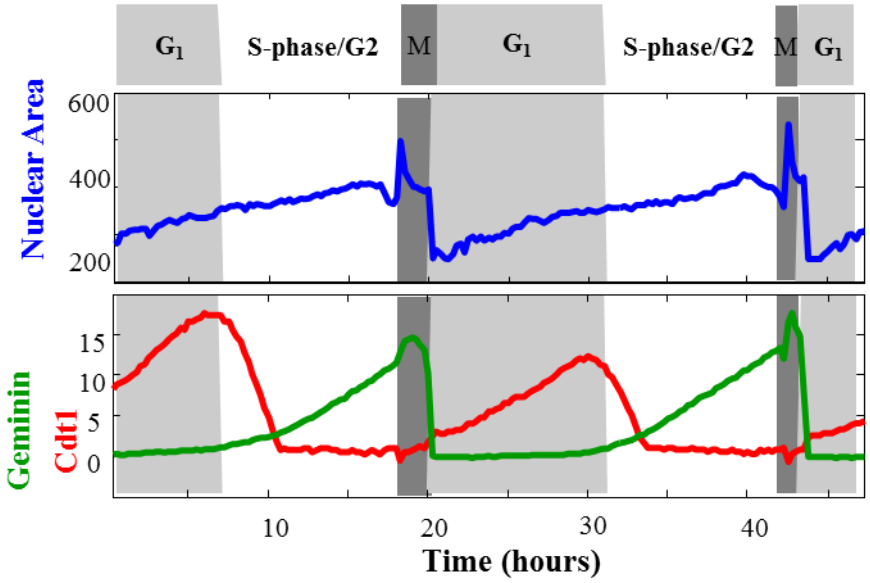

Figure 2.15: Monitoring growth of the nucleus in live cells. Cells are tracked yielding trajectories if nuclear area and cell cycle reporters, which are used to cut and synchronize traces to time of cell birth.

This technique reveals a negative correlation between a cell's nuclear size and its subsequent growth (fig. 2.16A). The strongest negative correlation was generally observed by comparing cells' nuclear size at a given time since birth to their growth rates four hours later. In figure 2.16B, the correlation coefficient (Pearson's r) between size at time "t" and growth rate at time "t + 4 hrs" is plotted as a function of cell age (i.e. time since birth). While the correlation is slightly negative throughout, we see it dip steeply at two points, recalling the two periods of size-dependent growth rate adjustment indicated by the $CV_{apparent}$ trends discussed above (fig. 2.12).

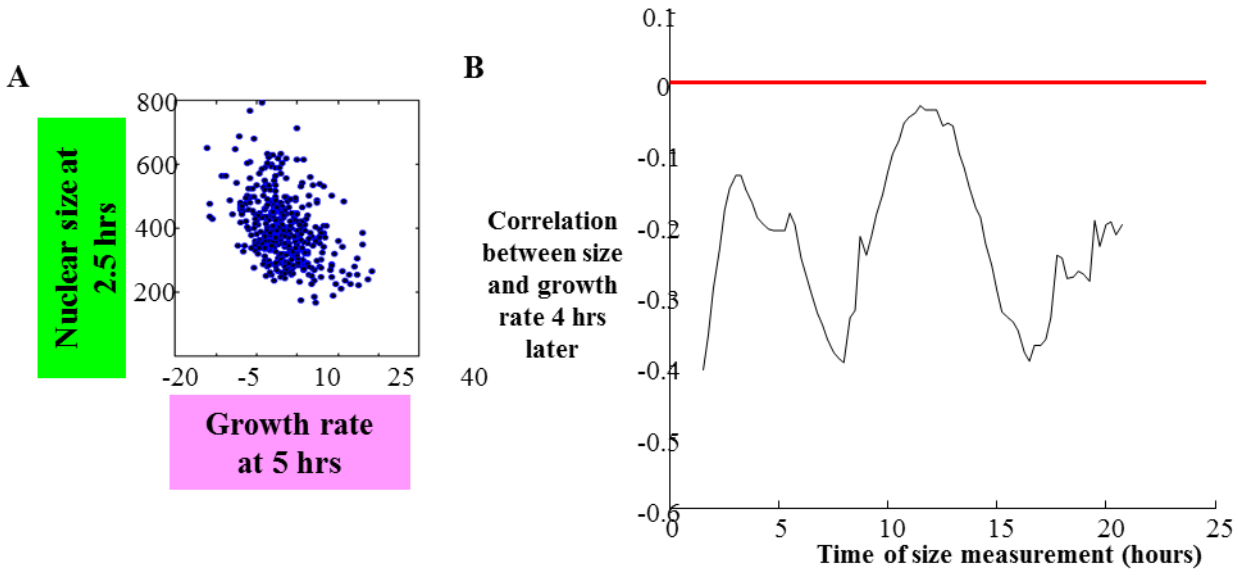

Figure 2.16: Negative correlation between nuclear size and subsequent growth rate. (A) Nuclear size of individual cells 2.5 hrs after birth plotted vs. growth rate of those same cells 5 hrs after birth. (B) Correlation coefficient (Pearson's r) between size and subsequent growth rate (4 hrs later), calculated as a function of age (time since birth).

Multiple experiments repeatedly show these two periods of negative correlation between nuclear size and subsequent growth, though the relative strength of the two dips in the correlation trajectory varies slightly (fig. 2.17A). The timing of the dips does not appear to be strictly tied to the G1/S transition, since it was not delayed in a population with extended G1 lengths (fig. 2.17B).

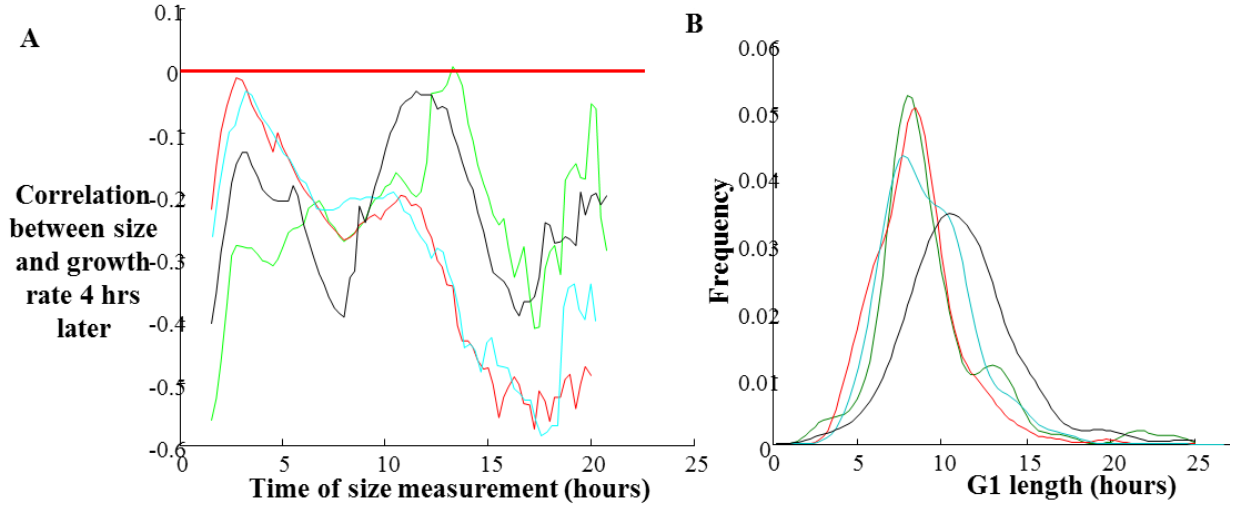

Figure 2.17: (A) Correlation coefficient (Pearson's r) between size and subsequent growth rate (4 hrs later), calculated as a function of age (time since birth), for four independent experiments. (B) Distribution of G1 lengths for those same experiments

Figure 2.18A presents the full matrix of correlations between nuclear size and growth rate at any two times, showing the generally negative correlation between size and subsequent growth rate (lower right triangle) and the expected positive correlation between growth rate and subsequent size (upper left triangle). The diagonal line marks the "size at t vs. growth rate at t+4" trajectory plotted in fig. 2.16B. Figure 2.18B shows that the same behavior is observed in Rpe1 cells.

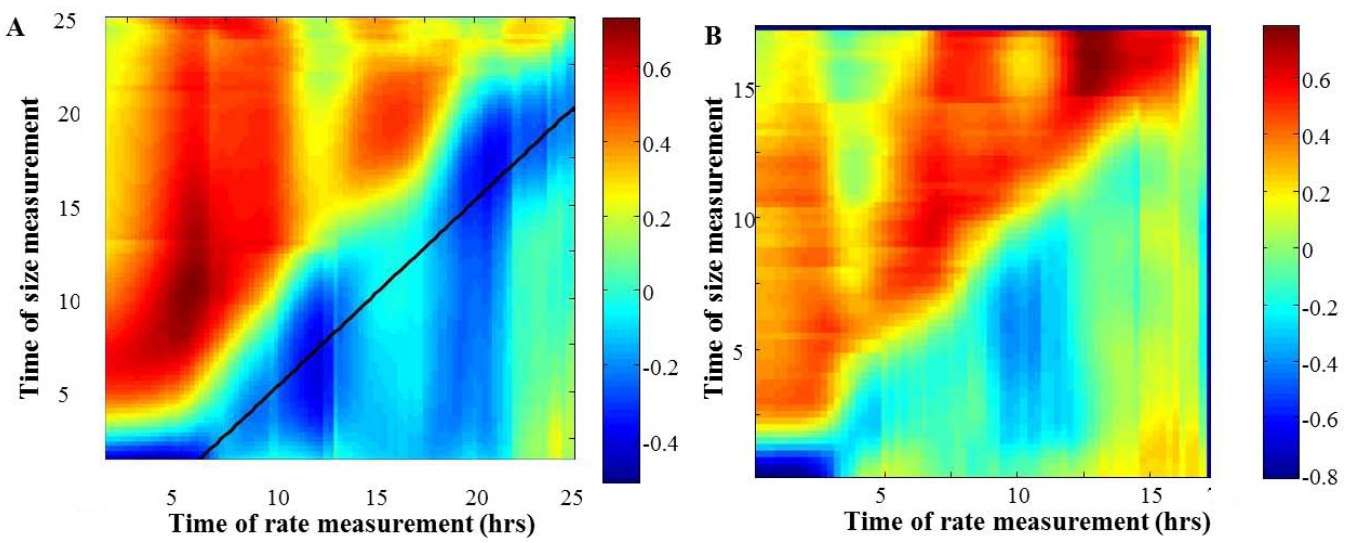

Figure 2.18: Correlation between size of cells (taken at time on y-axis) and their growth rates (taken at time on x-axis). Color corresponds to correlation coefficient. Shown for (A) HeLa and (B) Rpe1 cells

The most striking demonstration of growth rate adjustment can be seen by comparing the behavior of the largest cells and smallest cells during periods of growth rate regulation. In figure 2.19, cells are sorted based on their size at a particular time point and the full nuclear size trajectories for the ten largest cells and ten smallest cells are plotted. For each of the four time points at which cells were sorted (fig. 2.19A-D), the largest cells slow or stop their growth following this time point, while the smallest cells increase their growth rate. This behavior increases size uniformity in the population, as is demonstrated by the convergence of the size trajectories following the growth rate adjustment. The qualitative differences between growth curves of differently-sized cells also highlights the fact that cell growth does not follow a simple linear or exponential rule and that cells are highly heterogeneous in their behavior, in part due to cell-autonomous size regulation.

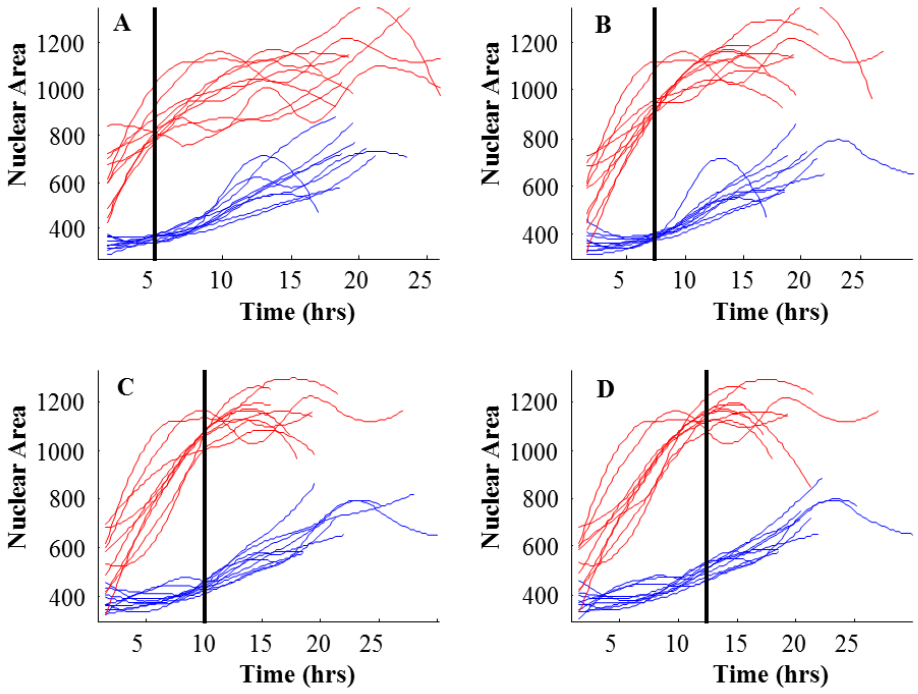

Figure 2.19: Comparison of growth trajectories of smallest and largest cells. Hela cells were sorted based on their size at 5 (A), 7.5 (B), 10 (C), and 12.5 (D) hours after birth. Nuclear size trajectories for the ten largest (red) and smallest (blue) cells are shown.

Compensatory growth over the cell cycle actively reduces size disparities

In measuring the buoyant mass of growing lymphocytes, Son et al.[24] found a negative correlation between cellular growth rate and G1 length, but no correlation between buoyant mass and G1 length. An alternate model of size homeostasis for proliferating cells, is that cell cycle length is dependent on a growth rate, not size, measurement so that cells add a constant amount of mass each cell cycle. The addition of a fixed amount of mass each cycle (linear growth), combined with regular divisions will stabilize the size distribution. This mechanism only works when all cells are cycling.

In our measurements of nuclear growth, we see a positive correlation between nuclear growth rate and subsequent size, strongest if size is measured ~3 hrs after growth rate. This is reflected in the red-colored upper-left triangle of figure 2.18A. For this reason, we can't rule out the idea that cells measure their growth rate. However, since growth rate is predictive of

subsequent size, with a relatively short delay, this would mean that growth rate can act as a proxy measurement for size. The effect of this is not to enforce a fixed, size-independent amount of growth each cell cycle. Rather, overall growth is compensatory, actively correcting deviations of large or small cells from the mean.

To demonstrate this we plot cells' total nuclear growth over the cell cycle as a function of their birth size in figure 2.20. The negative correlation between them supports a size-corrective mechanism rather than a fixed-growth model. This can be quantified by calculating the quantity

$$M = \frac{\mathrm{Var}(S_{t2})}{\mathrm{Var}(S_{t1}) + \mathrm{Var}(\Delta S)}$$

as a metric of compensatory growth. If growth is independent of size, $M = 1$, as per eq. (1) above, whereas values of M less than 1 suggest a variance-reducing mechanism. We find that M is consistently less than 1 in multiple independent experiments (ranging from0.5 to 0.8), in a statistically significant manner ($p<0.001$ by resampling test).

One caveat to the nuclear size measurement is that spurious correlations can result if segmentation of the nucleus becomes more accurate with cell age (perhaps due to increase in fluorescence intensity). We have observed the results reported above using two different nuclear-localized cell-cycle probes, making this concern unlikely. To confirm we are monitoring nuclear growth in a cell line with a very bright nuclear probe, and preliminary results replicate the compensatory growth, and the negative correlation between size and subsequent growth reported above.

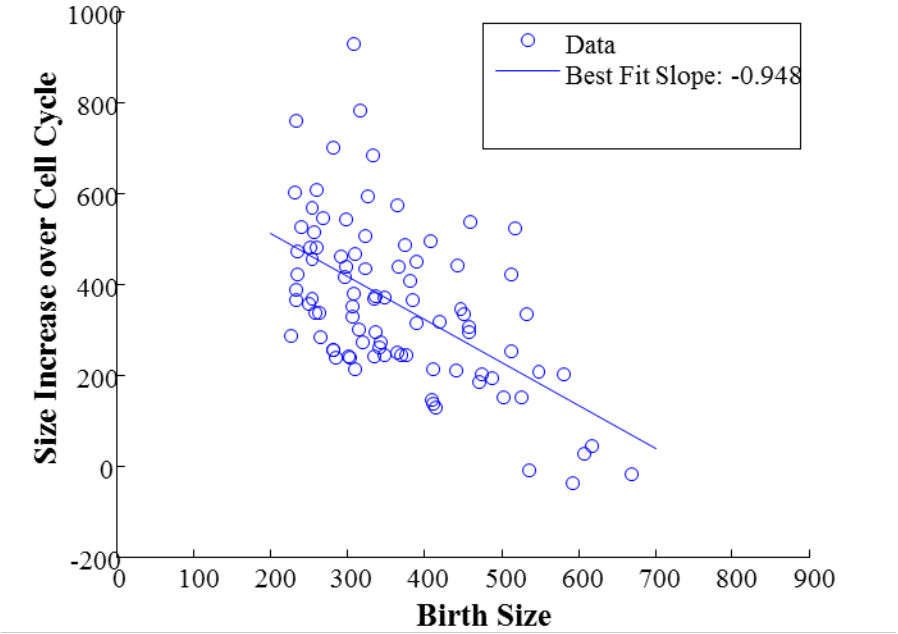

Figure 2.20: Compensatory growth over the cell cycle. Total increase in nuclear size during the cell cycle plotted vs. birth size for HeLa cells

Discussion

The results above suggest that cells regulate their size by adjusting both cell cycle length and growth rate, providing the first evidence of size-corrective cell-autonomous growth rate regulation. This indicates that animal cells have a mechanism with which to measure their own size, which feeds into both cell cycle and growth control pathways. The search for such a mechanism will be aided by the techniques developed above, which can be combined with molecular perturbations or immunofluorescent detection of signaling molecules.

With the calculation of $CV_{apparent}$, based on the combination of time-lapse microscopy and fixed-cell measurements, allows us to circumvent the experimental difficulty of monitoring protein accumulation in live cells, and may prove useful as a tool to study regulation of other difficult-to-measure properties, like protein phosphorylation. By invoking a simple statistical

principle, we are able to assay growth rate regulation (on the level of protein) without having to directly measure growth rates.

Current efforts are focused on: (1) further confirmation of these results (2) identifying what correlate of cell size is actually measured (3) elucidating the mechanism by which cell size is reported to cell cycle and growth regulators. Together these approaches can bring us towards a comprehensive understanding of cell size control.

1. *Cancer medicine 7*. (Elsevier, 2006).

2. Nguyen, C. V. *et al.* Pleomorphic ductal carcinoma of the breast: predictors of decreased overall survival. *Am. J. Surg. Pathol.* **34,** 486–493 (2010).

3. Nurse, P., Thuriaux, P. & Nasmyth, K. Genetic control of the cell division cycle in the fission yeast Schizosaccharomyces pombe. *Mol. Gen. Genet. MGG* **146,** 167–178 (1976).

4. Fantes, P. & Nurse, P. Control of cell size at division in fission yeast by a growth-modulated size control over nuclear division. *Exp. Cell Res.* **107,** 377–386 (1977).

5. Johnston, G. C., Pringle, J. R. & Hartwell, L. H. Coordination of growth with cell division in the yeast Saccharomyces cerevisiae. *Exp. Cell Res.* **105,** 79–98 (1977).

6. Rupes, I. Checking cell size in yeast. *Trends Genet. TIG* **18,** 479–485 (2002).

7. Martin, S. G. & Berthelot-Grosjean, M. Polar gradients of the DYRK-family kinase Pom1 couple cell length with the cell cycle. *Nature* **459,** 852–856 (2009).

8. Moseley, J. B., Mayeux, A., Paoletti, A. & Nurse, P. A spatial gradient coordinates cell size and mitotic entry in fission yeast. *Nature* **459,** 857–860 (2009).

9. Conlon, I. & Raff, M. Differences in the way a mammalian cell and yeast cells coordinate cell growth and cell-cycle progression. *J. Biol.* **2,** 7 (2003).

10. Weitzman, J. B. Growing without a size checkpoint. *J. Biol.* **2,** 3 (2003).

11. Conlon, I. J., Dunn, G. A., Mudge, A. W. & Raff, M. C. Extracellular control of cell size. *Nat. Cell Biol.* **3,** 918–921 (2001).

12. Lloyd, A. C. The regulation of cell size. *Cell* **154,** 1194–1205 (2013).

13. Roberts, S. A. & Lloyd, A. C. Aspects of cell growth control illustrated by the Schwann cell. *Curr. Opin. Cell Biol.* **24,** 852–857 (2012).

14. Zetterberg, A. & Larsson, O. Coordination between cell growth and cell cycle transit in animal cells. *Cold Spring Harb. Symp. Quant. Biol.* **56,** 137–147 (1991).

15. Jorgensen, P. & Tyers, M. How cells coordinate growth and division. *Curr. Biol. CB* **14,** R1014–1027 (2004).

16. Dolznig, H., Grebien, F., Sauer, T., Beug, H. & Müllner, E. W. Evidence for a size-sensing mechanism in animal cells. *Nat. Cell Biol.* **6,** 899–905 (2004).

17. Kafri, R. *et al.* Dynamics extracted from fixed cells reveal feedback linking cell growth to cell cycle. *Nature* **494,** 480–483 (2013).

18. Mitchison, J. M. Growth during the cell cycle. *Int. Rev. Cytol.* **226,** 165–258 (2003).

19. Curl, C. L. *et al.* Quantitative phase microscopy: a new tool for investigating the structure and function of unstained live cells. *Clin. Exp. Pharmacol. Physiol.* **31,** 896–901 (2004).

20. Sakaue-Sawano, A. *et al.* Visualizing spatiotemporal dynamics of multicellular cell-cycle progression. *Cell* **132,** 487–498 (2008).

21. Cardoso, M. C. *et al.* Mapping and use of a sequence that targets DNA ligase I to sites of DNA replication in vivo. *J. Cell Biol.* **139,** 579–587 (1997).

22. Nie, J. *et al.* SAD-A kinase controls islet β-cell size and function as a mediator of mTORC1 signaling. *Proc. Natl. Acad. Sci. U. S. A.* **110,** 13857–13862 (2013).

23. Jorgensen, P., Nishikawa, J. L., Breitkreutz, B.-J. & Tyers, M. Systematic identification of pathways that couple cell growth and division in yeast. *Science* **297,** 395–400 (2002).

24. Son, S. *et al.* Direct observation of mammalian cell growth and size regulation. *Nat. Methods* **9,** 910–912 (2012).

Chapter 3

Identifying signaling pathways responsible for size specification

Introduction

Several pathways have been found to influence cell size, by promoting or suppressing growth. In particularly, the mTOR pathway plays a central role in adjusting cell growth in response to the extracellular environment[1–3]. The atypical serine/threonine protein kinase mTOR interacts with several proteins to form two distinct complexes, mTOR complex 1 (mTORC1) and 2 (mTORC2)[3,4]. Research on cell growth has primarily focused on mTORC1, which has been shown to integrate signals from growth factors, nutrient availability and energy status to regulate global rates of protein synthesis and autophagy[5], thereby influencing cell size[3,6]. Active mTORC1 promotes translation of 5' TOP-motif containing mRNAs, largely by inhibiting the 4E-BP family of translation inhibitors, thus increasing rates of cap-dependent translation[7]. mTORC1 also promotes growth by activating the S6 Kinase 1 (S6K1) family of translational activators and the eIF4G translation initiation factors [4,8].

The influence of growth factors, such as insulin and insulin-like growth factor 1 (IGF1), on mTORC1 activity are largely mediated by the PI3K/Akt pathway[2,9]. Receptor activation initiates recruitment and activation of PI3K, resulting in the generation of lipid products that recruit Akt and other kinases to the plasma membrane, leading to their activation and downstream signaling, which promotes mTORC1 activation. Counteracting PI3K signaling is the phosphatase, PTEN. Notably, PTEN is responsible for the cell growth arrest that occurs in

response to DNA-damage-induced cell cycle arrest, suggesting that this pathway may mediate crosstalk between cell cycle progression and growth[10].

The effects of mTORC1 activation on cell size have been well documented. Constitutive activation of Akt results in a dramatic mTORC1-dependent increase in cell size[11]. Similarly, knockdown of tuberous sclerosis 1 (TSC1) and TSC2, key upstream regulators of mTORC1, also results in an mTORC1-dependent increase in cell size[12]. In contrast, knockdown of S6K1, a downstream effector of mTORC1, results in small cells and smaller body size in both mice and flies[13–15]. As discussed in chapter one, S6K1 and its substrate ribosomal protein S6 (rpS6) have also been shown to play a role in regulating pancreatic beta cell size[16].

Yet other pathways that influence cell size include Wnt, TGFβ, Hippo, and MAPK. Of particular interest, a recent report has demonstrated that the Wnt pathway influences cell size by protecting proteins from SCF mediated degradation rather than by increasing translation[17]. Additionally, there is crosstalk between these pathways. For example, mTOR has been shown to respond to Hippo, WNT and Notch signaling[18].

Growth in cell size reflects a balance in the rates of global protein translation, degradation and secretion (of extracellular proteins, for example). Previous reports have shown that translation and degradation rates are coordinated and co-regulated by mTOR[19]. Also, in a recent report, the Wnt pathway was shown to influence cell size by stabilizing proteins from SCF mediated degradation rather than by increasing translation[17].

While the pathways discussed here can all stimulate or suppress cell growth, we still don't know what induces a cell to grow to a *specific* size. The results in chapter two indicate that cells autonomously regulate their size, by both coordinating growth with cell cycle progression and tuning their growth rates to correct deviations from the population mean. This raises the

question of how a cell measures its size, in order to respond with the appropriate correction. What signal communicates information about a cell's mass to its cell cycle and protein production machinery?

To search for the signals responsible for the specification of cell size, we took two parallel approaches:

1. We used drugs to perturb the activity of various candidate proteins, to test for their involvement in size regulation. We looked for perturbations that increase size heterogeneity in a population by decoupling size from cell cycle progression and/or growth rate regulation. This approach will be discussed in chapter four.
2. We used antibodies to monitor the expression and activation of candidate proteins and signaling events as a function of cell size and cell cycle, in unperturbed populations. We searched for proteins that display cell-size-dependent expression or modification in unperturbed populations. The results of this approach are described below.

These approaches are complementary. Since the relevant signaling pathways are highly interconnected, drug perturbations can have unintended effects, making the study of unperturbed populations essential. However, while correlation of a particular signal with cell size and/or cell cycle stage may suggest its role, perturbations are necessary to firmly establish causality.

We used immunofluorescence to quantify the association of proteins of interest with cell cycle stage and cell size, using a four-color system to measure the size (protein content assayed by SE-A647 staining), cell cycle position, and level of antibody target, of each cell. Cell cycle positions were identified using the same mAG-hGem/DAPI axis mentioned earlier and illustrated in figure 2.8. We used high-throughput microscopy and automated image processing

to sample large populations of cells, in order to survey the joint distribution of size/cell-cycle/antibody-target states. The automated segmentation strategies described in chapter two were used to identify the nucleus and cell boundaries in each image and quantify the intensity of the antibody stain in each compartment. Figure 3.1 shows two examples of antibody-labelled cells, stained for cMyc (fig. 3.1A) and phospho-rpS6 (fig. 3.1B). The plots on the left show the mAG-hGem and DAPI levels for each cell. The colored dots represent the cells with the highest levels of cMyc or phospho-rpS6 and reveal the cell-cycle trend of these signals.

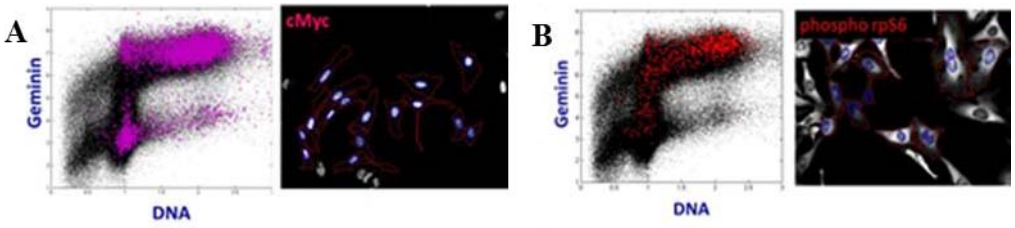

Figure 3.1: HeLa cells were stained with cell cycle markers and (A) anti-cMyc or (B) anti-phospho-rpS6. Scatter plots show mAG-hGem vs. DAPI intensity. Colored dots represent cells with antibody fluorescence above a high threshold.

We used this experimental design to:

1. Screen many antibody targets to look for size-sensor candidates, i.e. signals associated with size throughout the cell cycle or at particular stages.
2. Investigate known growth-regulatory pathways and characterize their behavior over the cell cycle, as well as search for any size-dependent signaling.

Results

Antibody-based screen to identify size-dependent signals

The results in described earlier indicated that cells can sense their own size, and respond to this information by altering their growth and cell cycle progression accordingly. We sought to identify potential size-sensor components by screening a range of antibodies for association with cell size. We tested 80 high-quality antibodies, each specific towards a different signaling molecule, covering nodes in numerous signaling cascades. We focused on signaling proteins in this experiment, avoiding structural components of the cell that may have a trivial correlation with cell size. We screened for signals that are differentially regulated in large and small HeLa cells, which could feed into the pathways controlling cell cycle progression and/or growth, thereby linking those processes to cell size. Signals that displayed cell-size-dependent activity were collected as "hits" for further analysis.

In order to identify meaningful "hits", we had to resolve the following challenges:

1. Cell size increases with progression through the cell cycle. Therefore signals which are present only in the later stages of cell cycle, such histone H3 phosphorylation, are expected to appear preferentially in larger cells even if they have no connection to cell size. Similarly, G1-specific proteins will be flagged a potential small-cell markers.
2. Trends may be obscured by non-specific binding and noise, especially if cells expressing high levels of the target protein are rare in the population.

Distinguishing size- and cell-cycle-based trends

To remove the confounding effect of cell cycle on size/signal correlations, we sorted cells based on their cell cycle stage and looked within each stage for an association of the signal with cell size. To do this, we used Shannon-Weaver conditional mutual information[20,21] as a metric to quantify each signal's association with size when cell cycle stage is held constant, I(*ab;s|cc*):

$$I(ab;s|cc) = \sum_{cc}\sum_{ab}\sum_{s} p(ab,s,cc) \log\left(\frac{p(ab,s|cc)}{p(ab|cc)\,p(s|cc)}\right)$$

where *ab* is the intensity of the antibody signal, *s* is cell size, and *cc* is cell cycle stage.

To calculate I(*ab;s|cc*), we assigned cells one of five discrete cell cycle stages, based on their mAG-hGem level and DNA content. The cells in each stage were binned based on their antibody level and size (fig. 3.2).

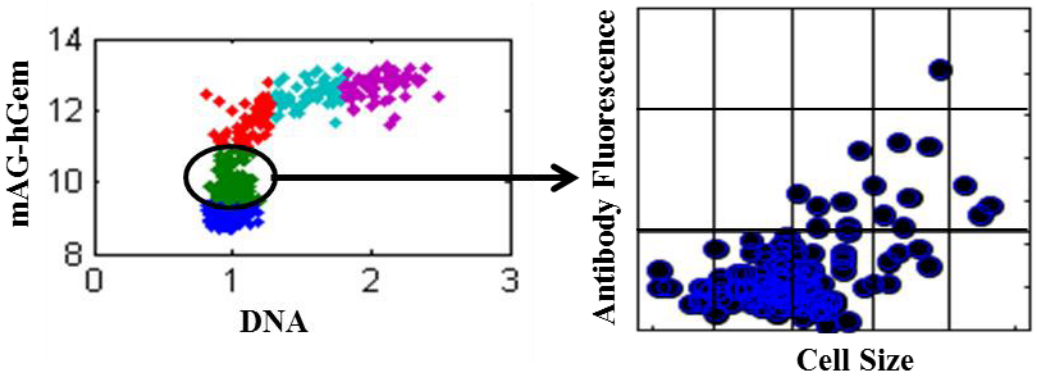

Figure 3.2: Cells are sorted into cell cycle stages based on DAPI and mAG-hGem intensity. The association of antibody signal with cell size (protein) is calculated for each stage and summed.

The statistic I(*ab;s|cc*) compares the proportion of cells in each bin, p(*ab,s|cc*) to the proportion expected if size and signal are independent, p(*ab|cc*) p(*s|cc*). A bin with more cells than expected contributes positively to I(*ab;s|cc*). The calculation is dominated by bins with many cells, reducing the effect of outliers and ensuring that I(*ab;s|cc*) is always positive. An analogous

strategy was used to calculate I(*ab;cc*|*s*), to identify cell-cycle-dependent signals in a manner unbiased by cell size.

Automatic thresholding to detect trends with high sensitivity

If a signal is active in a small subpopulation of cells, measures of its association with size (or any other parameter) will be dominated by the majority of "dark" cells. This will result in no association, or a gradual positive trend due to non-specific binding of the antibody to other proteins in the cell, obscuring the true behavior of the signal. In these cases, trends can be highlighted by quantifying the proportion of cells with high levels of an antigen as a function of size, rather than the general trend of antigen level with size. In other words, if we can identify the subpopulation of active cells, we can compare their size distribution to that of the dark cells, to see if they are over-represented at a particular size. In calculating I(*ab;s*|*cc*), this means sorting cells into only two bins (with the "off" bin containing all of the dark cells, while the "on" bin contains the cells that are truly expressing the signal) rather than evenly binning the signal distribution (fig. 3.3A). The question then becomes: what threshold of fluorescence intensity reliably distinguishes cells with high pathway activity? The optimal threshold will vary depending on the antibody.

To allow high-throughput screening of many antibodies, we developed an algorithm which automatically identifies the appropriate threshold for each sample. Our method works by iteratively raising the threshold, and finding the threshold that yields the maximum value of I(*ab;s*|*cc*) (fig.3.3B). This process looks for a threshold below which cells are dispersed in sizes and above which the population is confined to a particular size. In the example shown in figure 3.3A and 3.3B, the optimal threshold reveals that cyclin D1 is elevated exclusively in large cells,

during late G1. This trend that would not have been detected with regular binning or a threshold based on the population median. Note that the threshold that yields the highest value of I(*ab;s|cc*) is typically identical or very close to the threshold maximizing I(*ab;cc|s*), further evidence that we are finding the boundary between real signal and noise.

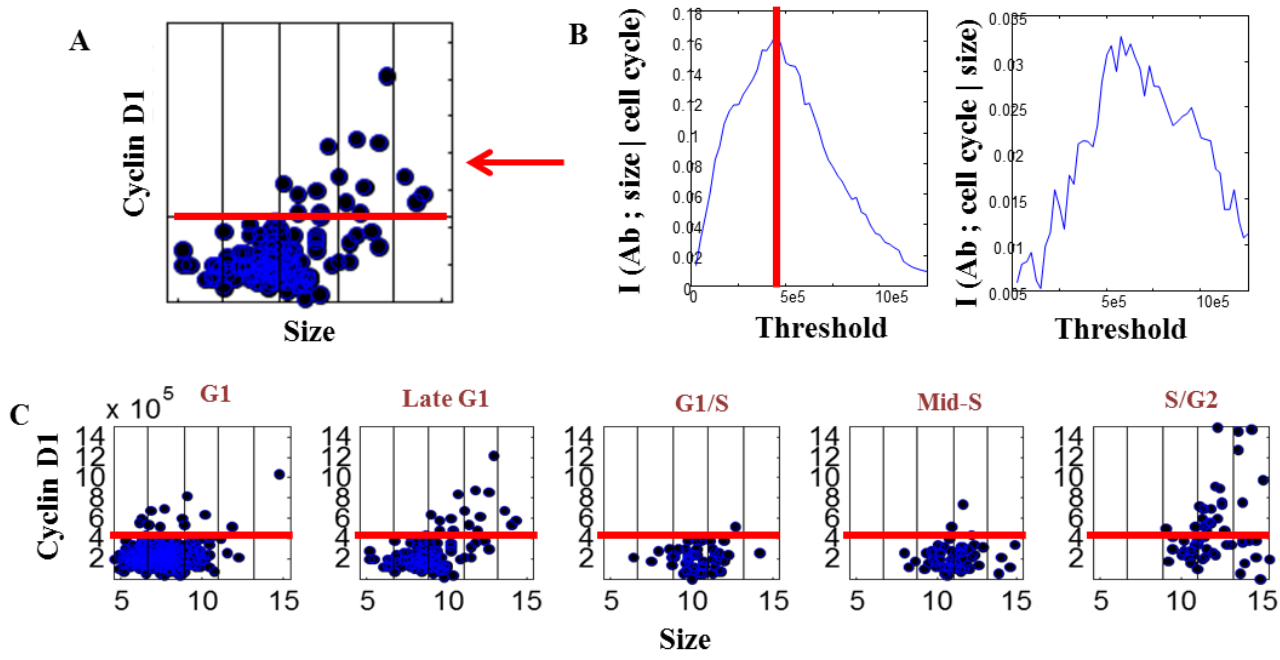

Figure 3.3: (A) A threshold reveals that the subpopulation if high-expressing cells are found at larger sizes. (B) The threshold was determined by finding the maximal conditional mutual information of antibody (cyclin D1) and size given cell cycle position. (C) The threshold reveals a cell-cycle dependent trend.

Initial results of antibody screen

In figure 3.4, I(*ab;cc|s*) is plotted vs. I(*ab;s|cc*) for a selection of antibodies. Signals high on the y-axis are strongly cell-cycle dependent, independent of their association with cell size. These include several known cell-cycle-associated signals like phospho-histone H3 and phospho-Rb, demonstrating the validity of our approach. Signals falling on the right-hand side of the plot are associated with size within one or multiple cell cycle stages. These also include a mixture of

expected hits like phospho-rpS6, as well as novel findings like p21 and p27, which are both upregulated in large cells.

Table 3.1 lists the signals most strongly associated with cell size. The signals are sorted into those that are preferentially active in small cells vs. those that are preferentially active in large cells.

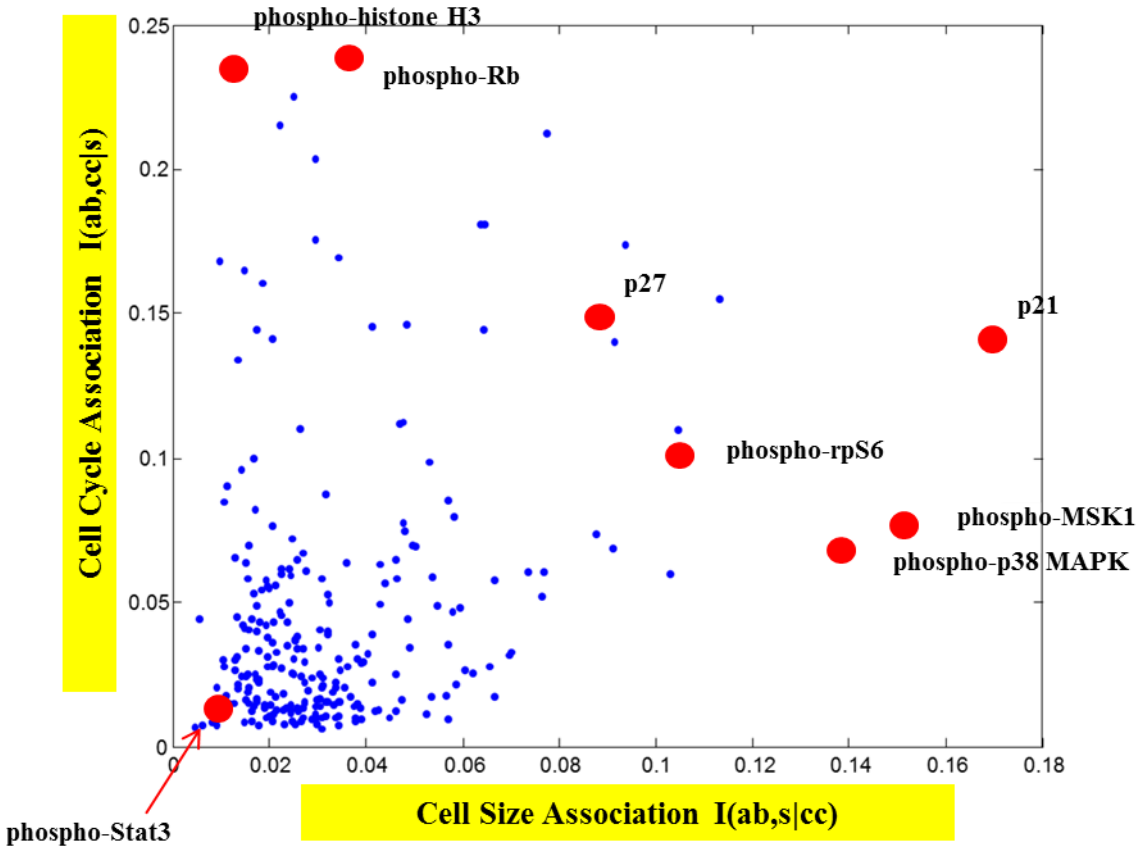

Figure 3.4: I(*ab;cc|s*) plotted vs. I(*ab;s|cc*) for a selection of antibodies.

Small Cells	Large Cells
pMAPKAPK2	p21
pSRC	p-p38MAPK
pY1137-EGFR	Ubiquitinylated proteins
pS376-MSK1	p-PDGF
EGR1	pMAPK
EGFR	p27
pSHP2	rpS6
pSTAT5	phospho-rpS6
phospho-(Ser) PKC substrates	S6K
	pS6K
	Cyclin D1
	p-PDGF
	ErbB2

Table 3.1: Antibodies associated with cell size in one or more cell cycle stages.

We are currently in the process of validating those hits and examining their associations with size as a function of the cell cycle in detail. As an additional precaution against trends resulting from non-specific antibody binding, we avoid antibodies that display only a general linear or monotonic increase with cell size, and focus on antibodies that display abrupt jumps in detection as a function of size, or interesting cell-cycle-dependent patterns.

Several of these hits seem like promising leads. Of particular note, an antibody targeting ubiquitinated proteins displayed a strong preference for large cells (fig. 3.5).

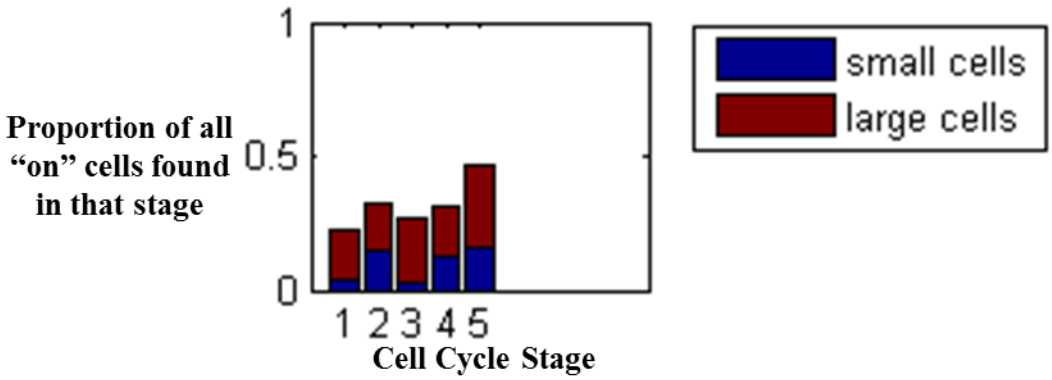

Figure 3.5: Cells with high levels of ubiquitinated proteins are predominantly large, during early G1 (stage 1) and late G1/early S-phase (stage 2).

The increased ubiquitination of proteins in large cells is prominent at two cell cycle stages, first in early G1 and again in late G1/early S-phase. This matches the timing of the two dips in $CV_{apparent}$ in HeLa cells (fig. 2.12F). Those dips indicated that during those periods growth rates are regulated so that small cells grow faster than large cells. Live imaging of nuclear growth suggested that this is accomplished by large cells slowing their growth. The increase in ubiquitination in large cells, during or close to those time windows, suggests that increased degradation may be responsible for the decrease in growth rate in large cells. This is also consistent with the possibility that very large cells may actually shrink, which is suggested by the presence of very large cells in G1 in Rpe1 populations and their absence during S-phase. We have replicated this size-dependent detection of ubiquitination in a cell-cycle-stage-specific manner in independent experiments and are following this up by testing the effect of the proteasome inhibitor bortezomib on cell size regulation.

Investigating the relationship between cell size, cell cycle stage, and the activity of the mTOR signaling pathways

In a parallel approach to the unbiased antibody screen, since the mTOR pathway has been established as a key player in the regulation of cell growth, we investigated the behavior of several mTOR pathway components as a function of cell size and cell cycle position. We posed two initial questions. Firstly, does mTORC1 activation follow a cell cycle dependency that mirrors the dynamics we observed in the regulation of growth rate? This would suggest that mTORC1 is the growth regulator that is receiving information about cell size. Secondly, is mTORC1 regulated differently in large and small cells? The results in chapter two suggested that large cells decrease their growth rate, narrowing cell-to-cell size variability. This means that growth-promoting signals that participate in the process of size specification must not only influence cell size but be influenced by cell size.

mTORC1 activity displays switch-like dependency on cell cycle progression

As a reporter of mTORC1 activity, we used immunofluorescence detection of Ser235/236-phosphorylated rpS6. Inhibition of mTORC1 by rapamycin completely abrogated rpS6 phosphorylation in HeLa cells (figure 3.6), confirming that in these conditions rpS6 phosphorylation is mediated by mTORC1 (presumably via S6K1) and not an alternate regulator, such as MAPK-activated RSK. We refer to phospho-rpS6 as a reporter of mTORC1 activity to avoid the assumption that any association of rpS6 phosphorylation with cell cycle progression or cell growth is effected through rpS6 itself, since mTORC1 has many downstream effectors. At the same time, we note that the activity of mTORC1 on different targets may be differentially regulated, so trends that are observed with a phospho-rpS6-specific antibody cannot be assumed

to be the same for other mTOR effectors without verification. We have confirmed that some of the trends below are reproduced by immunostaining of phospho-4EBP1.

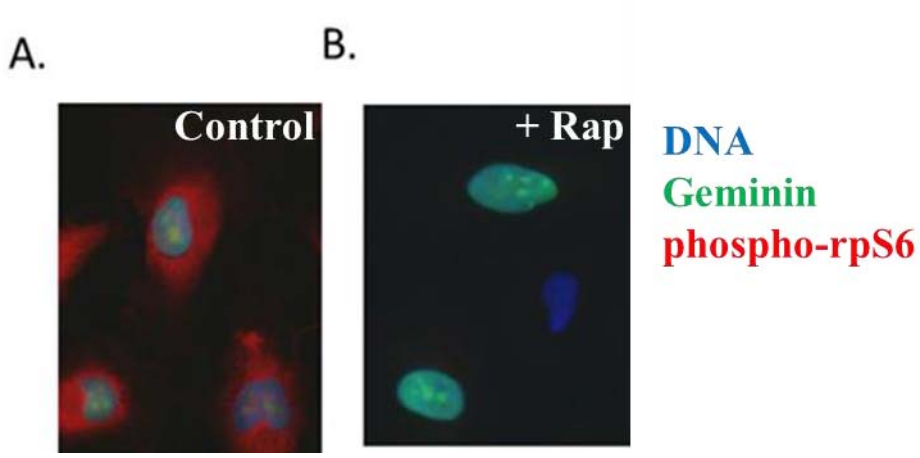

Figure 3.6: HeLa cells expressing mAG-hGem and stained with anti-phospho-rpS6 and DAPI. (A) Untreated cells. (B) cells treated with 70 nM rapamycin.

Figures 3.7A and 3.7B shows how the distribution of phospho-rpS6 levels changes as a function of cell cycle progression. The data reveal switch-like dynamics of mTORC1 activation; phospho-rpS6 levels rise abruptly during G1 and continue to increase throughout S-phase. This trend reflects rpS6 phosphorylation, not the abundance of rpS6, which is constant over the cell cycle (fig. 3.7C). While mTORC1 activity does correlate with cell cycle progression, these dynamics do not mirror the cell cycle periodicity we observed in the cell-size dependence of growth rate ($CV_{apparent}$). Nevertheless, these results do not preclude the possibility that mTORC1 plays a role in the modulation of $CV_{apparent}$.

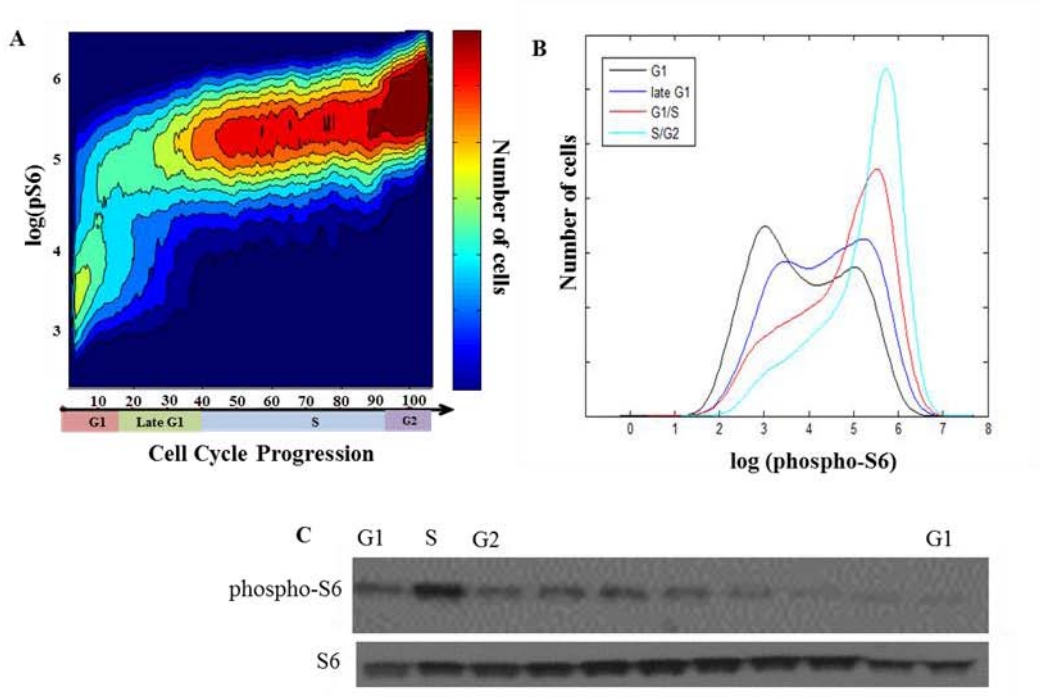

Figure 3.7: rpS6 phosphorylation over the cell cycle. (A) anti-phospho-rpS6 fluorescence (log scale) vs. cell cycle position. Color represents proportion of cells with that combination of phospho-rpS6 and cell cycle stage. Columns are normalized to sum to one, to highlight change in distribution shape over the cell cycle. (B) Histograms for data in (A), binned into discrete cell cycle stages. (C) Western blot for phospho-rpS6 and rpS6. Cells were synchronized in G1 (double thymidine block), and then sampled at intervals after release. phospho-rpS6 is highest when all cells are in S/G2 (second lane) and decreases as more and more cells divide and enter G1.

mTORC1 activity is more strongly correlated with cell size in S phase than in G1

To further test whether mTOR is involved in precisely specifying cell size, we checked whether mTORC1 signaling shows a dependency on cell size, which could indicate that it is differentially activated in large and small cells. We observed a significant correlation between cell size and levels of phospho-rpS6. Surprisingly, however, while phospho-rpS6 is present for most of cell cycle, phospho-rpS6 level and cell size only become strongly correlated upon G1-exit, in HeLa, Rpe1, and HT1080 cells (fig 3.8).

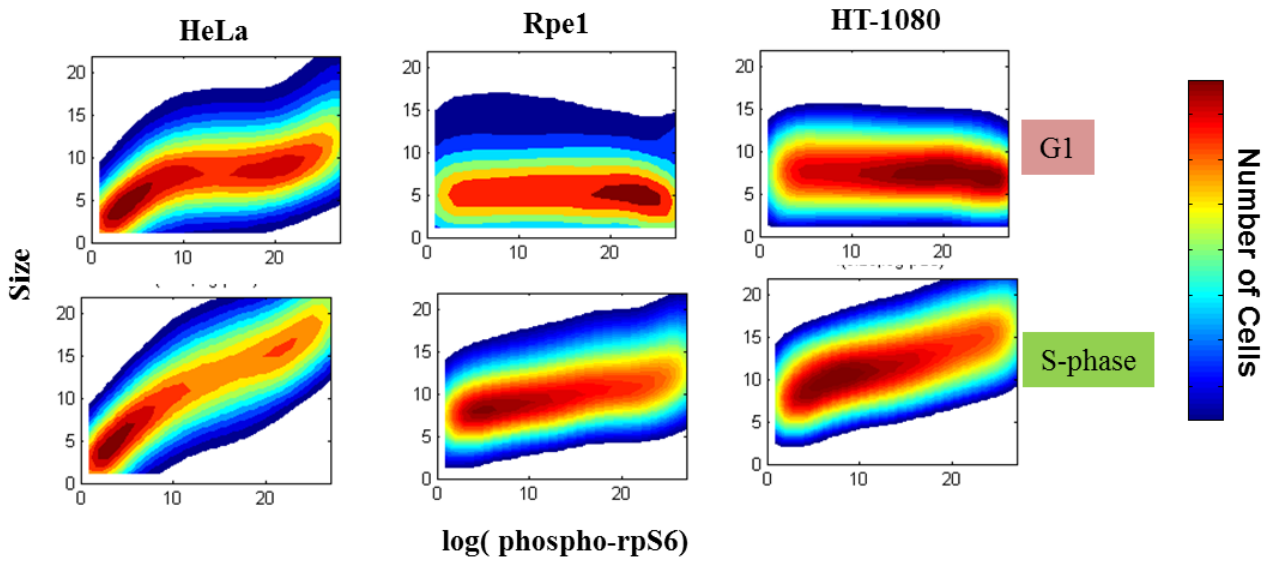

Figure 3.8: rpS6 phosphorylation is correlated with cell size in S-phase. Joint distribution of phospho-rpS level and size in HeLa (left), Rpe1 (middle), and HT1080 (right), during G1 (top) and late S-phase (bottom). Distributions are normalized by column.

This result shows a correlation of phospho-S6 levels with cell size that is surprisingly dependent on cell cycle stage. In figure 3.9A, this trend is quantified by plotting the mutual information of phospho-rpS6 and cell size as a function of cell cycle stage. (The sum of all stages would be I(*ab,s*|*cc*), with *ab* in this case referring to phospho-rpS6 level.) To confirm that the trend is not an artifact of non-phospho-specific antibody binding, we repeated the experiment on cells treated with rapamycin (fig. 3.9B) and saw very low values of I(*ab,s*), which did not follow the same trend. Further investigations will ask whether how trend relates to regulation of growth in small and large cells.

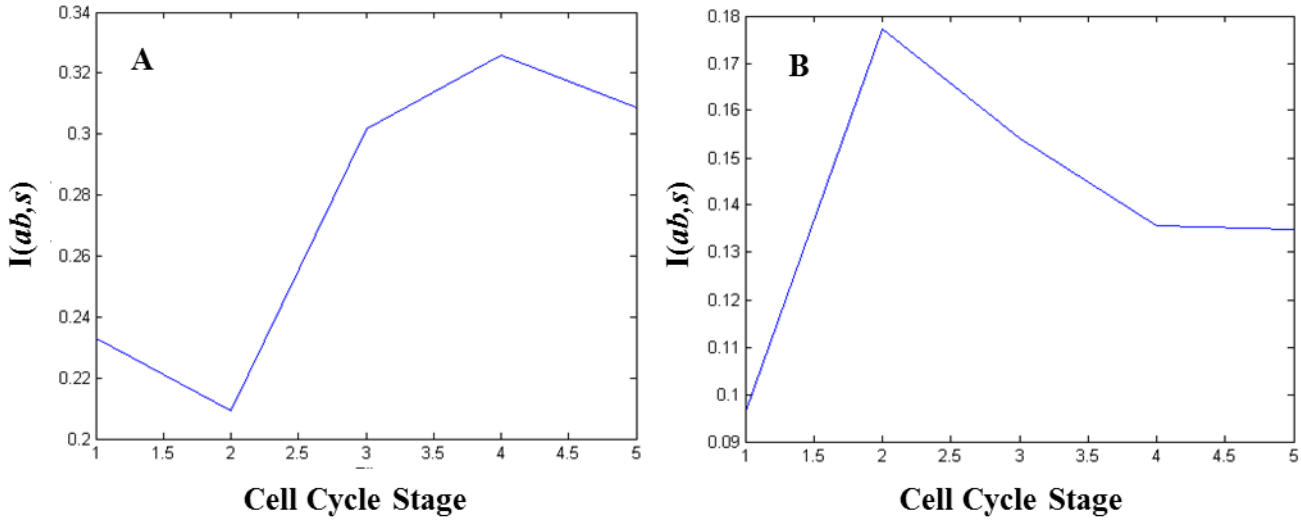

Figure 3.9: Mutual information of phospho-rpS6 and size, as a function of cell cycle stage in (A) control and (B) rapamycin treated cells. Note different scale on y-axis.

G1-exit is more dependent on cell size than on mTORC1 activity

Since phospho-rpS6 levels rise dramatically before S-phase entry, we asked whether this change plays a role in promoting G1-exit. Since we previously saw that cells exit G1 in a size-dependent manner, we tested whether cell size or phospho-rpS6 level is more predictive of G1 exit. The heat map in figure 3.10A shows the proportion of cells with any given combination of size and phospho-rpS6 level that have exited G1. The sharp vertical boundary seen in this representation reflects a strong influence of cell size on G1-exit. Following any row of the heat map from left to right, along the size axis, will reveal a large increase in the number of cells that have exited G1 as the critical size is passed. In contrast, phospho-rpS6 level does not strongly predict G1 exit, over most of the range of cell sizes. A horizontal gradient, i.e. association of phospho-rpS6 level with cell size, is only seen for cells in the critical size range.

This comparison is quantified in figure 3.10B, by assigning each cell a binary parameter g (0 for G1 cells, 1 for post-G1 cells) and calculating the conditional mutual information terms $I(g,s|ab)$ and $I(g,ab|s)$. These terms are divided by the total entropy of g:

$$H(g) = -\sum p(g_i) \log(p(g_i))$$

to assess how much of the variability in g is accounted for by either s or ab. The bar plot in figure 3.10B compares $I(g,s|ab)/ H(g)$ to $I(g,ab|s)/ H(g)$, and shows that cell size explains a much larger percentage of the variability in G1 status than phospho-rpS6 level does.

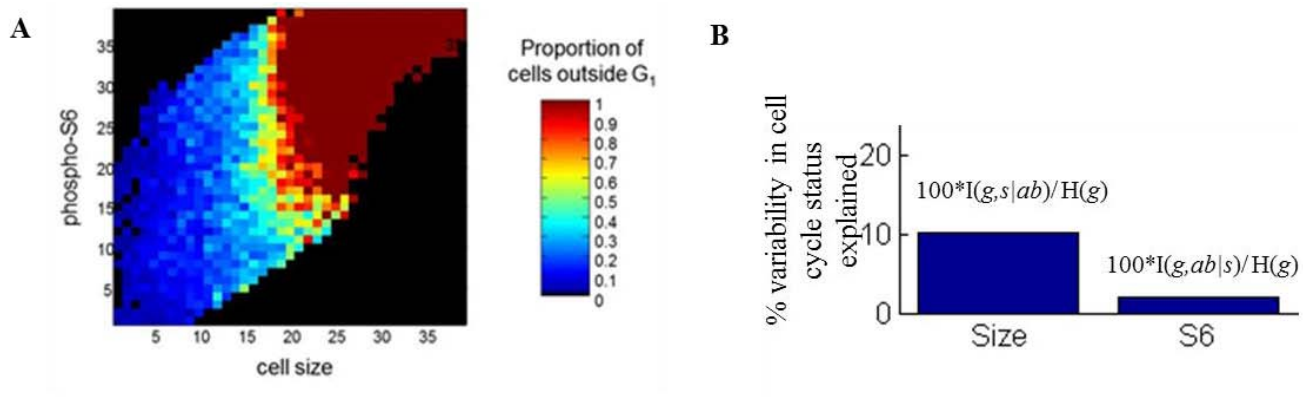

Figure 3.10: (A) Proportion of post-G1 cells as a function of phospho-rpS6 level and cell size. (B) Comparison of the percentage of variability in cell cycle state accounted for by size or phospho-rpS6.

To illustrate this result, we sorted the cells into four groups based on their phospho-rpS6, and looked at the joint distribution of size and cell cycle progression for each group. The heat maps in figure 3.11 show these distributions, with each row normalized in order to highlight the change in cell-cycle-stage distribution as a function of size. At low levels of phospho-rpS6, both small and large cells are concentrated in G1. At high levels of phospho-rpS6, large cells are depleted from G1 and spread into S-phase and G2. However, cells that have high phospho-rpS6 levels but are still small (a relatively rare state which high-throughput microscopy and image processing allows us to sample) are still restricted to G1. In HeLa and HT1080 populations, these

cells accumulate in two distinct clusters- in early and late G1, consistent with the idea that they cannot leave G1 until they reach a threshold size.

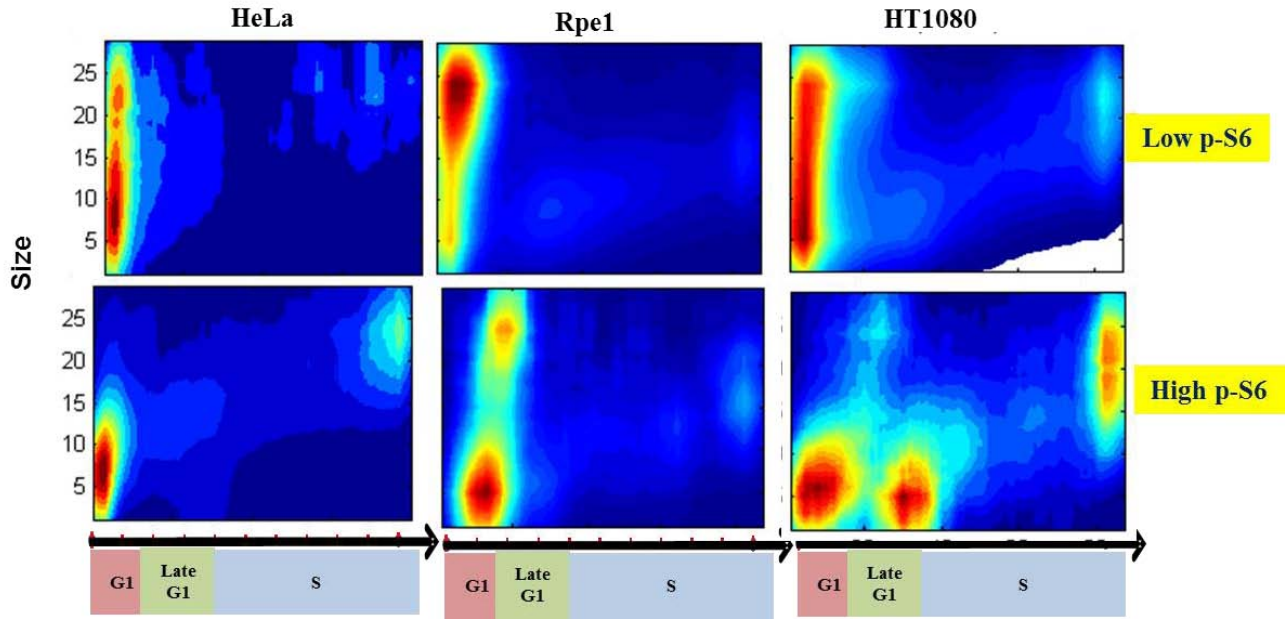

Figure 3.11: mTORC1 activity correlates with cell cycle progression in *large* cells. Joint distribution of size and cell cycle position in HeLa (left), Rpe1 (middle), and HT1080 (right) cells with low (top) or high (bottom) levels of phospho-rpS6. Distributions are normalized by row.

4EBP1 phosphorylation and rpS6 phosphorylation are co-regulated

To confirm that the trends reported above apply to mTORC1 activity more generally than just its phosphorylation of S6K, we stained cells for phospho-4EBP1, with similar results (fig. 3.12).

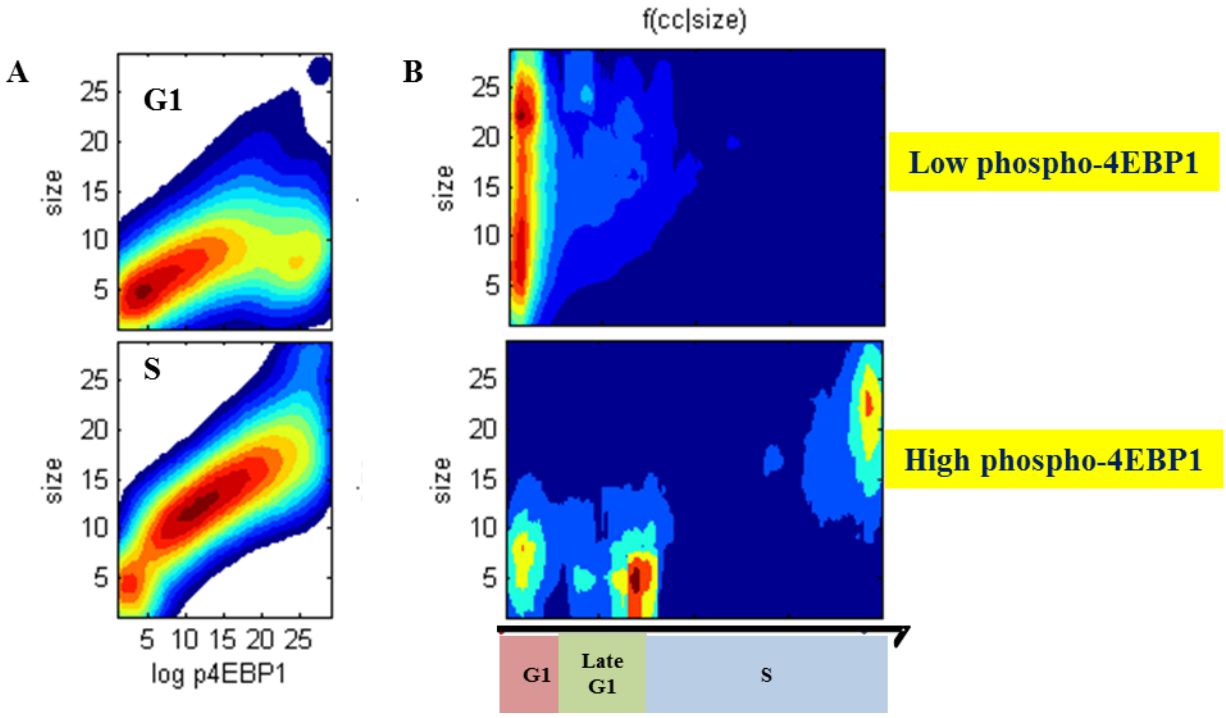

Figure 3.12: (A) Joint distribution of phospho-4EBP1 level and size in HeLa (left), during G1 (top) and S-phase (bottom). Distributions are normalized by column. (B) Joint distribution of size and cell cycle position in HeLa cells with low (top) or high (bottom) levels of phospho-4EBP1. Distributions are normalized by row.

Conclusions

The antibody screen has yielded a number of interesting leads that perturbation approaches will further explain. For example, the size-dependent ubiquitin detection in early and late G1 may relate to a question we have long pondered: does growth rate regulation occur through modulation of synthesis or degradation? One way to approach this is by perturbations, for example treating cells with a proteasome inhibitor and looking for differential effects on the size distribution at different cell cycle stages. In particular, the localized perturbation analysis method we have derived (which will be discussed in the next chapter) is suited to examining the effects of short inhibitor treatments.

However, using the approaches described here to look at additional signals in the synthesis and degradation pathways may be a valuable complement to perturbation experiments.

Even though they cannot prove causal relationships, these experiments provide the important advantage of examining unperturbed populations. This is particularly relevant to this problem, because perturbations to degradation or synthesis rates can induce what looks like regulatory behavior, if cells differ in their turnover rates. If large cells have a higher turnover rate than small cells, inhibiting synthesis can cause a drop in size variance that would not normally occur. Similarly, inhibiting degradation can increase variance, which can give the appearance of disrupting the growth rate control mechanism even if that is not the case. The ideal experiment may be to use labeled amino acids as well as antibodies to look at synthesis in combination with signaling events. Having a read-out of both signaling state and phenomenology in single cells can allow us to identify which signals are truly responsible for a particular behavior.

The approaches taken here will be useful in further exploring the interaction of the pathways controlling growth and cell cycle progression. The cell-cycle-dependence of rpS6 phosphorylation, as well as its cell-cycle-dependent correlation with size, raise the interesting question of whether growth in different cell cycle stages is controlled by different regulatory circuits. Supporting this idea, we see that rapamycin affects cell size particularly in S-phase (results in chapter four). We can further explore this possibility by looking for signals that are associated with cell size during G1, to build a comprehensive view of growth control over the cell cycle.

Our analyses here also indicate that size is a more important contributor to G1 exit than mTORC1 activity. This approach can be used to look for signals with the opposite outcome. Screening for signals that can override the restriction of small cells to G1, may answer the question of how a cell measures its own size.

1. Fan, Q.-W. *et al.* EGFR signals to mTOR through PKC and independently of Akt in glioma. *Sci. Signal.* **2,** ra4 (2009).

2. Harrington, L. S., Findlay, G. M. & Lamb, R. F. Restraining PI3K: mTOR signalling goes back to the membrane. *Trends Biochem. Sci.* **30,** 35–42 (2005).

3. Laplante, M. & Sabatini, D. M. mTOR signaling in growth control and disease. *Cell* **149,** 274–293 (2012).

4. Ma, X. M. & Blenis, J. Molecular mechanisms of mTOR-mediated translational control. *Nat. Rev. Mol. Cell Biol.* **10,** 307–318 (2009).

5. Fader, C. M., Aguilera, M. O. & Colombo, M. I. Autophagy response: manipulating the mTOR-controlled machinery by amino acids and pathogens. *Amino Acids* (2014). doi:10.1007/s00726-014-1835-7

6. Lloyd, A. C. The regulation of cell size. *Cell* **154,** 1194–1205 (2013).

7. Thoreen, C. C. *et al.* A unifying model for mTORC1-mediated regulation of mRNA translation. *Nature* **485,** 109–113 (2012).

8. Richter, J. D. & Sonenberg, N. Regulation of cap-dependent translation by eIF4E inhibitory proteins. *Nature* **433,** 477–480 (2005).

9. Cantley, L. C. The phosphoinositide 3-kinase pathway. *Science* **296,** 1655–1657 (2002).

10. Lee, C., Kim, J.-S. & Waldman, T. PTEN gene targeting reveals a radiation-induced size checkpoint in human cancer cells. *Cancer Res.* **64,** 6906–6914 (2004).

11. Faridi, J., Fawcett, J., Wang, L. & Roth, R. A. Akt promotes increased mammalian cell size by stimulating protein synthesis and inhibiting protein degradation. *Am. J. Physiol. Endocrinol. Metab.* **285,** E964–972 (2003).

12. Rosner, M., Hofer, K., Kubista, M. & Hengstschläger, M. Cell size regulation by the human TSC tumor suppressor proteins depends on PI3K and FKBP38. *Oncogene* **22,** 4786–4798 (2003).

13. Montagne, J. Drosophila S6 Kinase: A Regulator of Cell Size. *Science* **285,** 2126–2129 (1999).

14. Ohanna, M. *et al.* Atrophy of S6K1(-/-) skeletal muscle cells reveals distinct mTOR effectors for cell cycle and size control. *Nat. Cell Biol.* **7,** 286–294 (2005).

15. Shima, H. *et al.* Disruption of the p70(s6k)/p85(s6k) gene reveals a small mouse phenotype and a new functional S6 kinase. *EMBO J.* **17,** 6649–6659 (1998).

16. Ruvinsky, I. *et al.* Ribosomal protein S6 phosphorylation is a determinant of cell size and glucose homeostasis. *Genes Dev.* **19,** 2199–2211 (2005).

17. Acebron, S. P., Karaulanov, E., Berger, B. S., Huang, Y.-L. & Niehrs, C. Mitotic wnt signaling promotes protein stabilization and regulates cell size. *Mol. Cell* **54,** 663–674 (2014).

18. Shimobayashi, M. & Hall, M. N. Making new contacts: the mTOR network in metabolism and signalling crosstalk. *Nat. Rev. Mol. Cell Biol.* **15,** 155–162 (2014).

19. Zhang, Y. *et al.* Coordinated regulation of protein synthesis and degradation by mTORC1. *Nature* **513,** 440–443 (2014).

20. Cover, T. M. & Thomas, J. A. *Elements of Information Theory*. (Wiley, 2012).

21. Shannon, C. E. & Weaver, W. *The mathematical theory of communication*. (University of Illinois Press, 1964).

Chapter 4

Using drug perturbations to investigate size control circuitry

Introduction

To conclusively identify the cellular components responsible for cell size specification, we sought to use the experimental and analytical methods we have developed to characterize the response of cells to various drug perturbations. Specifically we will look for drugs that decrease cell size uniformity in a population, disrupt the coordination of growth and cell cycle progression, or disrupt the relationship between cell size and growth rate. This is an important complement to the immunostaining experiments described in chapter three, as it may provide a way to establish causality.

However, there are a number of difficult challenges that accompany perturbation-based experiments. These are listed below, along with the measures we took to address them.

1. Drugs disrupt multiple targets in the cell (off-target and multi-target effects), so we can't assume that a drug's effect reflects the role of an individual target. Furthermore, the signaling networks that control cell growth and cell cycle progression are highly interconnected as. Therefore, even a highly specific inhibitor will cause numerous downstream effects, making it hard to identify the target directly responsible for the drug's effect. For this reason, when probing the role of a particular protein, process, or pathway we need to compare the effects of multiple targeted inhibitors that have different secondary effects. Similarly, we can compare the effects of drugs with overlapping sets

of targets and downstream links, to identify the common target associated with a particular drug-induced phenotype.

2. Cell growth and cell cycle progression are integrated processes, and perturbing one will often affect the other. Furthermore, since cell size is affected by both growth and division, multiple types of perturbations may have similar effects on the assayed joint distribution of size and cell cycle position. For example, a decrease in cell size may reflect either slower growth or a shortened cell cycle, making it hard to know what process a drug actually altered. One way to resolve such ambiguities is to compare the effects of a drug over short and long timescales to observe both immediate and secondary changes in the size/cell cycle distribution. In the example above, a decrease in cell cycle length would cause a transient increase in the number of mitotic cells.

3. Because drug-treated cell populations are not in a stationary state, we can't rely on the assumptions underlying ERA and related analyses to infer dynamic behavior from measurements of fixed cells. The staggered-timescale approach mentioned above can aid in making inferences without these assumptions. Additionally, in a set of complementary experiments, we used low doses of drugs of particular interest to achieve a perturbed stationary state, where cells continue to proliferate at a constant rate while under the influence of the drug and maintain a stable cell size distribution.

Drug screen to identify cell size regulators

To conduct an unbiased search for proteins involved in size specification, we worked with collaborators at Novartis to use our assay to screen of thousands of well-characterized drugs for their effects on the joint distribution of cell size and cell cycle position. Measuring the full

distribution of states in each condition provides a wealth of information but also a complex analysis challenge. Analysis of high-content screens is a field that is still in its infancy[1]. In conventional screens, each tested compound is scored with a single number, for example level of a reporter target or the percent of surviving cells. In contrast, when assayed with high-content imaging, each screened condition yields a multi-dimensional scatter plot or histogram. In such cases, finding the appropriate metric to score differences between compounds and controls is not trivial.

As an illustrative example, figure 4.1 shows data retrieved from two wells in our screen, a negative control well (DMSO) and a positive control well (cycloheximide). While differences between the two conditions can clearly be discerned by visual inspection, it is not be immediately clear which metrics would best quantify these differences in a way that is biologically meaningful. For instance, comparison of the 2-d probability density maps in figures 4.1A and 4.1B reveal that cycloheximide increased the proportion of cells in S-phase and in G2. The 3-d probability density plots in figures 4.1C and 4.1D show that cycloheximide also decreased the proportion of large cells in G1.

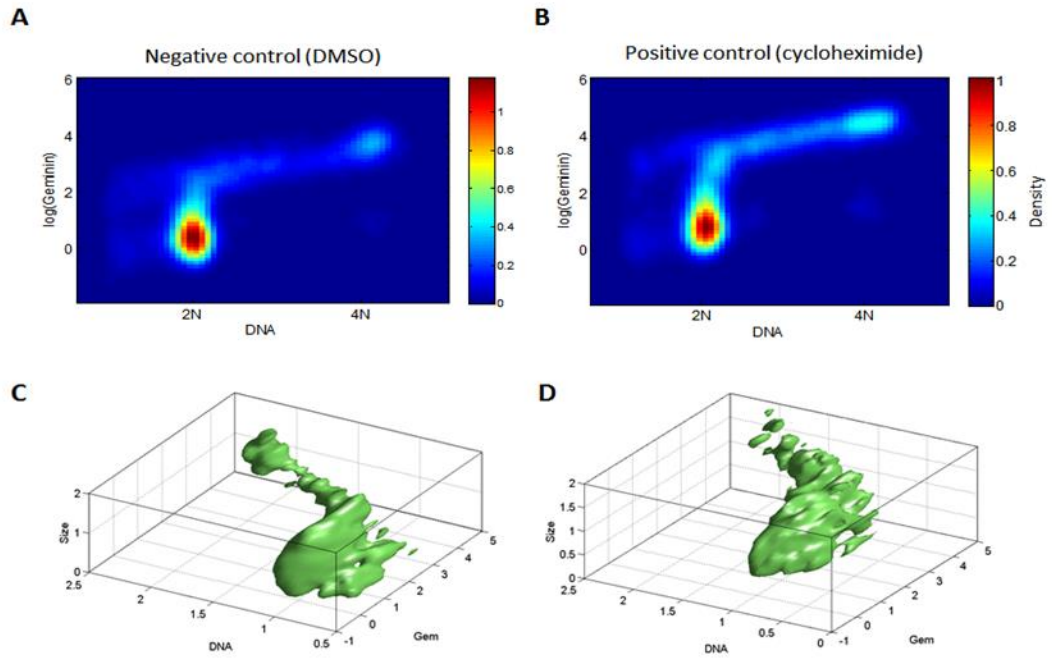

Figure 4.1: Comparison of data from a single well treated with DMSO (A, C) and a single well treated with cycloheximide (B, D). Data is represented in two ways: a 2D probability density (histogram) (A, B) showing the proportion of cells with different combinations of Geminin and DNA content, and a 3D probability density plot (C, D) showing the proportion of cells with different levels of Geminin, DNA and cell size.

One straightforward way to compare different screened conditions is to find metrics that quantify the general dissimilarity between scatter plots, such as the L^2-norm. Using such an approach may indicate that the conditions differ, but fail to tell if the differences are specific to particular stages of cell cycle or particular cell sizes. Thus, while high content imaging opens many doors, by enabling us to glean information from the heterogeneity in a cell population, tools and analyses designed to interpret the data have yet to be developed[2–4]. For example, there are many statistical tests that can be used to examine whether a compound increases or decreases cell size, but there is not available method to quantify how much a compound influence the coordination between cell size and cell cycle progression. To fully exploit the data gained from our screen, we need to derive summary statistics that allow us to compare drugs in the most meaningful way.

.

Results

Drug screen design

We used the strategy described in chapters two and three to simultaneously assay cell size (protein content), cell cycle position (DNA content and Fucci cell cycle reporters[5]), and proliferation (cell number). HeLa cells expressing a mAG-hGem and mKO2-hCdt1 (a reporter of SCF^{Skp2} activity[5]) were grown in 384 well plate, exposed to screened compounds for 24 hours before fixation, staining with SE-A647 and DAPI, and imaging. Following imaging, cell and nuclear borders were computationally identified and images were quantified for levels of each of the labeled channels. This resulted in a scatter plot of cell size and cell cycle stage for each of the screened compounds (fig 4.2A) which can be described by a probability density plot showing the proportion of cells at each size and cell cycle position (fig. 4.2B).

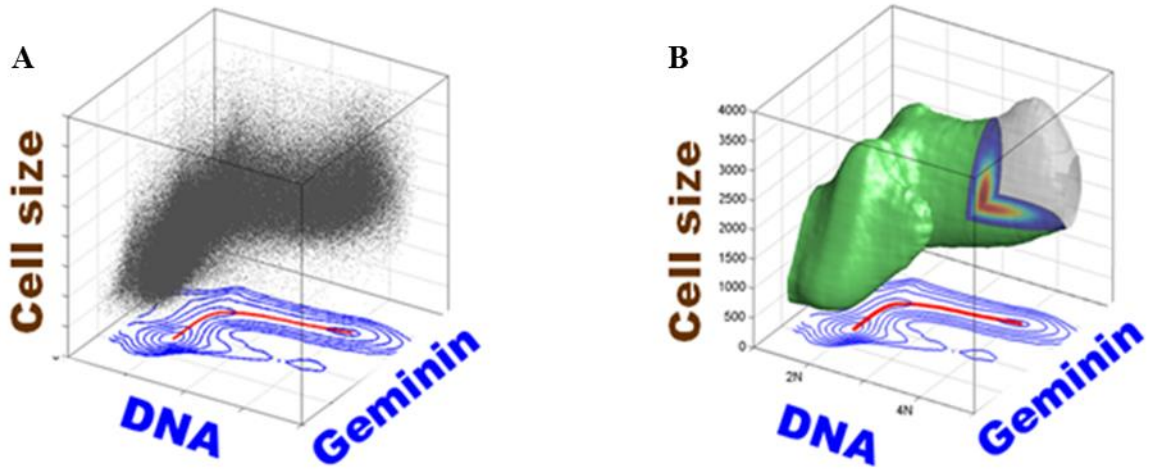

Figure 4.2: Two representations of the data generated from each screened condition

We limited the screen to compounds that are well characterized and annotated for affected targets, to facilitate follow-up of hit compounds by eliminating the need for target

identification. We started by screening the Novartis MoA (mode of action) library – a highly specialized compound library designed to maximize target coverage with a representative set of well characterized compounds.

Image processing and intensity corrections

We used the strategies outlined in chapter two (methods) to build an image-processing pipeline, tailored to meet the needs of the screen. In order to get accurate, quantitative measurements, it is critical to find an appropriate flat-field correction to eliminate the effect of uneven illumination across the wells during imaging. To do this, we took advantage of the fact that we know DNA histograms should have two peaks, with the second centered at a value double that of the first. We generated DNA histograms from the cells in local regions and used the ratios of the two peaks to generate an artificial "flat" and "dark" image, which was used to correct the screen images (fig. 4.3).

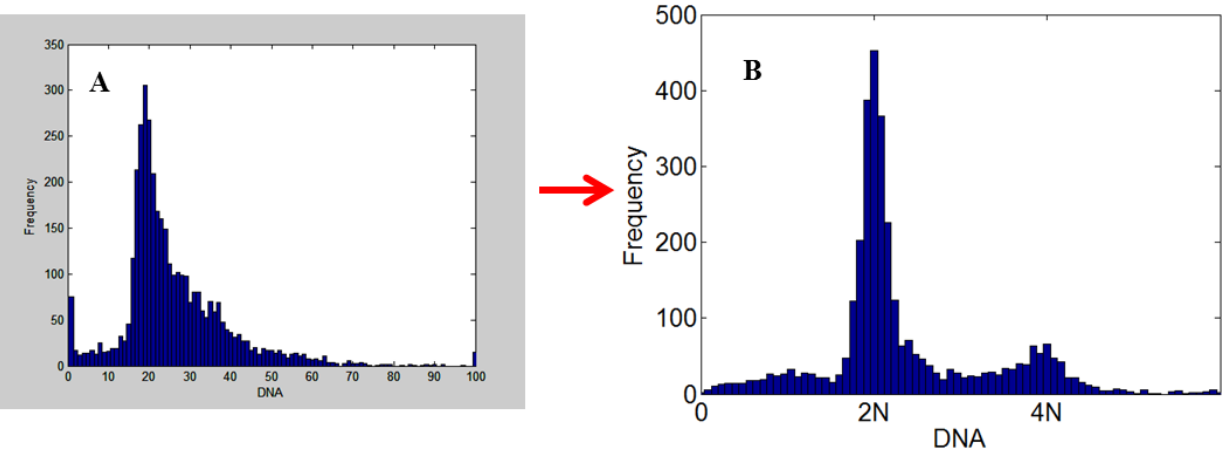

Figure 4.3: Histograms of cellular DNA content (A) before and (B) after locally generated flat field correction

Initial evaluation of screen data and preliminary hits

As a first step in the analysis, we examined the effects of different compounds on cell size, without considering data collected from the cell cycle reporters. As expected, when we classified drugs based on the signal transduction pathway they target, we identified mTOR inhibitors as potent influences on cell size (fig. 4.4B). Cells treated with mTOR inhibitors consistently displayed a smaller cell size. In further validation of the data, cycloheximide treatments consistently decrease cell size (fig. 4.4A).

We also identified pathways whose connection to cell size is largely unexplored. In particular, inhibitors of protein kinase C (PKC) signaling produced a dramatic increase in cell size. Twelve PKC inhibitors, targeting various PKC isozymes, showed significant effects on cell size. PKC signaling was also highlighted by our antibody screen (described in chapter three), where PKC substrates were found to be preferentially phosphorylated in small cells (chapter three, table 3.1), consistent with the result presented here.

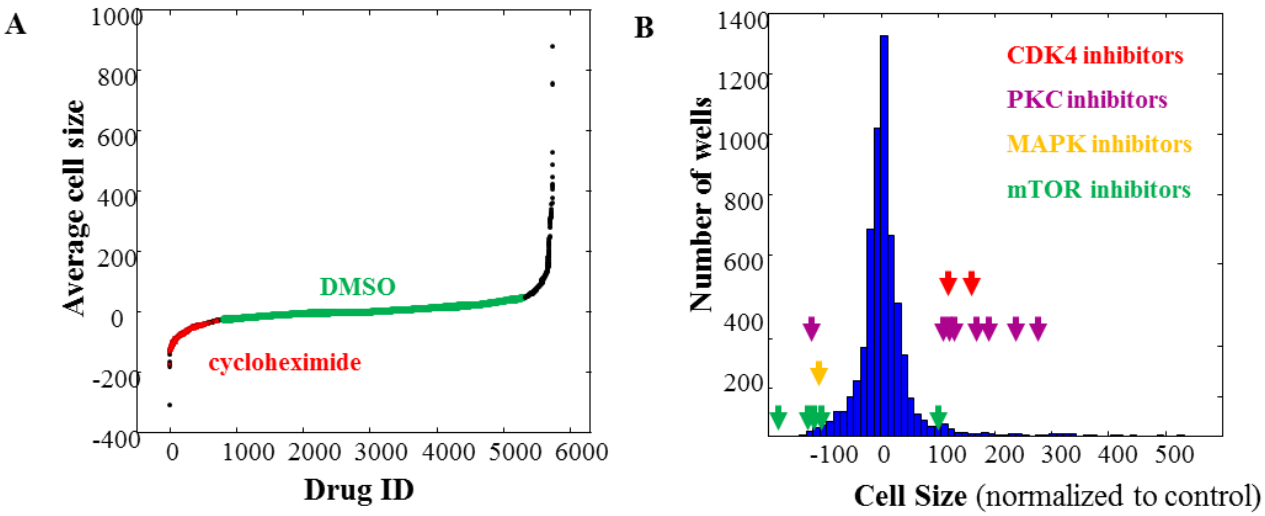

Figure 4.4: Initial screen results. (A) Populations of cells from the different wells were sorted for average cell size. Cell size is displayed as the difference of well mean from control mean. Wells treated with DMSO (negative controls) are highlighted in green. Wells treated with cycloheximide (positive controls) are highlighted in red. (Legend continues on next page.)

Figure 4.4 (continued): (B) Screened compounds were classified based on which molecule or signaling pathway they target. Colored arrows indicate the average cell size in wells treated with compounds that are associated with the specified target. The blue histogram describes the distribution of cell size when all screened compounds are collectively pooled.

We next looked at the effect of drugs on cell size variability- a critical indicator of disruption of size control. In figure 4.5, compounds are ranked based on their CV. We found a number of compounds that consistently either increase or decrease cell size variability, at both doses tested (1 uM and 10 uM). These are listed by target in table 4.1 and include several known members of growth-regulating pathways, such as a PI3K/mTOR inhibitor (which decreased CV) and EGFR and PDGFR inhibitors. Other notable hits include the hsp90 inhibitor radicicol and the microtubule stabilizer epothilone B. However, since each drug has multiple known targets, our first step was to add a set of drugs with targets that overlap with these to our next round of screening, in order to identify the proteins that actually influence size variability.

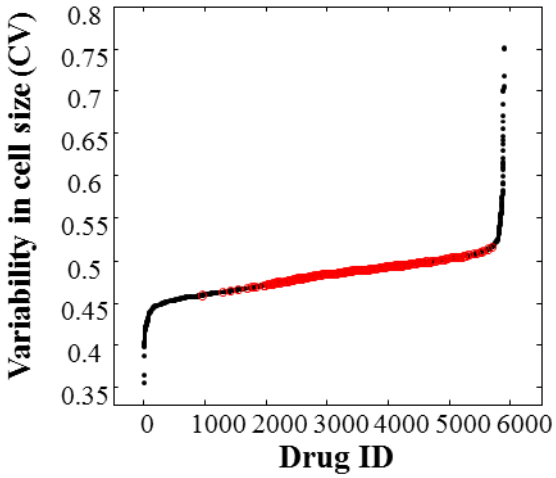

Figure 4.5: Effects of screened compounds on variability in cell size Compounds were sorted for their influence on CV of cell size. Red circles indicate control wells (DMSO).

Increased CV: Drug Targets	Decreased CV: Drug Targets
Microtubule-Stabilizing Agent; Apoptosis Inducer; Antimitotic Drug (Generic name: Epothilone B)	mTOR Inhibitor; PI-3-Kinase Inhibitor
hsp90 Inhibitor; MAP3K7 (TAK1) Inhibitor; Pyruvate Dehydrogenase Kinase Inhibitor;ATP Citrate Lyase Inhibitor (Generic name: Radicicol)	Glucocorticoid Receptor (GR) Modulator
EGFR Inhibitor; Abl Kinase Inhibitor; Protein Kinase C Inhibitor	Focal Adhesion Kinase (FAK) Inhibitor
PDGFR Inhibitor; Flt3 Inhibitor; Angiogenesis Inhibitor	Anti-inflammatory Drugs; Angiogenesis Inhibitor
Tyrosine Kinase Inhibitor	Antimetabolite; Dihydrofolate Reductase (DHFR) Inhibitor
beta-Amyloid Aggregation Inhibitor; Cyclooxygenase-1/2 Inhibitor; Free Radical Scavenger	HIV Protease Inhibitor
Aurora-A Kinase Inhibitors; MAPKAP-K2 Inhibitor; hsp 27 Inhibitor; TNF-alpha Release Inhibitor	Apoptosis Inducer; Caspase 3 Activator (Generic name: Brefeldin A)
Chemokine CXCR1 (IL-8 alpha Receptor) Antagonist;Chemokine CXCR2 (IL-8 beta Receptor) Antagonists	5-HT1B Agonist
	gamma-Secretase Inhibitor; Antiamyloidogenic Agent
	mu-Calpain (1/2) Inhibitor
	DNA Polymerase Inhibitor
	Apoptosis Inducer; BIRC4 Expression Inhibitor;Sphingosine Kinase Inhibitor;Tumor NADH Oxidase (tNOX) Inhibitor (Generic name: Phenoxodiol)

Table 4.1: Compounds that increased or decreased coefficient of variance in size.

Analysis of phenotypes without cell cycle parameterization

While the parameterization of a cell cycle axis is an intuitive and simple approach, it has fundamental drawbacks. The approach of integrating multiple reporters to form a cell cycle axis is a form of reduction in dimensionality. Instead of separately examining levels of DNA, Geminin and Cdt1, we use a single axis which we believe represents the process of cell cycle. As is the case with any form of dimensionality reduction, combining multiple reporters into a single axis is inevitably associated with a loss of information. In our case, lost information might be

critical for discriminating subtle differences between phenotypes of different compounds. In order to comprehensively compare different compound phenotypes, we are developing methods for direct comparison of the multi-dimensional scatter plots retrieved from the different compound treatments.

Our strategy is to first calculate, from each screened condition, the four-dimensional probability density function describing the distribution. Probability density estimation is performed using standard Gaussian kernel density estimates[6,7]. Figure 4.1C,D shows two such probability density estimates, one of a negative control well (DMSO) and one from a positive control well (cycloheximide). To test the capacity of these probability density functions to describe differences between tested compounds we used the L1-norm as a distance metric and clustered negative and positive controls (fig. 4.6). This resulted in a clear separation of the two conditions, showing a high degree of similarity between cycloheximide repeats and DMSO repeats and a distinct difference between DMSO and cycloheximide. We are exploring other metrics for comparing probability density functions as well, to use as a complement to our cell-cycle-axis-based analyses.

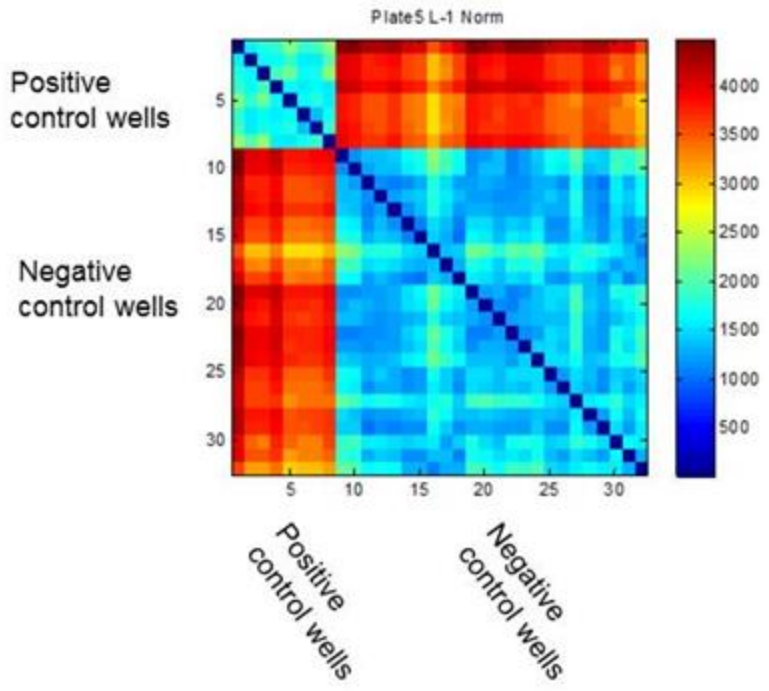

Figure 4.6: Clustering multidimensional phenotypes of wells treated with cycloheximide (positive controls) and wells treated with DMSO (negative controls). From each of the DMSO and cycloheximide repeat treatments we calculated a probability density estimate of DNA, Geminin, Cdt1 and cycloheximide. We then used L1-norm as a distance metric to score differences between the different treatments and used hierarchical clustering, resulting in a separation of the data into two groups.

Parameterizing a cell cycle axis

In a parallel approach, to probe the coordination of growth and cell cycle progression, we parameterized the three cell cycle labels (DNA, Geminin and Cdt1 reporters) into a single variable marking cell cycle progression. Three parameterization strategies were explored:

1. *Discrete cell cycle parameterization* (fig. 4.7). As we did in analyzing the antibody screen in chapter 3, we divided cells into groups based on their combination of cell cycle markers (fig. 4.7A). The addition of the cdt1 reporter allowed further discrimination of cell cycle position. Cells could be binned into 8 groups: early G1, late G1, G1/S transition, S phase, G2 phase, M phase and apoptotic cells (fig. 4.7B,C).

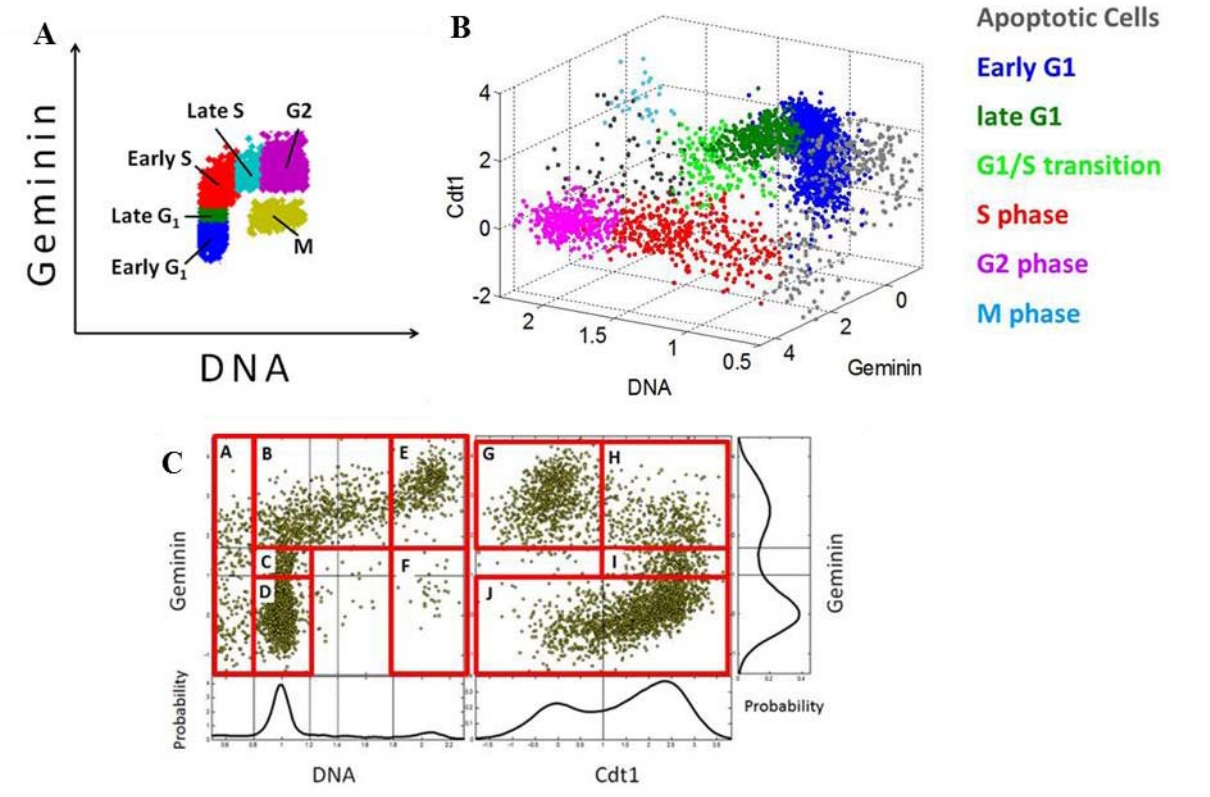

Figure 4.7: A discrete parameterization strategy for cell cycle progression. Cells from a single screened condition are described in terms of their levels of Geminin and DNA (**A**), or DNA, Geminin and Cdt1 (**B**). Based on defined thresholds for reporter levels, we classified cells from each screened condition into different cell cycle stages. Since the three dimensional scatter plot in (**B**) may be hard follow, we plot the same data as two separate two-dimensional plots (**C**) Also shown are the marginal distributions of each of the measured reporters. Based on these measurements cells from each screened condition were classified into eight cell cycle stages as depicted: Apoptosis (A), Early G1 (D, J), Late G1 (C, I), S phase (B, H) and G2 (E).

Drawbacks of discrete cell cycle parameterization: Thresholds used to classify cell cycle stage are, to some extent, arbitrary. Thus cells that are near transition from one cell cycle stage to another may be misclassified.

2. *Continuous cell cycle parameterization* (fig. 2.8). The continuous cell cycle axis approach described earlier has the advantage that it can report cellular dynamics within a cell cycle subdivision.

Drawbacks of the continuous cell cycle parameterization: We run the risk of over-interpreting differences between cells due to noise as differences in cell cycle position. This risk may be

increased with drug treatments, as the reporters used to parameterize the cell cycle (geminin, cdt1) may themselves be influenced by screened compounds.

3. *Piecewise continuous cell cycle parametrization.* To compromise between the discrete and continuous approaches, we followed a combined approach by dividing cells into groups of cell cycle state and parameterizing a continuous cell cycle axis in each group separately (Fig. 4.8).

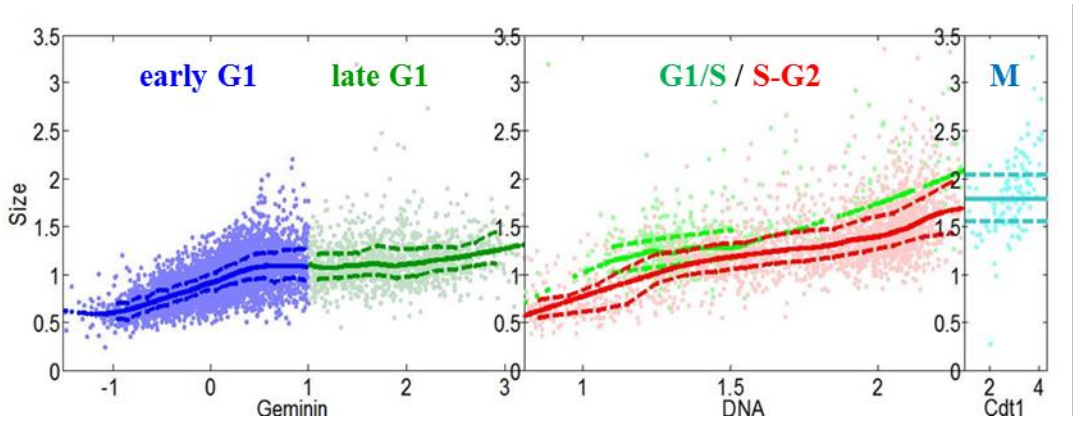

Figure 4.8: Cells are divided into three cell cycle groups, with cell cycle axes parameterized differently within each group. The solid lines represent the fitted mean cell size along cell cycle progression*. The upper and lower dashed lines represent the cell size of 75th and 25th percentiles respectively. Group 1 (left): G1 cells, cells are parameterized in cell cycle axis based on their Geminin level. Group 2 (middle): G1/S transition cells, S and G2 cells, cells are parameterized based on their DNA level. Group 3 (right): M phase cells, cells are arranged based on their Cdt1 level. In M phase, the solid line represents the median cell size of the subpopulation.

Finding compounds that disrupt the coordination of cell growth and cell cycle progression

In order to identify compounds that disrupt the link between cell size and cell cycle progression, we must define a quantitative measure of coordination. We explored two alternative strategies to score whether coordination of growth and cell cycle are perturbed by the different screened compounds. The first relied on established metrics from classical information theory[8,9].

Second, we derived a new measure - localized perturbation analysis – to test if the effects of a drug on cell size are confined to particular cell cycle stages.

Using relative entropy to parse the effects of a drug on the joint size/cell cycle distribution

In assessing the effect of a drug on the cell size distribution, we encounter the same situation that arose in analysis of the antibody screen data. Since cell size is correlated with cell cycle position, a drug that perturbs the cell cycle distribution may appear to have influenced cell size. For example, a drug that causes G2 arrest may appear to have increased cell size. To untangle these effects we used a similar approach, calculating the conditional relative entropy (or Kullback-Leibler divergence) of pairs of control and drug-treated size distributions, while holding cell cycle stage constant. This is a measure of how little the control and drug size distributions overlap, calculated separately for each cell cycle stage, and summed over all stages. An analogous calculation is used to quantify the drug-induced change in the cell cycle distribution independently of its effect on the size distribution.

In figure 4.9, the effects of compounds on the size distribution (KL divergence of the control and drug size distribution, given cell cycle stage) are plotted vs. their effects on the cell cycle distribution. The blue points represent control wells (compared to other control wells), while the black points represent drug-treated wells (compared to neighboring control wells). If we consider just the control wells, we see that natural variation in size is accompanied by coordinate changes in the cell cycle distribution. An example of this phenomenon was reported in chapter two, where we saw that mean size correlates with mean G1 among unperturbed populations. (Note that there is a trivial part of this correlation between controls in this representation, in addition to the real

correlation, due to the mathematical relationship between the two conditional KL divergence terms plotted. This can be subtracted out, but we plot the original terms here to make use of the intuitive and established interpretation of the quantities.)

Most of the drug-treated wells fall along the diagonal established by the controls, some extending it further. However, a subset of compounds cause a disproportionate change in either the size or cell cycle distribution, indicating a disruption in the normal relationship between the two. These compounds are candidates for further investigation, as they may target the mechanisms coordinating growth and cell cycle. The absence of drugs that strongly perturb cell size without affecting cell cycle distributions may reflect the robustness of the link between size and cell cycle progression (although it could possibly reflect a bias of the compound library towards cell cycle perturbants). Interestingly, one of the few drugs that affects size disproportionately is an hsp90 inhibitor that also increases the CV of size in the population.

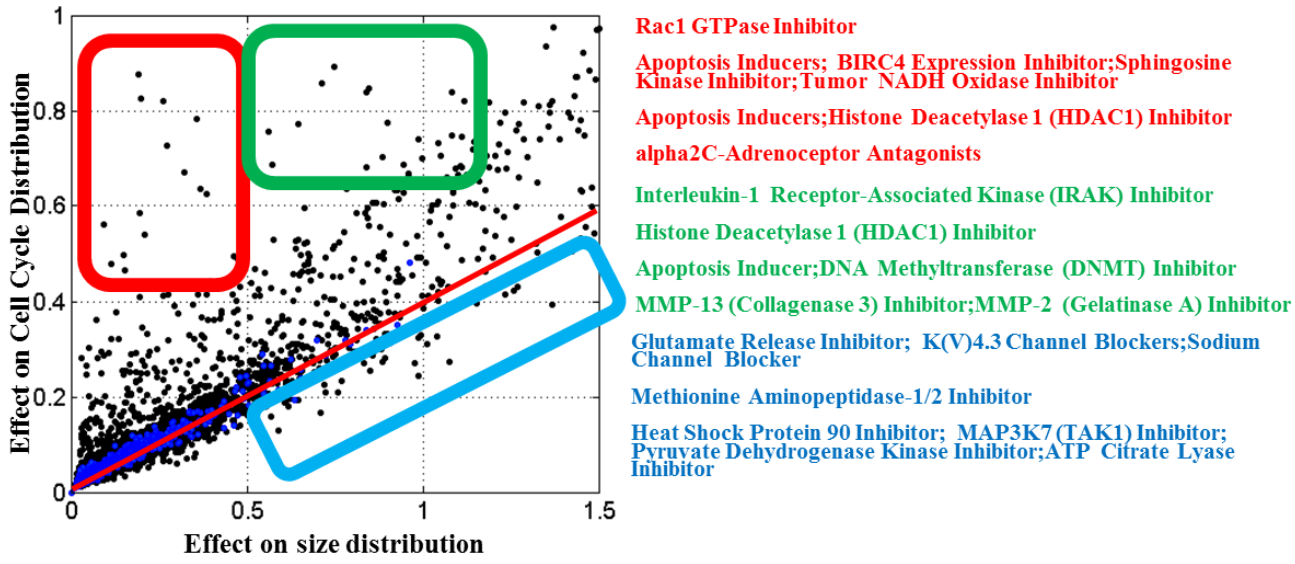

Figure 4.9: Effects of screened compounds on the joint distribution of cell size and cell cycle stage.
(Legend continues on next page.)

Figure 4.9 (continued): The joint distribution of cell cycle stage and cell size from each tested condition was compared to a control distribution from the same plate. Differences between compared distributions were calculated on two axes; (1) the KL divergence between the joint distributions when normalized to cell cycle stage (Change in cell size) and (2) the KL divergence between the two distributions when normalized to cell size (Change in cell cycle stage). Blue dots indicate controls (DMSO). The linear fit (red line) describes a trend existing in control conditions: control wells that are different in distributions of cell size are correspondingly different in the distributions of cell cycle stage. Black points represent difference between the distributions of cell size and cell cycle stage of control wells to distributions of the compound-treated samples.

Applying localized perturbation analysis to identify compounds that perturb coordination of growth and cell cycle.

Our initial data implies mechanisms of cell size regulation that are cell-cycle-stage dependent, suggesting that growth is regulated differently in the different stages of cell cycle. To identify pathways responsible for this coordinated regulation, we looked for compounds with an influence on cell growth that varies depending on cell cycle stage. To that end, we constructed an analysis to statistically establish whether size defects caused by a drug are or biased towards cells that are in a particular cell cycle position. The mathematical procedure involves subtracting the 2D probability densities of pre and post drug treatment size/cell cycle stage distributions and applying local binomial regression or bootstrapping.

To implement this analysis, we started by treating cells with a selection of drugs for just three hours. This was done to make interpretation of the results simpler, since we can assume that cells have not gone far in the cell cycle and more easily identify shifts in the distribution that are caused by altered growth during specific cell cycle stages. The drawback of this experiment is that the size differences caused during this time are small. However, spreading the distribution along the cell cycle axis allows us to detect subtle changes.

Using this method we observed that the catalytic mTOR inhibitor Torin 2[10], for example, results in an overall decrease in cell size that is independent of cell cycle stage (fig. 4.10A). In contrast, rapamycin and GSK3b inhibitor VIII and display perturbations on cell size that are cell-

cycle-stage-specific (fig. 4.10B,C). A short rapamycin treatment decreases the size of S-phase cells more than size of cells in G1 or the G2 phases of cell cycle. GSK3b inhibition seems to increase size variability after but not before G1-exit (i.e. cells are under-represented in the center of the size distribution and over-represented above and below it). This analysis can be expanded for use in the drug screen, with added consideration for cell cycle progression. We are exploring several ways of condensing this type of result into a set of metrics that can be used to cluster drugs or quickly pick out interesting hits.

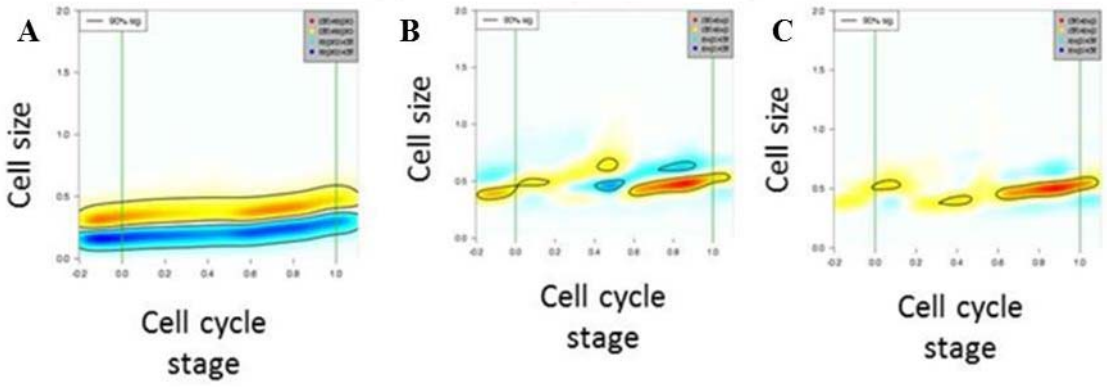

Figure 4.10: Localized perturbation analysis (LPA). Heat maps show regions of the size/cell cycle plane where drugs are over-represented (blue) or under-represented (red/yellow). Black outlines mark regions where the difference between control and drug is statistically significant. Plots are shown for Torin 2 (A), Rapamycin (B), and GSK3b inhibitor VIII (C).

Using perturbed stationary state populations to investigate size control mechanisms

Analysis of the drug screen data is complex, in part due to our uncertainty about whether and how the cell cycle progression of drugged cells has been altered. Short perturbations can reduce this uncertainty somewhat, but often have very small or negligible effects. As a complementary approach, we optimized conditions where cells can proliferate steadily while under the influence of a drug.

As described in chapter two, we found that HeLa cells can proliferate steadily in up to 70 nM rapamycin (fig. 2.5A and fig. 4.11A). They maintain a stable size distribution with a smaller

mean size (measured by SE-A647 staining, figure 2.5B) and volume (measured by Coulter counter, figure 2.5C) than controls. As a comparison, we found stationary-state conditions for inhibition of protein synthesis by cycloheximide (keeping in mind that this also stimulates mTOR activity[11]). Cells can also proliferate exponentially in 60 nM cycloheximide (fig. 4.11B), where they have a longer cell cycle length and maintain the same mean size as controls (fig. 4.11C).

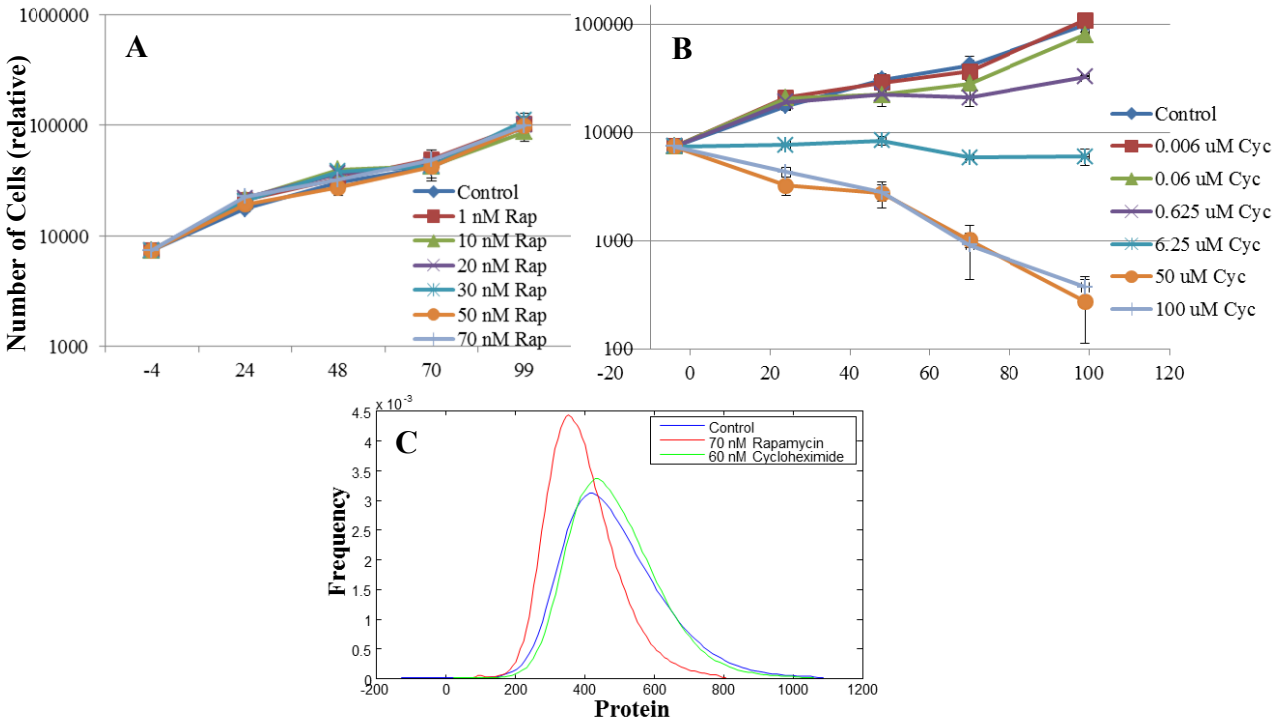

Figure 4.11: Stationary-state proliferation under drug treatment. (A) Proliferation curves (measured by Invitrogen Cyquant assay) for control and rapamycin-treated cells. (B) Proliferation curves for control and cycloheximide-treated cells. (C) Cell size (total protein as measured by SE-A647 staining) distributions of control (blue), rapamycin-treated (red), and cycloheximide-treated (green) cells.

Notably, rapamycin causes a small but reproducible increase in the coefficient of variation of size, while cycloheximide does not. Since we observed normal size-dependent control of G1 length in rapamycin-grown cells (chapter two), we questioned whether rapamycin increases size heterogeneity by disrupting size dependent growth rate regulation. To test this, we used the experiment described in chapter two to measure $CV_{apparent}$ under rapamycin treatment in

HeLa and Rpe1 cells. We found that rapamycin consistently eliminated the first dip in $CV_{apparent}$ in Rpe1 cells (fig. 4.12A-D). In HeLa cells, however, the result varied between experiments (fig. 4.13A-D). Further experiments are needed to resolve this ambiguity and determine if rapamycin-sensitive mTORC1 activity really plays a role in the first phase of growth rate regulation. This would imply that mTOR promotes growth in a size-dependent manner to maintain uniformity.

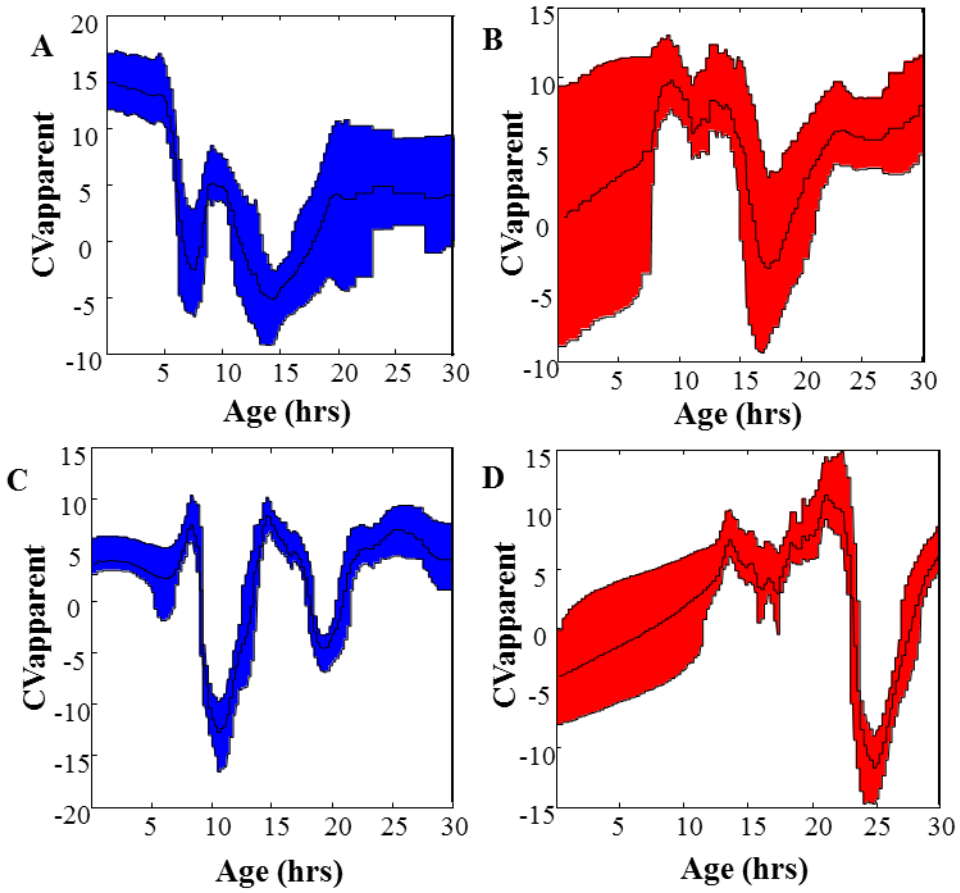

Figure 4.12: Effect of rapamycin on early growth rate regulation. $CV_{apparent}$ as a function of age for Rpe cells grown in rapamycin. Controls (blue) are shown next to the associated rapamycin (red) experiment. Experiments A and B were done side by side, as were C and D.

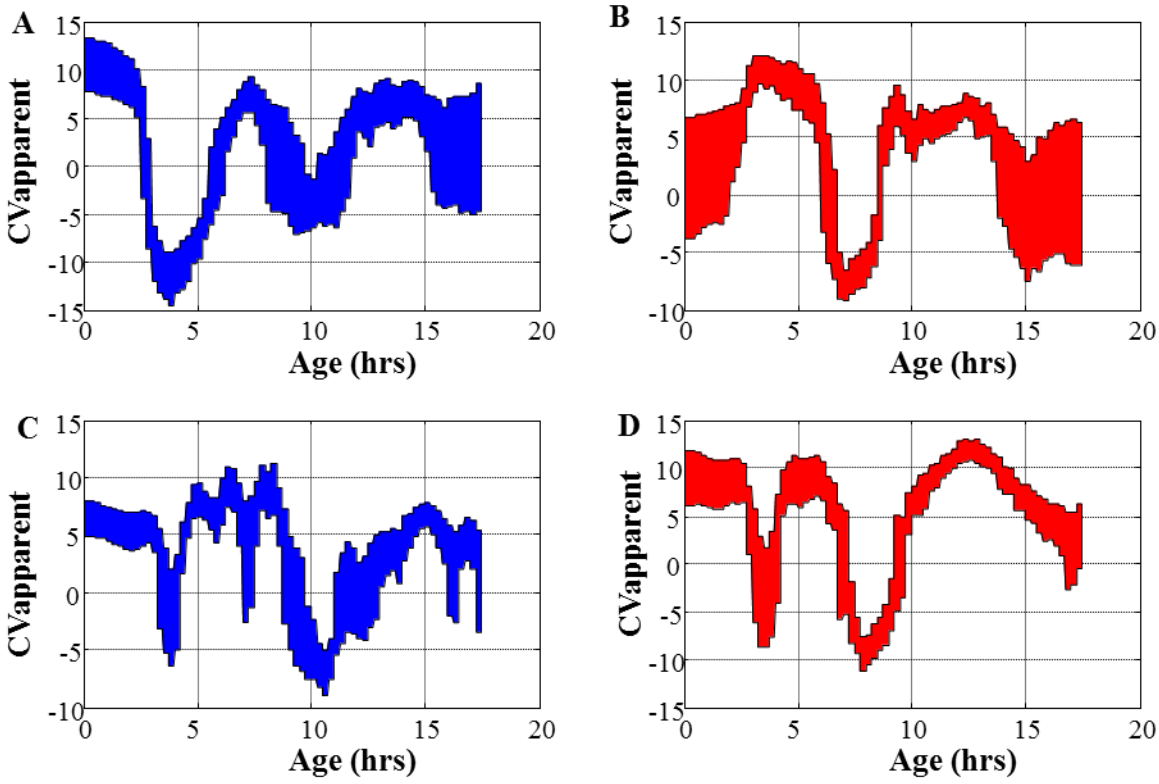

Figure 4.13: Effect of rapamycin on early growth rate regulation. $CV_{apparent}$ as a function of age for HeLa cells grown in rapamycin. Controls (blue) are shown next to the associated rapamycin (red) experiment. Experiments A and B were done side by side, as were C and D.

Discussion

The experiments and analyses described here represent a set of tools with which to probe the regulation of cell size, by quantifying what are often subtle changes in the joint distribution of cell size and cell cycle position. These approaches will be used to identify compounds disrupting size specification in a larger screen done by Novartis, as well as to follow up on the findings presented here. The metrics defined here will be used to further sort the compounds, in order to look for pathways that are enriched in particular sets of "hit" drug targets.

The initial hits also include a number of targets which may lead to interesting avenues of exploration, such as PKC, which was detected in both drug and antibody screens. The PKC family of kinases has diverse biological roles in various cellular events such as cellular growth,

proliferation, differentiation and cell death[12], but its connection to cell size control is unknown. In one of the few reports on the subject, Grumont et al[13] provide evidence that the increase in cell size that accompanies T cell activation is mitigated by the activity of PKCq.

The approaches here can also be used to pursue the question of whether mTOR plays a role in maintaining size uniformity. The comparison of different types of inhibitors (like Torin and rapamycin) is a promising strategy. These treatments may also be combined with antibody staining to monitor the effects of the drug on downstream mTOR effectors.

1. Young, D. W. *et al.* Integrating high-content screening and ligand-target prediction to identify mechanism of action. *Nat. Chem. Biol.* **4,** 59–68 (2008).

2. Young, D. W. *et al.* Integrating high-content screening and ligand-target prediction to identify mechanism of action. *Nat. Chem. Biol.* **4,** 59–68 (2008).

3. Singh, S., Carpenter, A. E. & Genovesio, A. Increasing the Content of High-Content Screening: An Overview. *J. Biomol. Screen.* **19,** 640–650 (2014).

4. Hutz, J. E. *et al.* The multidimensional perturbation value: a single metric to measure similarity and activity of treatments in high-throughput multidimensional screens. *J. Biomol. Screen.* **18,** 367–377 (2013).

5. Sakaue-Sawano, A. *et al.* Visualizing spatiotemporal dynamics of multicellular cell-cycle progression. *Cell* **132,** 487–498 (2008).

6. Wasserman, L. *All of statistics: a concise course in statistical inference*. (Springer, 2004).

7. Wasserman, L. *All of nonparametric statistics*. (Springer, 2006).

8. Cover, T. M. & Thomas, J. A. *Elements of Information Theory*. (Wiley, 2012).

9. IEEE Information Theory Society. *Information theory: 50 years of discovery*. (IEEE Press, 2000).

10. Simioni, C. *et al.* Activity of the novel mTOR inhibitor Torin-2 in B-precursor acute lymphoblastic leukemia and its therapeutic potential to prevent Akt reactivation. *Oncotarget* **5,** 10034–10047 (2014).

11. Beugnet, A., Tee, A. R., Taylor, P. M. & Proud, C. G. Regulation of targets of mTOR (mammalian target of rapamycin) signalling by intracellular amino acid availability. *Biochem. J.* **372,** 555–566 (2003).

12. Reyland, M. E. Protein kinase C isoforms: Multi-functional regulators of cell life and death. *Front. Biosci. Landmark Ed.* **14,** 2386–2399 (2009).

13. Grumont, R. *et al.* The Mitogen-Induced Increase in T Cell Size Involves PKC and NFAT Activation of Rel/NF-κB-Dependent c-myc Expression. *Immunity* **21,** 19–30 (2004).

Chapter 5

Conclusions

We set out to discover the means by which cell size is specified, looking for processes that act to maintain size uniformity in a population. Such processes would require differential regulation of cells sharing the same environment. We have seen evidence that cells autonomously adjust their own size, leading to a controlled behavior of size variance in the population. Surprisingly, cells appear to regulate both their cell cycle length and their growth rate to correct size aberrations. This raises a number of questions, the most obvious being: how does a cell measure its own size? A related question is, what determines the "correct" size for a particular cell type and environment, and how does a cell compare the two? We have developed a number of tools and approaches that may help to answer these and other questions. In this discussion, I will highlight some open questions, clues that our research has yielded, and potential approaches to solutions.

Phenomenology of cell size control

How do growth rate and cell cycle control work together to precisely specify cell size? How important is the relative contribution of each process? We began exploring these questions with a modeling approach, which can be expanded to explore more situations. We are also working on an analytical framework with which to approach these questions. The cooperation of multiple size-control mechanisms is not trivial. For example, if large cells can shrink during G1,

but exit G1 quickly because of their size, the mechanisms can counteract each other. The timing and restrictions of each mechanism's activity have a strong effect on the outcome.

This leads us to an additional question: Is the size-dependent regulation of growth rate linked to cell cycle progression? We repeatedly see indications of two phases of size regulation during the cell cycle: two dips of $CV_{apparent}$ below zero, two dips in the negative correlation between nuclear size and growth rate. This may indicate a cell-cycle dependence of the growth rate regulatory mechanism. However, it is important to keep in mind that the dips represent periods when size regulation is *occurring*, not necessarily when it is *allowed*. For example, if a large contribution to the observed regulation is made by large cells slowing their growth, we might see increased regulation when cells begin to approach larger sizes, which could be some time after birth. This could coincide with late G1, without being connected to cell cycle events. Indeed, several observations suggest that large cells dramatically slow their growth or even shrink. Most obviously, monitoring nuclear growth showed a clear switch from fast to slow growth in the largest cells. We also see depletion of very large Rpe1 cells in S-phase, as well as preferential ubiquitination in large cells in late G1. One way to approach this is to combine these techniques with gentle perturbations as we have begun to do with rapamycin. Another is to synchronize cells based on cell cycle reporters rather than birth and compare those results.

Do the roles of cell growth regulatory pathways change over the course of the cell cycle?

Is growth in different cell cycle stages controlled by different regulatory circuits? Immunostaining of unperturbed cells suggests a cell-cycle dependence of mTORC1 activity and its interaction with cell size. Using short drug treatments, we see that rapamycin slows growth more strongly in S-phase than G1, consistent with the correlation of rpS6 phosphorylation with

cell size that arises during S-phase. A number of other growth perturbations appear to have cell-cycle-specific effects, as well.

Using the approaches we've developed to look at the activation profile of other signaling proteins in growth-regulatory pathways, as a function of cell size and cell cycle progression, will further our understanding of how all of these pathways interact. A first step would be to check if other known regulators show complementary behavior to mTORC1 (such as a strong association with size specifically in G1). Co-staining cells for multiple regulatory signals can be particularly informative. For example, we can ask whether a particular pair of regulators can be active simultaneously in a cell, or if they are mutually exclusive. We can also look at multiple effectors of a single regulator in tandem, such as phospho-rpS6 and phospho-4EBP1. High throughput microscopy allows us to sample rare events, as we did when we looked at small cells with high mTORC1 activity. This can help untangle the roles of co-regulated effectors. For instance, even though rpS6 and 4EBP1 tend to be phosphorylated simultaneously, we can focus on cells at the edge of the distribution that have one but not the other, and ask how they behave.

What links cell size to growth rate and cell cycle progression?

We have developed several methods to screen for possible size-dependent growth regulators, which point to some interesting leads. Perhaps the most obvious question is whether mTOR-driven growth is size-dependent. We observed a weak increase in size variability in rapamycin, and see that it abrogates the first growth rate regulatory phase in Rpe1 cells (subject to the caveat above, that these may not be truly distinct phases). Comparing the effects of other mTOR pathway inhibitors may further clarify the role of mTOR. A possible approach is to use low doses of inhibitors to lower mTOR activity without getting rid of it completely. We can use

antibodies to assess the downstream effects of the inhibitor, in order to "tune" mTOR activity to intermediate levels. We are able to do this with rapamycin (fig. 5.1), which may be a useful tool.

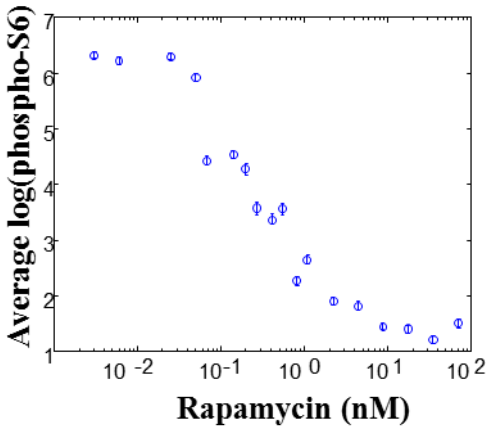

Figure 5.1: Modulating rpS6 phosphorylation with low doses of rapamycin. Cells were treated with a range of rapamycin doses. The average level of phospho-rpS6 in treated cells is plotted (log scale) as a function of dose.

Analysis of the drug and antibody screen data will also provide insight into the links between size, cell cycle, and growth rate, and have already highlighted some potential leads like the PKC pathway and hsp90. In addition to signaling pathways, the screen also includes compounds that affect structural components of the cell. For example, the microtubule stabilizer epothilone B increases variability in size. Cellular geometry may play a role in size measurement, as has been described in fission yeast[1].

Examination of signaling activity in unperturbed populations is an important complement to perturbation approaches. In this case, we might look for signals that are active in cells that "break the rules" of size regulation, such as small cells late in the cell cycle. We can also combine these approaches to see which regulators are responsive to drugs that decrease size uniformity or decouple growth from cell cycle progression.

Perhaps the most interesting question is that of the physiological importance of size uniformity. Studies that have investigated the relationship between cell size and cell function

(surveyed in chapter one) have generally done so by effecting dramatic changes in the mean size of cells in a tissue, with mixed results[2,3,4]. In some cases, changes in size seem to have no effect on cell function. Even in these cases, though, the question of whether it is important for cells in a tissue to be similarly sized has not been addressed. Subtle perturbations that increase the variance in size may be a way to approach this question.

---

[1] S. G. Martin, M. Berthelot-Grosjean, Polar gradients of the DYRK-family kinase Pom1 couple cell length with the cell cycle. *Nature* **459**, 852 (Jun 11, 2009)

[2] G. Fankhauser, Maintenance of normal structure in heteroploid salamander larvae, through compensation of changes in cell size by adjustment of cell number and cell shape. *The Journal of experimental zoology* **100**, 445 (Dec, 1945)

[3] G. Roth, J. Blanke, D. B. Wake, Cell size predicts morphological complexity in the brains of frogs and salamanders. *Proceedings of the National Academy of Sciences of the United States of America* **91**, 4796 (May 24, 1994)

[4] I. Ruvinsky *et al.*, Ribosomal protein S6 phosphorylation is a determinant of cell size and glucose homeostasis. *Genes & development* **19**, 2199 (Sep 15, 2005)

Appendix I

Dynamics extracted from fixed cells reveal feedback linking cell growth to cell cycle

**Ran Kafri[1], **Jason Levy[2], Miriam, B. Ginzberg[1], Seungeun Oh[1], Galit Lahav[1] and Marc, W. Kirschner[1]

[1]Department of Systems Biology, Harvard Medical School, Boston, MA 02115, USA

[2]Department of Mathematics and Statistics, University of Ottawa, Ottawa, ON, Canada K1N 6N5

*Correspondence: marc@hms.harvard.edu

** These authors contributed equally to this work

Author Contributions

R.K. and J.L. developed the method (ERA) for extracting dynamic information and calculating feedback spectra from fixed populations, designed algorithms, wrote all image-processing software and analyzed data. R.K. designed all experiments, and wrote the manuscript. J.L. contributed significantly to all conceptual challenges and to writing the manuscript. M.B.G. contributed conceptually, made important measurements and calculations and contributed to the writing of the manuscript. S.O. provided interferometry-derived cell mass measurements. G.L. and M.W.K. contributed to the formulation of the problem, development of the ideas and the writing of the manuscript.

Abstract

Biologists have long been concerned about what constrains variation in cell size; yet, progress on this question has been slow and stymied by experimental limitations. We describe a new method, ergodic rate analysis (ERA), which uses single cell measurements of fixed steady-state populations to accurately infer the rates of molecular events, including rates of cell growth. ERA exploits the fact that the number of cells in a particular state is related to the average transit time through that state. With this method, one can calculate full time trajectories of any feature that can be labeled fixed cells, for example levels of phospho-proteins or total cellular mass. Using ERA we find evidence for a size-discriminatory process at the G1/S transition that acts to decrease cell-to-cell size variation.

Introduction

Size is an obvious and distinguishing feature of cells, characteristic of their physiology and pathology. A barrier to studying size control in mammalian cells is the inaccuracy in measuring size, growth rate, and the dynamics of pathways controlling growth and proliferation. To overcome these obstacles, we developed ergodic rate analysis (ERA), a procedure for extracting dynamics and regulatory relationships from a single image of a population of individual fixed cells. ERA makes use of the fact that, at steady state, the number of cells in any particular molecular state is related to the rate at which cells transit through that state. Using this method, we calculated the dynamics of cell growth and cell cycle progression and investigated the processes that limit size variation.

Results

Precise cell cycle dynamics from a single image of fixed cells

Unsynchronized proliferating cells are often found to be in a quasi-steady state, in which the proportion of cells in each phase of the cell cycle is stable (fig. 6.1). We determine cell cycle position by measuring the levels of both DNA and a fluorescent reporter of the Geminin degron (mAG-hGem) [1]. In the context of the present study, mAG-hGem serves as a marker for activity of anaphase promoting complex (APC). The scatter plot in figure 6.1 demonstrates the well-known decrease in APC activity in late G_1 (resulting in mAG-hGem accumulation), which is followed by doubling of DNA in S-phase. Reactivation of APC at mitosis results in a sharp fall in mAG-hGem fluorescence followed by cytokinesis where DNA levels drop by one half (fig. 6.1).

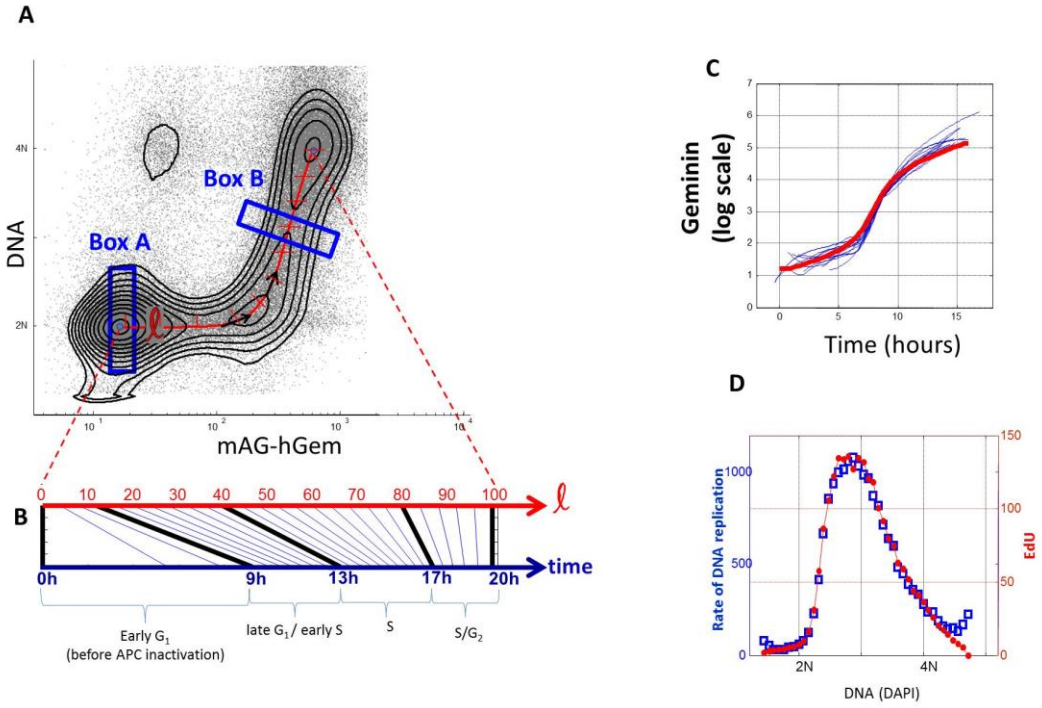

Figure 6.1: Dynamic information from static data using ERA. (**A**) Levels of DNA (DAPI) and Geminin (mAG-hGem) in an unsynchronized, exponential population of HeLa cells. (Legend continues on next page.)

Figure 6.1 (continued): The black contour lines denote the distribution, *f*, of cells within the DNA/Geminin plane. Also shown is the average cell cycle trajectory, *l*, (red). The different densities of cells in boxes A and B result from the different rates at which cells traverse those regions. (**B**) The transformation of the cell cycle axis, *l*, to a real time axis. For convenience we chose 100 units of *l* to represent a complete path from the beginning of G_1 to the end of G_2. Comparison of ERA with direct dynamical measurements (**C-D**). (**C**) Accumulation of Geminin (mAG-hGem) was followed in 10 individual live cells by time lapse microscopy (blue lines) and compared to the dynamics of mAG-hGem calculated from fixed cells using ERA (red). (**D**) DNA replication rate was measured by exposing cells to a 20 min. pulse of EdU (5-ethynyl-2′-deoxyuridine, Invitrogen) prior to fixation. Average levels of EdU fluorescence per cell (indicating rate of DNA replication) are plotted (blue) as a function of DAPI, giving a measure of the mean rate of DNA replication as a function of passage through S. For comparison, ERA was used to calculate DNA replication rates directly from fixed cells not treated with EdU (red).

For populations 12 hours post fixation that have not reached confluence, the distribution, *f*, of cells in the plane defined by these two measurements is independent of the time at which cells were sampled and fixed, as shown in the supplementary material. The existence of a stationary state condition imposes a quantitative relationship between the proportion of cells in different regions of the plot and the rates of molecular events (i.e. changes in DNA and APC activity). For example, in figure 6.1, because every cycling cell passes through the labeled regions A and B, the higher cell count in region A must mean that cells traverse this region at slower rates than in region B (see Box 6.1).

Box 6.1: The ERA Balance Equation.

ERA rests on the fact that at steady state the difference, $-N_t del\cdot(fv)$, between the rates at which cells enter and leave any given molecular state must be balanced by the increase in cell count in that state. N_t is the total number of cells in the population at time t, f is the proportion of cells in the given state (indicated by the black contour lines in Fig 1), and v is the rate at which cells pass through that state. Since f does not change with time, the number of cells at any given state as a function of time is $fN_t = f_{N0}e^{\alpha t}$. These considerations result in a simple balance equation:

$$-\bigtriangledown\cdot(fv)+B=\alpha f \quad \text{(Eq. 6.1)}$$

where α is the proportion of cells dividing per unit time and B is a term accounting for cell division (see Supplementary material). As we will show, Eq. 6.1 can be used to derive accurate

time profiles from a single measurement on a population of fixed cells. If more parameters are measured, the dimensionality of the plot increases but the analyses remain the same.

Eq. 6.1 is free of any mechanistic assumptions or free variables and is grounded only on a basic conservation principle akin to conservation of mass. Eq. 6.1 and its implementations throughout this study are based on two main assumptions outlined in detail in the Supplementary material: the first is that the representation axes (which in the present study are DNA and APC activity) appropriately represent both individual and collective cell behavior and the second is that the steady state assumptions described above apply.

Reduction in dimensionality.

Our goal in this study was to use Eq. 6.1 (Box 6.1) to determine the growth rate of cells at different points in the cell cycle, in other words to solve for *v*. To solve Eq. 6.1 we reduced the number of dimensions from DNA (1st dim) and APC/C activity (2nd dim) to a single dimension, *l*, representing cell cycle progression over time (see Box 6.2). While *l* is not directly measured, it can be calculated from *f,* which is obtained experimentally (see Supplementary material). Figure 6.1A shows *l* (red curve) superimposed on the single cell measurements.

Box 6.2. Reducing the dimensionality of Equation 1.

Confining Eq. 6.1 to the cell cycle trajectory, *l*, and integrating results in an expression (Eq. 6.2) that relates measured probability density, *f*, to the rate, ω, of progression through the cell cycle, we have:

$\omega(l) = \alpha*(2\text{-}F(l)/f(l)$ (Eq. 6.2)

where $F(l) = {}_1^{l}\int f(l)\, dl$. Furthermore, since $\omega(l) \equiv dl/dt$, we can use results of Eq. 6.2 to calculate a complete time axis for the dynamics of the measured processes using: $t(l_0) = {}_{l=1}^{l0}\int 1/\omega\, dl$ (Eq. 6.3)

where $t(l_0)$ is the time it takes for cell starting at position l=1 (G1) to reach position l_0 on the cell cycle axis, l. As shown in figure 6.1, Equations 6.1-6.3 transform a single, non-temporal, measurement on fixed cells into temporal trajectories represented on time axis, t. Fig 6.1B shows the non-linear transformation (the ERA transform) of a path, l, defined by molecular events, onto a time axis. We conveniently chose 100 units of l to represent a complete path from G_1 to G_2. We do not include M (metaphase) in this analysis since the number of cells in M is very small. Real time enters this calculation through the doubling time of the population, $\tau = \frac{log(2)}{\alpha}$.

For solutions of ERA in more than 2 dimensions see supplementary material.

Comparison of ERA with direct measurements.

Fig. 1C compares mAG-hGem dynamics of live cells obtained from time lapse microscopy to dynamics of fixed cells calculated by ERA. There is near perfect agreement. To further demonstrate the utility of ERA, we compared the rate of DNA replication obtained by labeling live cells with EdU to the rate of DNA replication obtained by ERA of DAPI stain intensity in fixed cells (Fig. 1D). As with the previous example, we obtained a striking overlap between the measurements. Both examples demonstrate that ERA calculations can resolve dynamics on the order of minutes.

Cell growth dynamics during the cell cycle

We quantified the protein mass of individual cells by measuring the total fluorescence intensity from cells stained with a succinimidyl ester dye (SE-A647), which covalently reacts with lysyl groups. This is a good measure of protein mass[2] and correlates well with physical measurements of dry mass by quantitative phase microscopy (QPM), whose accuracy is better than 1%[3] (fig. 6.2C). From these measurements, we assembled a 3-dimensional single-cell dataset simultaneously reporting cell size and cell cycle stage for millions of fixed cells (fig 6.2 A,D,E). As expected, our data demonstrates an approximate doubling in protein fluorescence in a single cell cycle (Figure 6.2B).

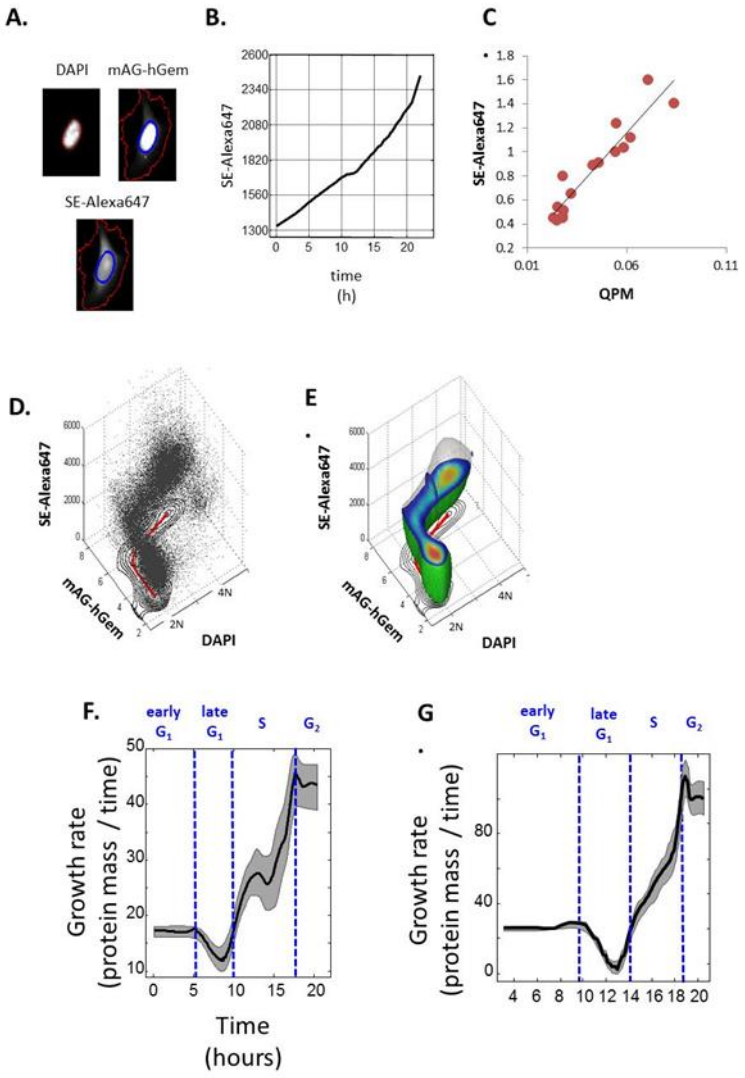

Figure 6.2: Calculation of growth as a function of cell cycle progression using ERA. (A) Cells were stained and imaged for DNA content (DAPI), the geminin degron (mAG-hGem) and for protein content (succinimidyl ester-Alexa 647 (SE-A647)). (B) Growth during cell cycle progression, computed by ERA. (C) Comparison of SE-A647 fluorescence intensity with quantitative phase microscopy measurements in single cells. Each data point represents a single cell measured for both protein content (SE-647) and phase retardation (QPM). (**D**) A scatter plot for the levels of DNA (DAPI) Geminin (mAG-hGem) and cell size (SE-A647) in an unsynchronized population of HeLa cells. Also shown is the projection of the 2-dimensional distribution of Geminin and DNA overlaid with l. (**E**) The 3-dimensional probability distribution from the data shown in 2D (**F**, **G**) Growth rate versus time for HeLa (F) and RPE1 (G) calculated by ERA. Confidence intervals are shown as described in Supplementary material.

For four very different cell lines the growth in mass during the cell cycle, as calculated by ERA, produced very similar trajectories that are neither linear nor exponential (fig 6.2F, 6.2G and Supplementary material). The results show that growth rates increase with progression in cell cycle and reach a maximum during G_2, consistent with a recent study using QPM[4]. What is

novel is a transient slowdown in protein accumulation rate at the G_1/S transition in all cell lines (fig 6.2 F-G). Since this slow down occurs for a relatively short time, it is not surprising that it was not detected in previous time course measurements on synchronized populations. Further, by aligning cells using molecular markers of cell cycle progression rather than time, ERA avoids the clouding effects of imperfect synchronization. Plots of growth rate as a function of mass are similar to those obtained recently with the suspended microchannel resonator[5] (supplementary material).

Feedback between growth and proliferation.

The existence of stable and narrow distributions of cell size suggests cell-autonomous feedbacks controlling size variability. To search for such feedbacks we calculated the joint dependency of growth rate, v, on size, s, and cell cycle position, l (fig. 6.3). The size distribution within any interval along the cell cycle path l, $\Delta_\ell = (\ell - w, \ell + w)$, is governed exclusively by (fig. 6.3): (i) the size distribution of cells entering the interval from the previous cell cycle stage, (ii) the size distribution of cells leaving the interval into a later cell cycle stage, and (iii) cell growth within the interval. Such a formulation allows the construction of a 3-term balance equation relating growth rate to cell size within the interval (see Box 6.3).

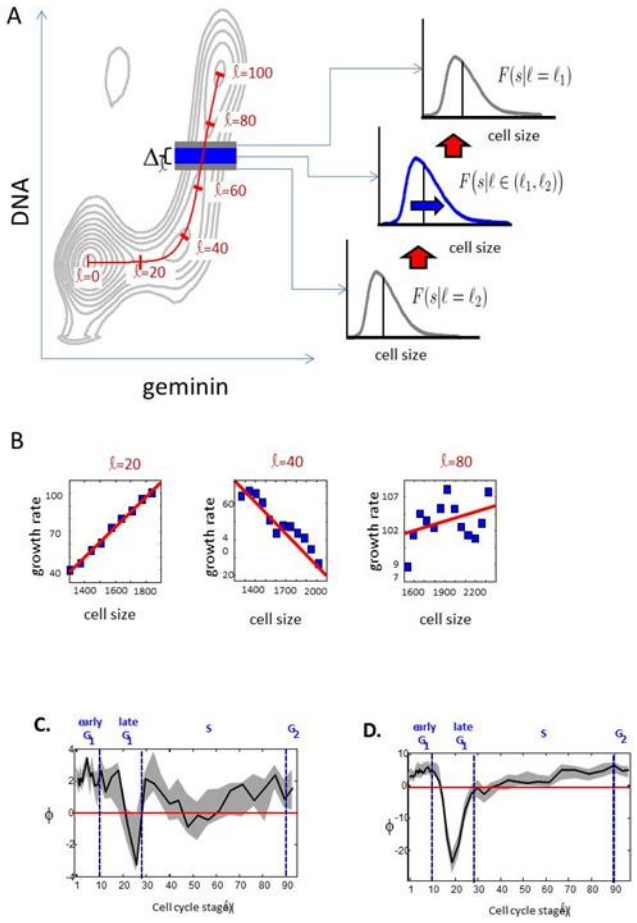

Figure 6.3: Rate of cell growth as a function of size and cell cycle. Size discrimination at the G1/S transition. (**A**) Calculation of growth rate as a function of size for a defined interval, Δ_l, on the cell cycle axis, l. To calculate feedback regulation as a function of cell size, the size distributions of cells entering and leaving Δ_l are estimated from the sizes of cells on the boundary of Δ_l. (**B**) Plots of growth-rate vs. cell-size at late G_1 ($l = 20$), the G_1/S transition ($l = 40$) and late S-phase ($l = 80$). (C,D) The slope, ϕ, of growth rate vs. cell size plotted as a function of l, for (C), HeLa cells and (D), RPE1 cells. The red horizontal line positioned at $\phi = 0$ is added to emphasize the distinction between positive and negative slopes (positive and negative feedbacks). Blue vertical lines demarcate borders between different stages of cell cycle. Confidence intervals are in gray.

Box 6.3. Analyzing growth as a function of size.

To obtain the size distributions of cells entering and leaving a given interval we consider the size distributions of cells positioned at the borders of that interval (fig. 6.3A). These distributions are formally approximated by the conditional probability distributions, $F(s \mid \ell - w)$ and $F(s \mid \ell + w)$, where $F(s \mid \ell - w)$ is the cumulative probability distribution of cell size, s, among cells in the

state $\ell - w$ at the entrance to the interval $\Delta_\ell = (\ell - w, \ell + w)$, and similarly with $F(s \mid \ell + w)$. The width, $\Delta\ell = 2w$, represents the resolution limit of the calculation. Using this construction we obtain an equation for the rate of cell growth as a function of cell size:

$$v(s, \Delta\ell) = \alpha \frac{(2 - \lambda_A)F(s \mid \ell - w) - (2 - \lambda_A - \lambda_B)F(s_0 \mid \ell + w) - F(s \mid \Delta\ell)\lambda_B}{f(s \mid \Delta\ell)\lambda_B} \quad \text{(Eq. 6.4)}$$

Where $F(s \mid \Delta_\ell) = F\big(s \mid (\ell - w, \ell + w)\big)$ is the size distribution within the interval , Δ_ℓ, λ_A is the fraction of cells occupying all cell cycle stages preceding Δ_ℓ, and λ_B is the fraction of cells in Δ_ℓ. We use the notation *F* and *f* to refer to cumulative and non-cumulative probability distributions, respectively. To further evaluate how the growth-rate/cell-size dependency relates to cell cycle progression, we translate $_l$ along the cell cycle axis and repeatedly solve Eq. 6.4 for all points on *l*.

Figure 6.3B plots how growth rate, v, depends on cell size, s, at three different points in the cell cycle; late G_1 (*l*=20), the G_1/S transition (*l*=40) and late S-phase (*l*=80). A surprising result of this analysis is the shift to a negative slope of growth rate versus cell size for cells around the G_1/S transition (see slope for *l*=40). This negative slope is surprising as it implies that at this point small cells have higher growth rates than larger cells. This cell-size dependent growth rate implies a negative feedback linking growth rate to cell size, effectively constraining cell-to-cell size variability in the population.

Figures 6.3A & 6.3D show the slope, ϕ, of the growth rate vs. cell size as a function of the cell cycle progression axis, *l*. A positive ϕ implies that larger cells have higher growth rates than smaller cells, while negative ϕ implies the opposite; ϕ = 0 indicates that growth is

independent of cell size. Calculating ϕ for four different cell lines (fig. 6.3A, 6.3D and supplementary material) yields feedback spectra that consistently acquire negative values at the G_1/S transition.

The strict interpretation that cell size negatively feeds back on growth rate at G_1/S depends on the assumption that progression along *l* is independent of cell size (see supplementary material). This is not the only possibility. An alternative interpretation is that size variation is limited not by repressing the growth rate of large cells but by inhibiting the rate at which small cells progress along the cell cycle. Whichever of these interpretations is correct, Eq. 6.4 identifies fingerprints of a cell-size discriminatory process, occurring at the G1/S transition, that distinguishes small and large cells and results in an increase in the homogeneity of cell size in the proliferating population. These results support very early findings suggesting cell size regulation at the G1/S transition[6].

To test further whether growth at G1/S is different for large and small cells, we treated HeLa cells for one hour with a proteasome inhibitor (MG132), a translation inhibitor (cycloheximide), or an mTOR inhibitor (Rapamycin). If growth rates and cell cycle progression were independent of cell size, both large and small cells would be equally affected by any treatment. Our results show that MG132 increased the variation in the size of cells at G_1/S. (Fig. 6.4B). Cycloheximide had the opposite effect (Fig 6.4C). mTOR inhibition also decreased cell-to-cell size variability, but to a lesser extent than cycloheximide (Fig 6.4D). These results suggest that the decrease in cell size variance is at least partially driven by a cell-size discriminating proteasome activity. The possibility that size variation is further controlled by size dependent translation activity seems less likely in light of the decreased size variation following cycloheximide treatment.

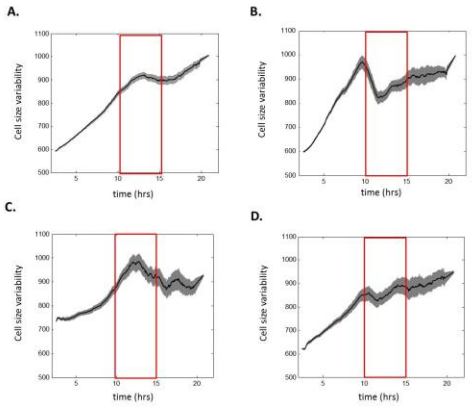

Figure 6.4: Cell size variability (full width/half maximum) as a function of cell cycle time for HeLa cells incubated for 1hr with (A) 0.001 v/v Dimethylsulfoxide; (B); 1uM cycloheximide; (C); 10uM MG132; (D) 100nM rapamycin. Confidence intervals are shown in gray.

Discussion

Proliferating cells in an unsynchronized population are distributed among different molecular states (i.e. cell cycle stages). In situations where this distribution does not change with time and where individual cells shift from state to state in a defined sequence, it is possible to calculate dynamical features from simple static single cell measurements[7,8] which may be obtained from microscopy or flow cytometry.' We have showed that both our primary measurements and the functions derived from them are time-invariant (see Supplementary material), thereby meeting these criteria. Others[9] previously suggested that data from fixed cells could, in principle, be used to extract dynamic information; we have now provided an explicit mathematical framework to make this analysis possible. Using ERA we show that cell-to-cell size variation is regulated by a negative feedback at the G1/S transition. We can also use ERA to characterize other dynamic processes that cannot in general be measured in real time in living cells, such as the temporal changes in phosphoproteins during the cell cycle (supplementary material)

Methods Summary

Reagents, cells and antibodies are described in the supplement. Cells were plated and fixed at 10^5 cells per ml in 15cm dishes. They were fixed in paraformaldehyde, permealized and stained with 0.04 ug/ml succinimidyl ester linked Alexa dyes diluted in DMSO (Alexa Fluor 647 carboxylic acid, succinimidyl ester, Invitrogen, A-20106). Slides were imaged on a with a Nikon Ti Inverted Fluorescence Microscope with Perfect Focus controlled by Nikon Elements software. We used the scan-slide function to image the full area of the slide at 20X magnification. Image analysis was performed with custom written software (EnsembleThresher). The details of the software and the calculation of the ERA parameters are discussed in detail in the supplement.

Acknowledgements

We thank Allon Klein, Yifat Merbl, Shay Tal and Jared Toettcher for consistent and valuable insights at the beginning of and throughout this project. We thank Jennifer Waters and the staff of The Nikon Imaging Center at Harvard Medical School for help and support. We especially thank Rebecca Ward for her critique of the paper and the National Institute of General Medical Sciences (GM26875) for support of this work.

1 Sakaue-Sawano, A. *et al.* Visualizing spatiotemporal dynamics of multicellular cell-cycle progression. *Cell* **132**, 487-498 (2008).

2 Mitchison, J. M. *The biology of the cell cycle*. 128 (University Press, 1971).

3 Popescu, G. *et al.* Optical imaging of cell mass and growth dynamics. *Am J Physiol Cell Physiol* **295**, C538-544 (2008).

4 Mir, M. *et al.* Optical measurement of cycle-dependent cell growth. *Proc Natl Acad Sci U S A* **108**, 13124-13129 (2011).

5 Son, S. *et al.* Direct observation of mammalian cell growth and size regulation. *Nat Methods* **9**, 910-912 (2012).

6 Killander, D. & Zetterberg, A. A quantitative cytochemical investigation of the relationship between cell mass and initiation of DNA synthesis in mouse fibroblasts in vitro. *Exp Cell Res* **40**, 12-20 (1965).

7 Collins, J. F. & Richmond, M. H. Rate of growth of Bacillus cereus between divisions. *J Gen Microbiol* **28**, 15-33 (1962).

8 Tzur, A., Kafri, R., LeBleu, V. S., Lahav, G. & Kirschner, M. W. Cell growth and size homeostasis in proliferating animal cells. *Science* **325**, 167-171, (2009).

9 Jacobberger, J. W., Avva, J., Sreenath, S. N., Weis, M. C. & Stefan, T. Dynamic epitope expression from static cytometry data: principles and reproducibility. *PLoS One* **7**, e30870 (2012).

Appendix II

Force exerted along the length of astral microtubules contributes to spindle centering

Miriam Ginzberg, Sophie Dumont, Tim Mitchison

Abstract: The position of the mitotic spindle is regulated to ensure proper segregation of components between daughter cells. Several models for mammalian spindle positioning via astral microtubules (MTs) have been proposed, including anchored motor proteins pulling at MT tips or along MT sides. To probe forces acting on astral MTs, we used laser ablation to detach individual astral MTs from the spindle in symmetrically-dividing Ptk2 cells and monitored subsequent movement of the severed MT fragments by confocal microscopy. Upon release from the spindle, in both metaphase and anaphase, astral MTs move outward toward the cell boundary, demonstrating that astral MTs exert an outward-directed pulling force on the spindle. Released MT velocities of up to 2 μm/s are observed, consistent with dynein-driven movement. Furthermore, long MTs are often observed to buckle against the cell cortex, when they reach the cell boundary, indicating that the MTs are driven outward by forces exerted along their sides. These results support a model in which the spindle is centered by length-dependent pulling forces exerted by dynein along astral MTs.

Introduction

The position of the spindle within a mitotic cell plays a key role in cell division and is tightly regulated in most cell types. In animal cells, the spindle position during anaphase dictates the location of the cleavage plane, which will perpendicularly bisect the spindle midzone.[1] In most mitoses, the spindle is maintained at the cell center, resulting in symmetric cell cleavage and two equally sized daughter cells. Spindle-centering deficits are often found in cancer cells displaying numerical chromosomal instability.[2, 3]

Spindle centering requires dynamic astral microtubules (MTs)[4]. Based on observations in various cell types, several plausible microtubule-based centering mechanisms have been proposed[4]. In the fission yeast S. pombe, MTs with minus ends anchored at the nucleus (analogous to astral MTs in the spindle) grow outward to the cell cortex, and MT polymerization against the cortex produces an inward pushing force at the nucleus. A symmetric distribution of microtubules about the nucleus, along with a probability of MT catastrophe that grows with MT length, ensures that the net force keeps the nucleus in the cell center (fig. 7.1A)[5]. This mechanism is not likely used in cells much larger than the 14 μm yeast cell, since long MTs buckle under compressive loads, making them inefficient pushing-force producers[4], unless astral

MTs are reinforced by interactions with the surrounding cytoskeleton.[6]

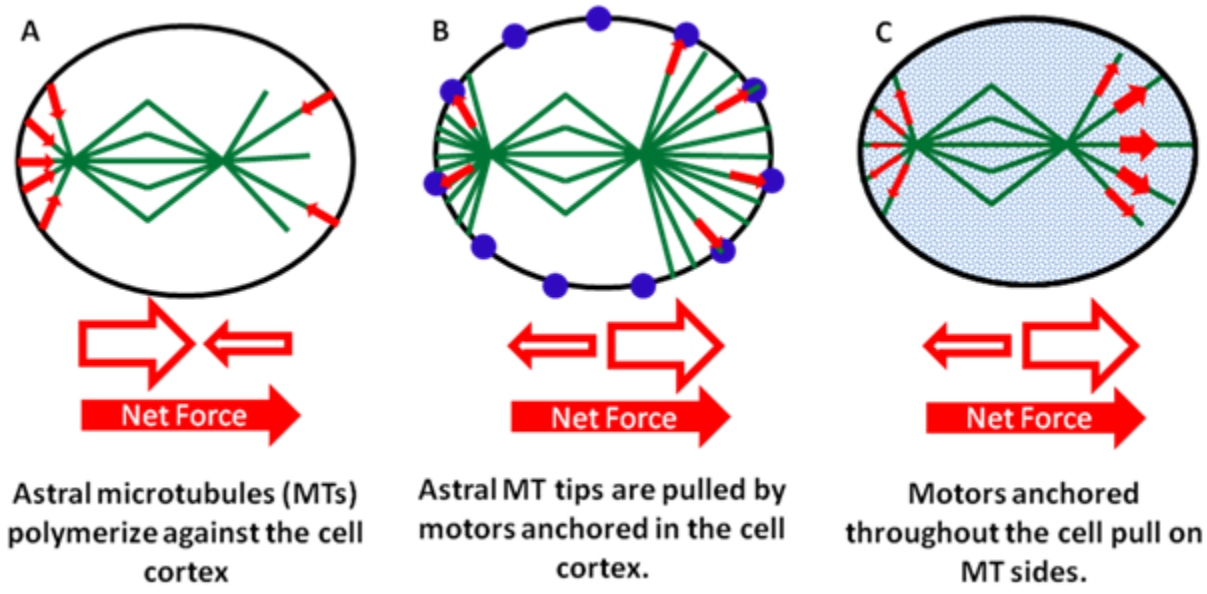

Figure 7.1: Several proposed spindle-centering mechanisms. In each case, forces on individual astral MTs (small red arrows) combine to produce a net force (large arrows below cells) moving the spindle toward the cell center. Blue dots symbolize motor proteins. (A) Astral MTs push against the cell boundary. If the spindle is close to one side of the cell, more MTs on that side will reach the cell edge, causing a net force directed toward the center. (B) Pulling at astral MT tips. If there are a limited number of motors available, symmetrically distributed about the cell boundary and "saturated" by astral MTs, an off-center spindle will experience a net force toward the cell center, since more motors will be pulling it from that direction. (C) Length-dependent pulling on astral MTs. The force applied by a MT is proportional to its length. An off-center spindle will be experience a net force toward the cell center, since MTs extending in that direction will be longer than those extending in other directions.

Mammalian cells require dynein, in addition to dynamic astral MTs, for accurate spindle centering, suggesting that their astral MTs are pulled, rather than pushed[7]. Experiments done in NRK cells indicate that symmetrically dividing mammalian cells continuously monitor and maintain their spindles at the cell center. If the shape of a cell is changed during metaphase or anaphase, the spindle will migrate to the new cell center in a dynein- and astral-MT-dependent fashion, indicating that the centering mechanism is active throughout mitosis[7].

Based on their studies of asymmetric spindle positioning in the C. elegans embryo, Grill and Hyman proposed a spindle-positioning mechanism in which cortically localized minus-end motors trap and pull on astral MT plus ends[8]. Each captured MT exerts the same amount of pulling force on the spindle, regardless of MT length, since pulling only occurs at the MT tip. If

every astral MT tip is trapped by a cortical motor, an off-center spindle will experience no net force, because astral MTs are symmetrically distributed about the spindle. However, if there are a limited number of cortical pulling sites evenly distributed about the cortex, an off-center spindle will be pulled toward the cell center (fig. 7.1B). If the cortical pulling sites are unevenly distributed, the spindle will be positioned asymmetrically[9]. In the case of the C. elegans embryo, the asymmetrically distributed protein GPR1/2 binds to both cortically-localized Gα and to LIN-5, which recruits the LIS-1/dynein/dynactin complex and creates a functional cortical pulling site[10].

While cortical GPR1/2-dependent forces pull spindles towards the posterior cortex to generate asymmetry in the first division of the C. elegans zygote, the earlier centration of the male pronucleus is likely achieved by a different type of positioning mechanism. Kimura and colleagues argued that endosome- and lysosome-bound dynein exerts force along the length of MTs in the pronucleus-associated aster and is responsible for movement of the pronucleus toward the cell center[11]. Evidence for pulling forces acting along the length of astral MTs has also been obtained from a number of other embryonic systems. In echinoderm zygotes, sperm pronuclei move in the direction of the longest MTs[12], and forces acting on centrosomes in physically deformed embryos can be fit by a model in which pulling force increases with microtubule length[13]. In frog and fish embryos, centrosome movements depend on dynein and also tend to occur in the direction of the longest MTs[14].

These observations can be explained if minus-end motors anchored throughout the cytoplasm exert a pulling force all along the length of astral MTs. Since longer MTs will interact with more motors, astral MTs will exert a force on the aster (or on the spindle in mitotic cells) that is proportional to their length. The length of astral MTs is limited by the cell boundary,

resulting in a net pulling force toward the cell center (fig. 7.1C)[14]. In flat cells, where astral microtubules grow along the basal cell cortex, the centering force can be provided by cortically localized motors pulling on MT sides. In contrast to the "pulling at MT tips" mechanism described above, this "pulling along MT length" mechanism requires a high density of cortical motors, rather than a limited number of cortical pulling sites.

Most work on spindle position and orientation in mammalian tissue has focused on MT-tip pulling sites at the cell border, such as dynein anchored at adherens junctions[15]. These studies have revealed the role of MT-tip-pulling in asymmetric divisions in polarized cells. For example, in neuroepithelial progenitor cells LGN (a mammalian homologue of GPR1/2) links cortically localized Gα to the spindle protein NuMA, which in turn can bind to dynein/dynactin to create a cortical MT-pulling site which orients the spindle[13,16].

The spindle-positioning strategy employed by symmetrically-dividing cells is less clear. Recent work by Collins et al revealed that cell-cycle-dependent regulation of cortical dynein and dynactin are critical for spindle pole positioning and symmetric cell division in LLCPK1 cells[17]. However, whether a MT-tip-pulling mechanism alone can robustly center the spindle within the cell is unknown. Additionally, the possibility that a generalized pulling force active throughout the cell applies tension on astral MTs hasn't been well explored. To probe the nature of forces acting on astral MTs throughout mitosis, we used laser ablation to generate free MT fragments in a controlled manner and monitored the movement of the fragments upon release from the spindle. This technique allowed us to compare the force acting on MTs at various positions in cell, and also to observe how these forces change with cell cycle progression.

Results

Astral MTs are under tension and are pulled toward the cell periphery.

Laser ablation assay probes force on individual MTs

As the example in fig. 7.2 demonstrates, Ptk2 cells center their spindles and align them with the long axis of the cell prior to cell cleavage. Laser ablation was used to detach individual astral MTs from the spindle, or interphase array, in Ptk2 cells expressing GFP-tubulin. After laser cutting of microtubules, the newly-created plus ends quickly depolymerized, while the minus ends were stable, leaving the resulting microtubule fragments detached from the centrosome (fig. 7.3). Plus-end depolymerization allowed us to identify MT severing and exclude cases where the MT was photobleached but not truly cut. After ablation, subsequent movement of the MT fragments was observed by spinning-disk confocal microscopy. In the interphase cell shown in figure 7.3, the MT fragment does not move, indicating that it experiences no net force.

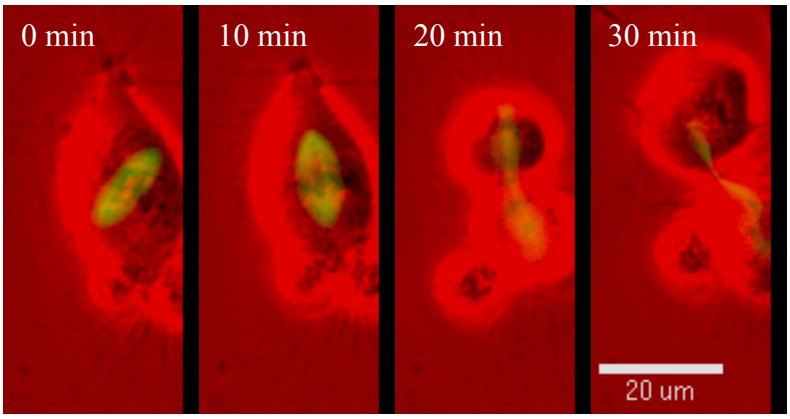

Figure 7.2: The spindle is positioned at the cell center and aligned with the cell's long axis. A representative example of a Ptk2 cell, where the mitotic spindle is centered and its long axis is aligned with the long axis of the cell prior to cytokinesis.

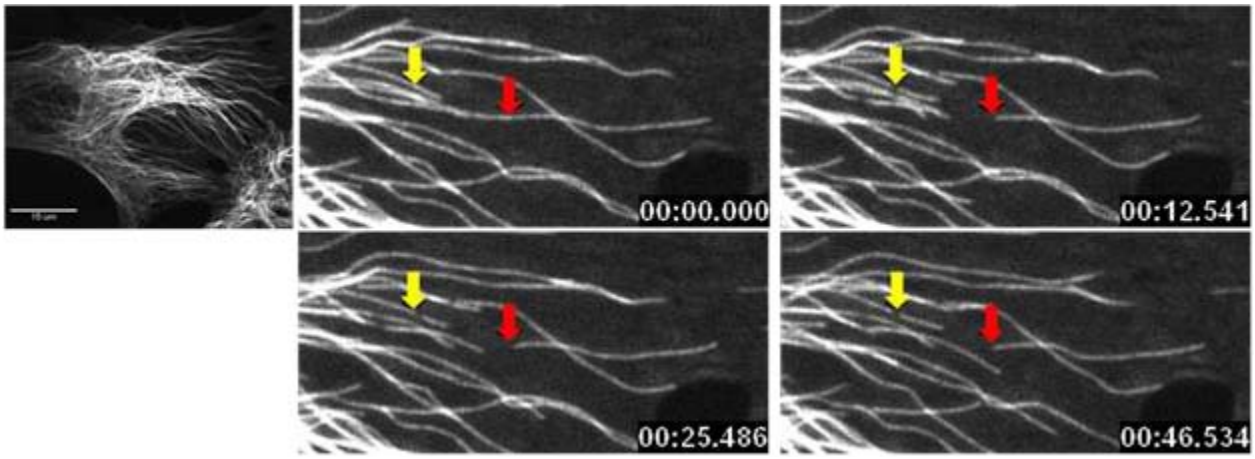

Figure 7.3: Laser ablation is used to generate free MT fragments within the cell. A MT is severed in an interphase cell. Red arrow indicates ablation site. Severing of the MT is confirmed by rapid depolymerization of the newly-generated plus end, while the newly-generated minus end remains stable. The yellow arrow indicates a site where the MT was photobleached, but not severed.

Astral MTs are transported away from the spindle upon release from the spindle pole.

In contrast to the interphase example in figure 7.3, in mitotic cells, severed astral MTs move away from the spindle (fig. 7.4 and table 7.1). This indicates that the astral MTs are under tension and exert a pulling force on the spindle. Severed MTs moved outward along the basal cortex of the cell with their plus ends leading, at speeds ranging from 20-140 um/min, which is consistent with dynein-driven movement (and too fast to be the result of MT treadmilling). Most MTs stay the within the imaged confocal plane, suggesting that cortically-anchored dynein is responsible.

Figure 7.4: A cell-edge-directed pulling force acts on astral MTs. (A) Representative example of a severed astral MT moving away from the spindle. Top left panel shows the whole spindle in a metaphase cell. Subsequent panels (close-up images of the upper spindle pole) are selected frames from a movie of the spindle pre- and post-ablation. The yellow arrow points to the severed MT. Scale bar 9 um. (B) In a metaphase cell, a non-kinetochore MT extending inward from the spindle pole is pulled toward the cell edge upon detachment from the spindle. (C) The results presented in (A) and (B) demonstrate that the direction of the force acting on a MT is determined by MT orientation. Both astral and interpolar MTs are pulled toward their plus ends. (D) A severed astral MT and (E) non-kinetochore interpolar MT in anaphase cells also move toward the cell periphery.

Figure 7.4 (continued)

A

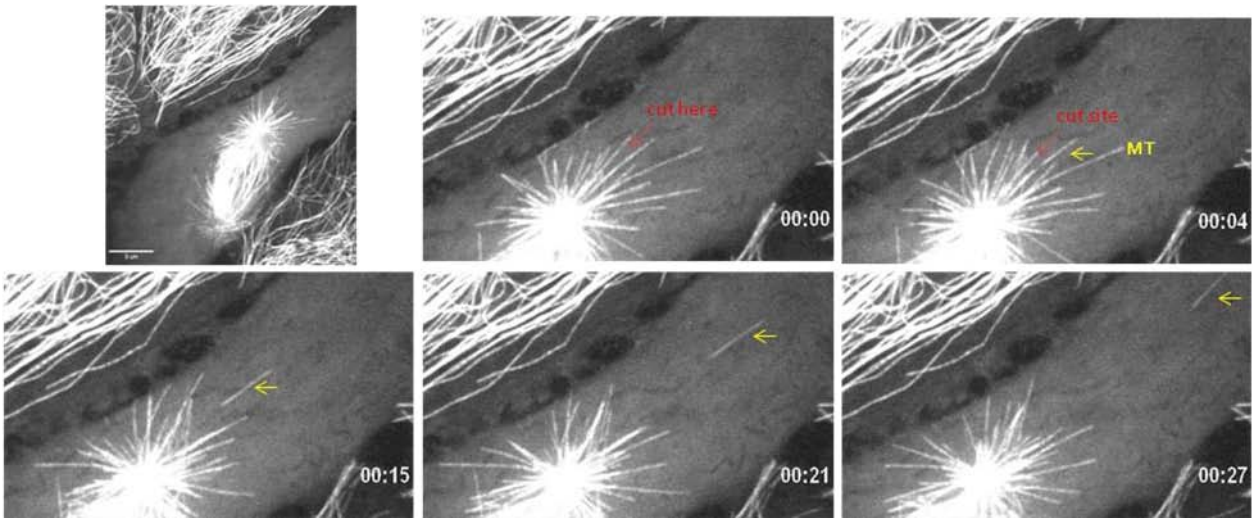

B

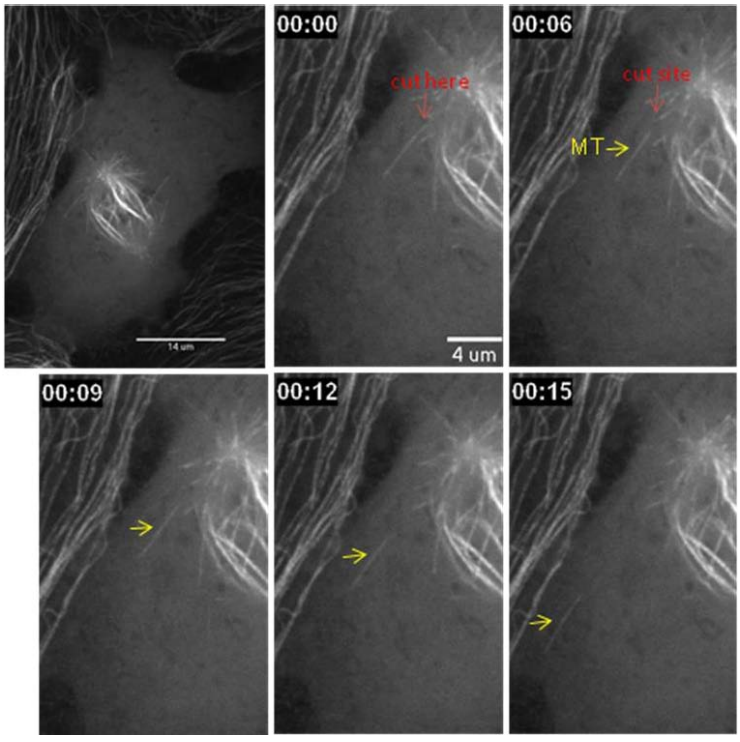

C

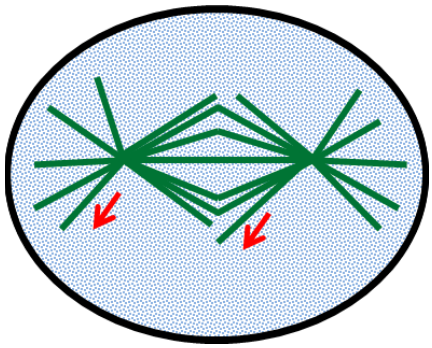

Figure 7.4 (continued)

D

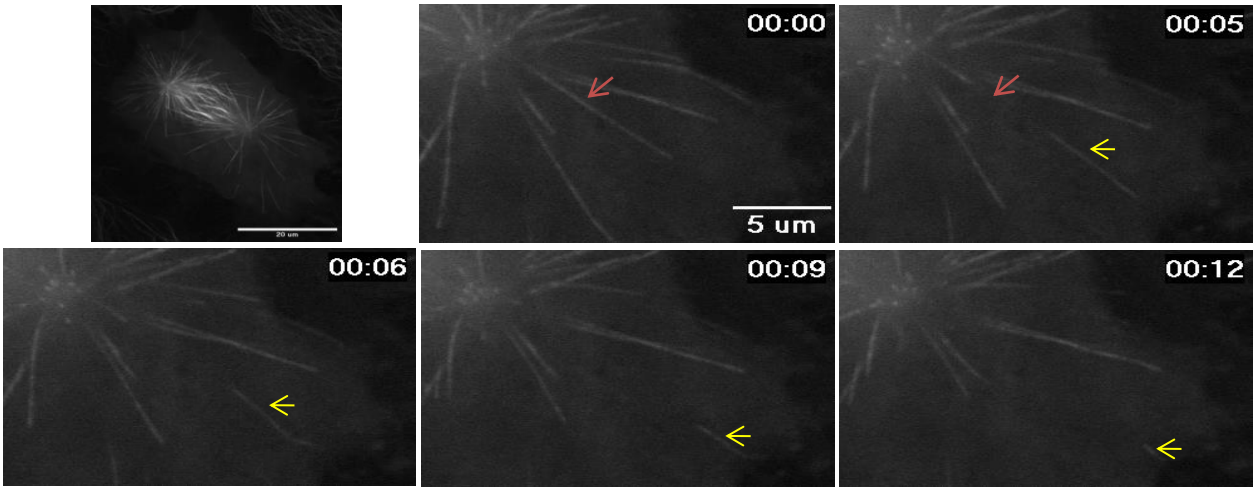

E

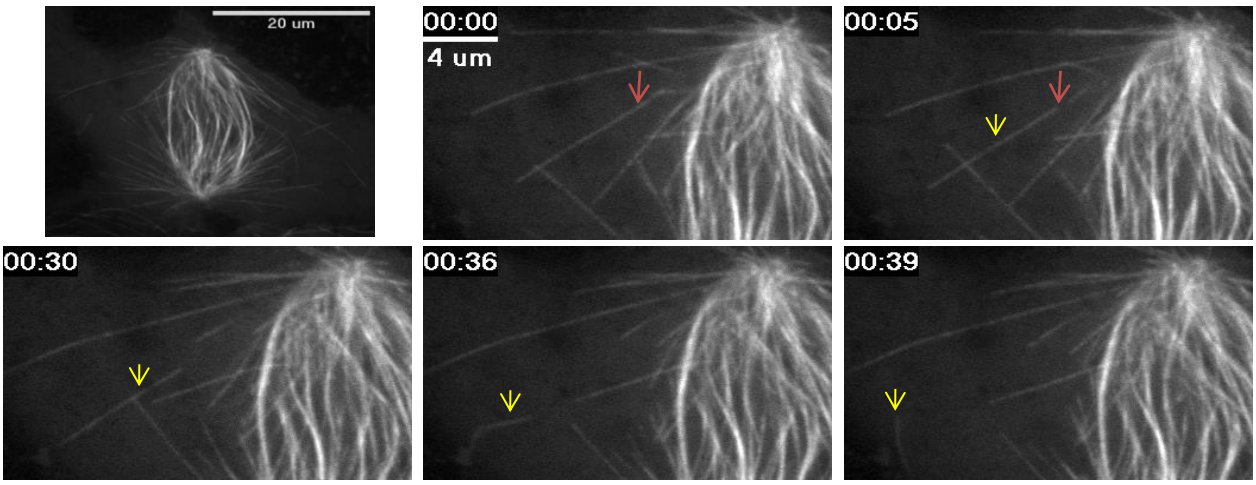

	Interphase	Metaphase	Anaphase
No movement	18	4	4
Sliding toward cell edge	10	30	24
Poleward sliding along neighboring MT	1	2	4

Table 7.1. Movement of severed MTs. MT sliding under nucleus has been left out of this tally.

The direction of MT movement is determined by MT orientation

Non-kinetochore MTs growing toward the chromosomes from the spindle poles also moved in the direction of their plus ends when severed (fig. 7.4, B and E). This indicates that minus-end-directed motors are distributed all along the cortex, and that the direction of the force on an astral MT depends on its orientation (fig. 7.4C). This configuration allows MT organization to determine the net force on the spindle.

Force is exerted along the sides of astral MTs.

Released astral MTs are carried to the cell periphery and buckle against the cell edge.

Released MTs move outward, even if they do not extend all the way to the cell edge (fig. 7.4). This indicates that astral MTs are pulled by motors anchored throughout the cell, rather than just at the cell boundary. Furthermore, released MTs sometimes buckle against the cell cortex, upon reaching the edge of the cell (fig. 7.5). This shows that force is exerted along the sides of

astral MTs, not just at their plus ends, as these MTs are still being driven into the cell boundary even when their plus ends no longer move. The critical force required to buckle MTs of the lengths observed was calculated, assuming the MT behaves as a stiff rod under compression, and using the equation, Critical Force = $\pi^2(EI/L^2)$, where EI is the flexural rigidity of a MT (~26e-24 $N \cdot m^2$) and L is the MT length.[18] We assumed that the ends of the MTs are free to rotate, but not move laterally and only considered MTs where lateral movement of the MT tip was not observed during buckling[19]. These calculations revealed that forces >10 pN sometimes act on buckling MTs (fig. 7.6, mean critical force = 8 pN, std. dev. = 6 pN, n=21), suggesting that multiple motors act on a single MT, since a single motor can generate forces up to ~5 pN. Taken together, these results reveal a general pulling mechanism acting along MTs throughout the cell. If the pulling motors are distributed throughout the cell (as indicated by the fact that no severed MTs remained stationary, regardless of their location), this would give rise to length-dependent pulling on astral MTs.

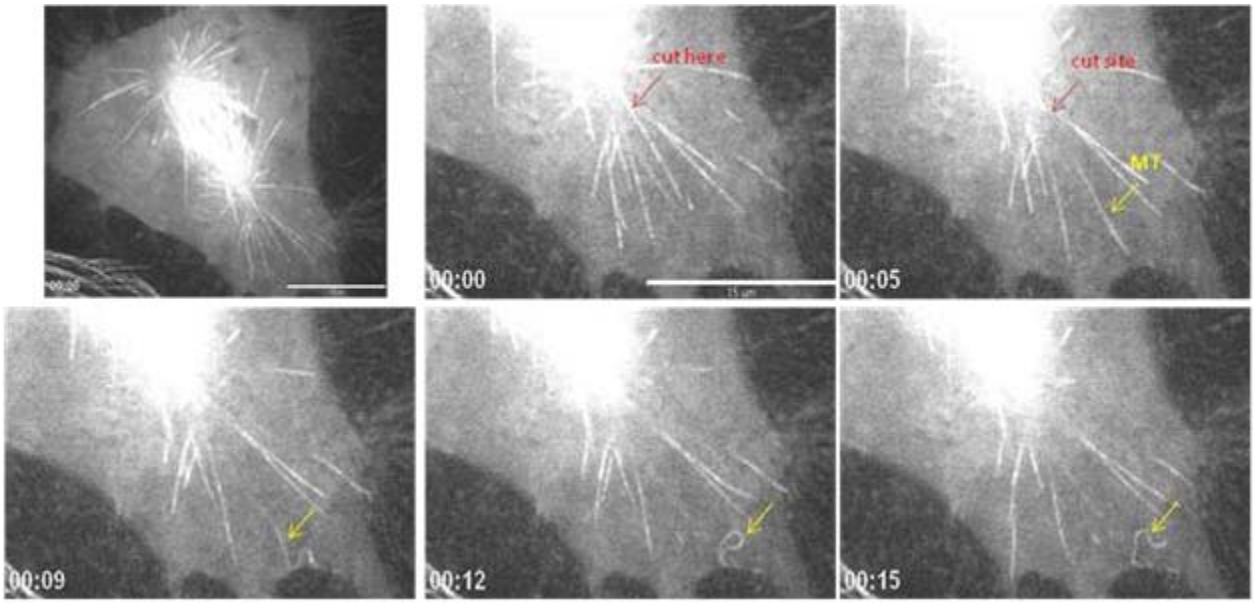

Figure 7.5: Force is exerted along the sides of severed astral MTs. A severed MT buckles against the cell boundary. Top left panel shows a whole metaphase spindle. Subsequent panels (close-up images of the lower spindle pole) are selected frames from a movie of the spindle pre- and post-ablation. The yellow arrow points to the severed MT. Scale bar 15 um.

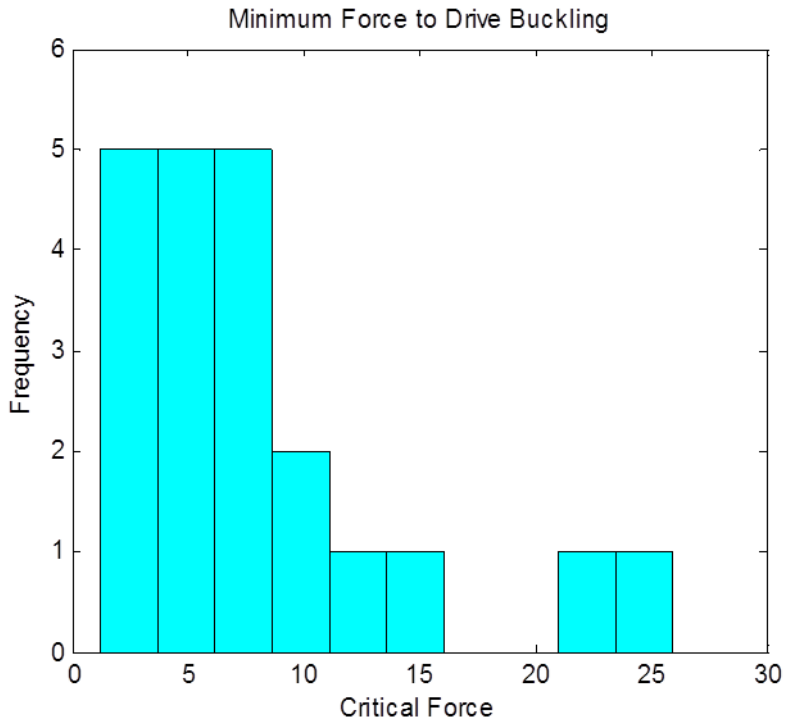

Figure 7.6: MT buckling requires force generated by simultaneous action of multiple motors. Histogram of calculated critical forces required for observed buckling events (n = 21). Only events where the ends of the MT were clearly distinguished, and no lateral movement of MT tips was observed, were included in this count.

Astral MTs are under tension throughout mitosis.

Astral MTs are pulled toward the cell periphery during both metaphase and anaphase.

Released astral MTs are pulled away from the spindle during both metaphase (fig. 7.4 A, B) and anaphase (fig. 7.4 D, E). The movement of severed MTs during metaphase and throughout anaphase shows that the force pulling MTs toward the cell periphery is present long before MTs begin to be released from the spindle poles, at the appropriate times for it to play a role in spindle centering. No difference in MT speeds[20] (fig. 7.7) or buckling forces (fig. 7.6) were observed between metaphase and anaphase, suggesting that force generation by cortical motors is not differentially regulated between these two stages.

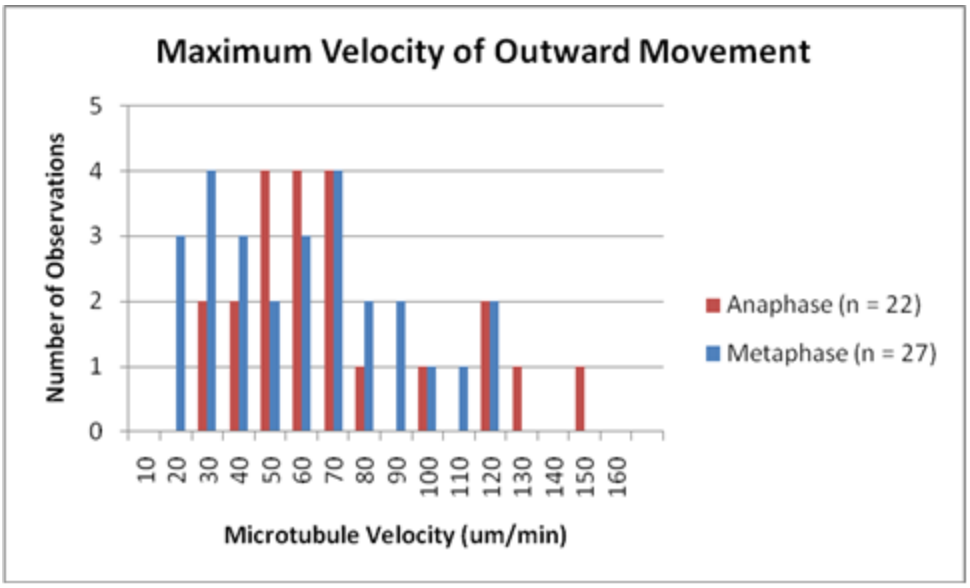

Figure 7.7: Severed MTs move at similar speeds during metaphase and anaphase. Histogram of velocities of MTs released at metaphase and anaphase. In many instances, the speed of a severed MT varied as it moved outward. The histogram reflects the maximum speed attained by each MT.

Released MTs can be pulled back toward the spindle pole by sliding along neighbor MTs.

In a few cases, during both metaphase and anaphase, severed MTs were transported inward toward the pole along neighboring intact MTs, leading to the repair of an astral MT bundle (fig. 7.8 and table 7.1). These events appear similar to the capture of non-centrosomal MTs during spindle assembly, which were shown to be due to dynein-driven MT-MT sliding[21]. Even once a MT was moving outward, its direction could be reversed by MT-MT sliding. Thus, astral MTs are subject to competing inward- and outward-pulling forces.

Poleward sliding was more often observed in areas of high MT density, consistent with the requirement that the severed MT be "caught" on a pole-attached MT for this to take place. This could account for the fact that spontaneously released MTs are transported asymmetrically away from the spindle during anaphase, as MTs released into the MT-dense interpolar region are likely to be kept at the poles via MT-MT sliding.

Severed interphase MTs (even at the cell periphery) were occasionally pulled in to nearby MT bundles (fig. 7.9), just as seen during mitosis, demonstrating that MT-MT sliding can pull MTs toward the centrosome(s) throughout the cell cycle.

A

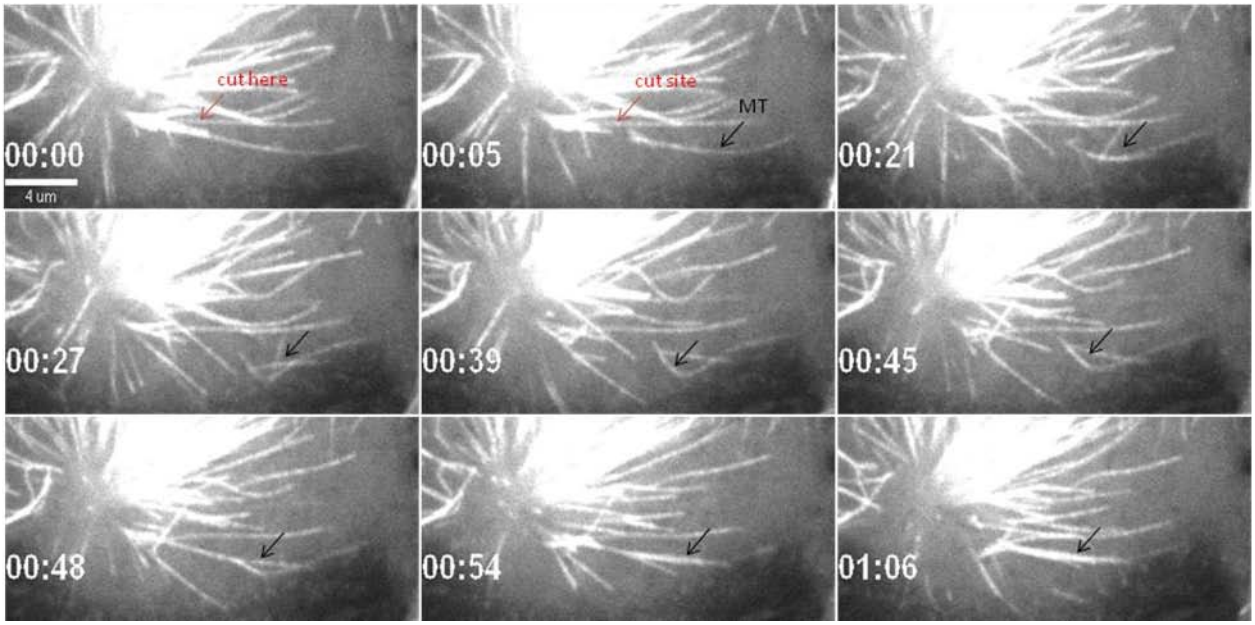

B

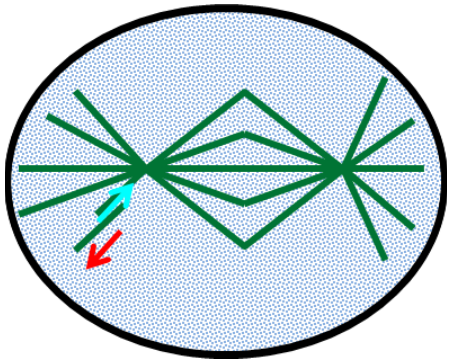

Figure 7.8: Released MTs can be pulled back toward the spindle pole by sliding along neighbor MTs. (A) An astral MT bundle is repaired via MT-MT sliding. Red arrow indicates cut site. Black arrow indicates severed MT bundle. Scale bar 4 um. (B) The cartoon illustrates the competing forces that may act on an astral MT. Force generated by cortical motors (red arrow) pulls the MT toward the cell periphery, while force generated by MT-MT sliding (blue arrow) pulls the MT back toward the spindle pole.

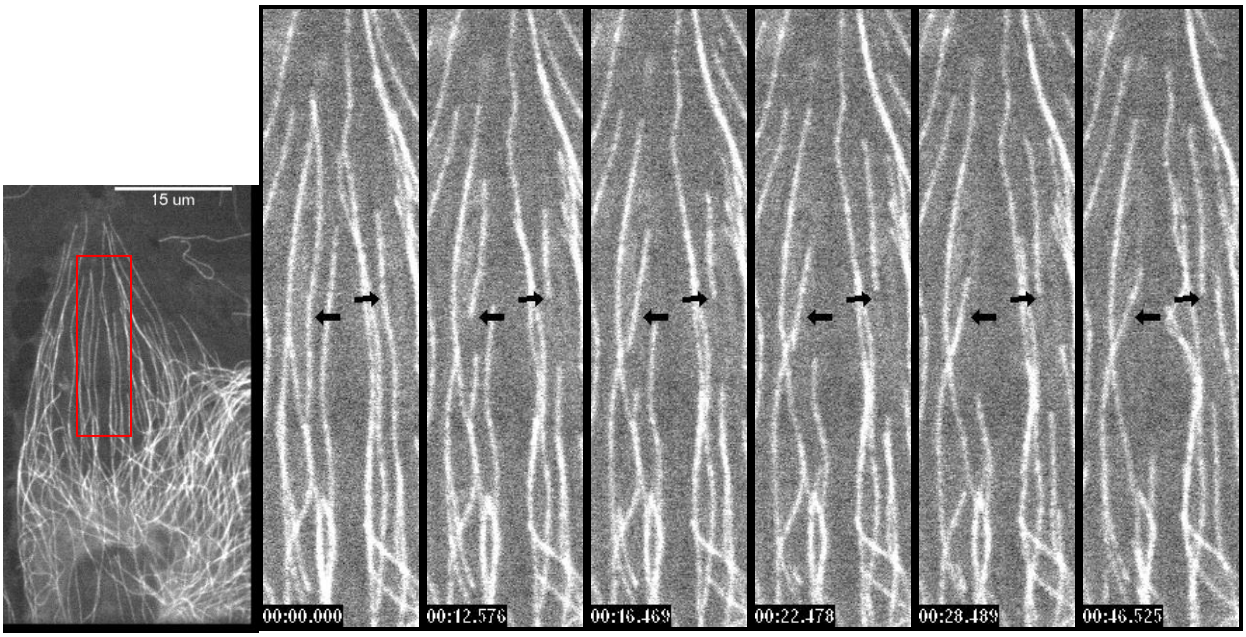

Figure 7.9: Isolated MTs are not pulled outward along the cortex during interphase. Two MTs at the cell periphery are ablated during interphase. Left panel shows an interphase cell. Scale bar 15 um. Subsequent panels (close-up images of MTs inside red box) are selected frames from a movie of the MTs pre- and post-ablation. Two MTs were cut. Black arrows indicate cut sites. The severed MT on the right remains still, while the one on the left is pulled into a nearby MT bundle.

Conclusions

Our results show that astral MTs are under tension and transmit a pulling force to the spindle. The astral MTs, with their plus-ends extending outward from the spindle poles, are pulled toward the cell periphery by minus-end-directed motors. Force is exerted along the sides of astral MTs, as evidenced by MT buckling, consistent with a spindle centering mechanism in which astral MTs exert a force proportional to their length on the spindle. This mechanism could robustly center and align the spindle, in the absence of any specialized spindle-positioning cues originating from cell-cell junctions.

In cultured mammalian cells, most astral MTs do not extend all the way to the cell boundary. In this case, an "MT tip" centering mechanism would utilize only a small fraction of MTs, and would require that there be a very low number of cortical motors in order for the

pulling force to be limited by the number of cortical pulling sites available. Spindle centering by length-dependent pulling on astral MTs, rather than an MT-tip-pulling-based centering mechanism, would allow all astral MTs to contribute to the centering process and would likely be more robust. Additionally, the presence of length-dependent MT pulling would explain why the long axis of the spindle tends to align with the long axis of the cell. Since astral MTs grow longer in anaphase, if a length-dependent force is active they would experience a stronger pulling force than metaphase MTs, even without a change in the force-producing mechanism. This is consistent with the report that, in LLCPK cells, spindles that are off-center at Anaphase B can be corrected by accelerated movement of the pole with longer astral MTs[17]. If metaphase MTs are too short to contact multiple motors, length-dependent pulling could first arise in anaphase.

The spindle-centering strategy described here could also play a role in asymmetric cell divisions, which commonly occur in stem cells to produce daughter cells with differing fates[22,23]. Most models of stable asymmetric spindle positioning require a directional force on the spindle counterbalanced by a centering force[24]. In C. elegans embryos depleted of Gα, GPR1/2, or LIN-5, the spindle is positioned at the cell center. This supports the theory that this asymmetric positioning mechanism is superimposed over a centering mechanism.

The Gα-LGN-NuMA pulling mechanism is active in symmetrically dividing HeLa cells[25], and recent work has shown that asymmetric dynein localization is responsible for spindle oscillations seen in these cells[26]. When a spindle pole comes within 2 um of the cortex, pole-localized polo-like kinase disrupts the binding of dynein/dynactin to LGN NuMA at the proximal cortex, and the dynein remaining at the distal cortex pulls the spindle back toward the cell center. This mechanism may be responsible for spindle centering in small HeLa cells, but would not account for centering in larger cells where the spindle pole is rarely within 2 um of the cortex.

(Additionally, disruption of this mechanism by LGN RNAi or membrane-targeted Plk1 was not reported to cause spindle centering defects in HeLa.)

In Ptk2 cells, the dynein applying force to astral MTs is likely anchored all along the basal cell cortex, possibly through Gα-LGN-NuMA [27] linkage, or other linkage to cortical actin. In Hela cells, siRNA knockdown of LIMK1 (a kinase which regulates the organization of cortical actin and astral MTs) abolishes spindle centering and also causes mitotic arrest[28]. In large, round cells, dynein would need to be anchored throughout the cytoplasm in order to exert length-dependent force on MTs. Recently, dynein localized to intracellular organelles was shown to play a role in centrosome centration C. elegans embryo.

Systematic probing of different populations of MTs, at various positions in the cell and throughout the cell cycle revealed that all astral MTs are subject to motor-generated pulling forces applied all along their length. These direct observations of the force acting on individual MTs show that conditions in the mitotic cell of favor an MT-length-dependent spindle centering mechanism.

In addition to positioning the spindle, forces acting on MTs contribute to the reorganization and maintenance of microtubule arrays during the cell cycle. During spindle assembly, non-centrosomal MTs are carried by dynein along astral MTs, moving in toward the spindle poles and becoming part of the forming spindle[21]. As the spindle is disassembled, in late anaphase and telophase, astral MTs (along with segments of the centrosomes) are spontaneously released from the poles and are transported outward toward the cell periphery, leading to reestablishment of interphase MT morphology[29]. Our experiments show that although astral MTs can be subject to forces pulling them away from the poles (provided by cortical motors) as well as towards them (provided by MT-MT sliding), throughout metaphase and anaphase most astral

MTs extending from the spindle poles experience a net force pulling them away from the spindle.

In contrast to mitotic astral MTs, MTs severed at the periphery of interphase cells stayed still, as long as they were not touching other MTs. The cortical-motor-driven pulling mechanism observed in mitosis does not appear to be active during interphase. Interphase MTs severed beneath the nucleus were often observed to slide, as previously reported, possibly driven by motors on the nuclear membrane.[30] MTs severed in the tangled MT array at the cell center sometimes moved, possibly sliding along the network of neighboring MTs. The idea that these MTs are transported by MT-linked motors, rather than cortical motors, is supported by the observation that MTs at the cell periphery which contacted few other MTs were relaxed and didn't exhibit the buckling seen in the MT-dense cell center. A recent report that MT-MT sliding in interphase Drosophila S2 cells is mediated by kinesin, not dynein, supports the idea that dynein-mediated outward pulling force on MTs is specific to mitosis[31]. Reports of MT sliding along the interphase cell cortex[32,33] may reflect a difference between cell types, but they could also be due to MT-MT sliding along the interphase MT network. This type of sliding would still support the MT-pulling centrosome-centering mechanisms reported by Burakov et al.[34] and Wu et al[33].

Severed interphase MTs (even at the cell periphery) were occasionally pulled in to nearby MT bundles (fig. 7.9), just as seen during mitosis, demonstrating that MT-MT sliding can pull MTs toward the centrosome(s) throughout the cell cycle. This suggests that the balance of forces pulling MTs toward and away from the centrosome/spindle poles is adjusted by regulation of cortical motors. Cortical-motor-driven force, which tends to pull MTs away from centrosomes, is

reduced following cytokinesis, possibly to facilitate inward MT flux during the next round of spindle assembly.

Materials and Methods

Cell Culture. Ptk2 cells stably expressing GFP-tagged alpha tubulin were grown in Minimal Essential Medium (Gibco 11095), supplemented with 10% heat-inactivated fetal bovine serum (Gibco 10438-026), 1 mM sodium pyruvate (Gibco 11360-070), 1% MEM non-essential amino acids solution (Gibco 11140-050), 100 I.U./mL penicillin, and 100 ug/mL streptomycin (Cellgro 30-002-CI). Cells were grown at 37°C in a humidified 5% CO_2 atmosphere.

Timelapse Microscopy.

Laser Ablation. Cells were plated on 25 mm round #1.5 coverslips (Warner Instruments CS-25R15) coated in poly-L-lysine (Sigma P-1524). Immediately prior to ablation experiment, the coverslip was transferred to a microscope-mounted, heated imaging chamber filled with Leibovitz's L-15 CO_2-independent media without phenol red (Gibco 21083-027), supplemented with 10% fetal bovine serum, 100 I.U./mL penicillin, and 100 ug/mL streptomycin. Imaging was done on a confocal microscope with a 100x oil objective lens. Ablation was done with a Micropoint laser. Microscope and ablation laser were controlled by Metamorph cropoint. Cell was imaged every 3 seconds after ablation.

[1] S. Oliferenko, T.G. Chew, M.K. Balasubramanian. Positioning Cytokinesis. Genes Dev. 23 (2009) 660-74

[2] D.O. Morgan The Cell Cycle: Principles of Control New Science Press, London (2007) 258-63

[3] H. Beamish, L. de Boer, N. Giles, F. Stevens, V. Oakes, B. Gabrielli. Cyclin A/cdk2 Regulates Adenomatous Polyposis Coli-dependent Mitotic Spindle Anchoring. *J. Biol. Chem.* **284** 29015-23 (2009)

[4] M. Wuhr, S. Dumont, A.C. Groen, D.J. Needleman, T.J. Mitchison. How Does a Millimeter-sized Cell Find its Center? *Cell Cycle* **8** 1115-21 (2009)

[5] M. Piel, P.T. Tran. Cell Shape and Cell Division in Fission Yeast. *Curr. Biol*. **19** R823-7 (2009)

[6] C. Brangwyyne, F.C. MacKintosh, S. Kumar, N.A. Geisse, J. Talbot, L. Mahadevan, K.K. Parker, D.E. Ingber, D.A. Weitz. Microtubules Can Bear Enhanced Compressive Loads in Living Cells Because of Lateral Reinforcement. *J. Cell Biol*. **173** 733-41 (2006)

[7] C.B. O'Connell, Y. Wang. Mammalian Spindle Orientation and Position Respond to Changes in Cell Shape in a Dynein-dependent Fashion. Mol. Biol. *Cell* **11** 1765-74 (2000)

[8] S.W. Grill, J. Howard, E. Schaffer, E.H.K. Stelzer, A. Hyman. The Distribution of Active Force Generators Controls Mitotic Spindle Position. *Science* **301** 518-21 (2003)

[9] S.W. Grill, A.A. Hyman. Spindle Positioning by Cortical Pulling Forces. *Dev. Cell* **8** 461-5 (2005)

[10] T. Nguyen-Ngoc, K. Afshar, P. Gonczy. Coupling of Cortical Dynein and Gα Proteins Mediates Spindle Positioning in Caenorhabditis Elegans. *Nature Cell Biol*. **9** 1294-1302 (2007)

[11] K. Kimura, A. Kimura. Intracellular organelles mediate cytoplasmic pulling force for centrosome centration in the Caenorhabditis elegans early embryo. *PNAS* **108** 137-42 (2011)

[12] Hamaguchi MS, Hiramoto Y. Analysis of the role of astral rays in pronuclear migration in sand dollar eggs by the Colcemid-UV method. *Dev. Growth Differ***. 28** 143-56 (1986)

[13] Minc N, Burgess D, Chang F. Influence of cell geometry on division plane positioning. *Cell* **144** 414-26 (2011)

[14] Wühr M, Tan ES, Parker SK, Detrich HW 3rd, Mitchison TJ. A model for cleavage plane determination in early amphibian and fish embryos. *Curr Biol.* **20** 2040-5 (2010)

[15] K.H. Siller, C.Q. Doe. Spindle Orientation During Asymmetric Cell Division. *Nature Cell Biol*. **11** 365-74 (2009)

[16] Q. Du, I.G. Macara. Mammalian Pins is a Conformational Switch that Links NuMA to Heterotrimeric G Proteins. *Cell* **119** 503-16 (2004)

[17] Collins ES, Balchand SK, Faraci JL, Wadsworth P, Lee WL. Cell cycle-regulated cortical dynein/dynactin promotes symmetric cell division by differential pole motion in anaphase. *Mol. Biol. Bell.* **23** 3380-90 (2012)

[18] F. Gittes, E. Meyhofer, S. Baek, J. Howard. Directional loading of the kinesin motor molecule as it buckles a microtubule. *Biophys. J.* **70** 418-29 (1996)

[19] J. Howard. *Mechanics of Motor Proteins and the Cytoskeleton* Sinauer Associates Inc. (2001) Sunderland, MA

[20] J.E. Martinez, M.D. Vershinin, G.T. Shubeita, S.P. Gross. On the use of in vivo cargo velocity as a biophysical marker. *Biochem. Biophys. Res. Comm.* **353** 835-40 (2007)

[21] U.S. Tulu, N.M. Rusan, P. Wadsworth. Peripheral, non-centrosome-associated microtubules contribute to spindle formation in centrosome-containing cells. *Curr. Biol*. **13** 1894-9 (2003)

[22] K.H. Siller, C.Q. Doe. Spindle Orientation During Asymmetric Cell Division. *Nature Cell Biol*. **11** 365-74 (2009)

[23] T. Lechler, E. Fuchs. Asymmetric Cell Divisions Promote Stratification and Differentiation of Mammalian Skin. *Nature* **437** 275-80 (2005)

[24] A. Kimura, S. Onami. Local Cortical Pulling Force Repression Switches Centrosomal Centration and Posterior Displacement in C. elegans. *J. Cell Biol*. **179** 1347-54 (2007)

[25] J.B. Blumer, R. Kuriyama, T.W. Gettys, S.M. Lanier. The G-protein Regulatory (GPR) Motif-containing Leu-Gly-Asn-enriched Protein (LGN) and Giα3 Influence Cortical Positioning of the Mitotic Spindle Poles at Metaphase in Symmetrically Dividing Mammalian Cells. *Eur. J. Cell Biol*. **85** 1233-40 (2006)

[26] T. Kiyomitsu, I.M. Cheeseman. Chromosome- and spindle-pole-derived signals generate an intrinsic code for spindle position and orientation. *Nat. Cell Biol*. **14** 311-17 (2012)

[27] G.E. Woodard et al. Ric-8A and Gi alpha recruit LGN, NuMA, and dynein to the cell cortex to help orient the mitotic spindle. *Mol. Cell Biol.* **30** 3519-30 (2010)

[28] N. Kaji, A. Muramoto, K. Mizuno. LIM Kinase-mediated Cofilin Phosphorylation during Mitosis is Required for Precise Spindle Positioning. *J. Biol. Chem.* **283** 4983-92 (2008)

[29] N.M. Rusan, P. Wadsworth. Centrosome fragments and microtubules are transported asymmetrically away from division plane in anaphase. *J. Cell Biol.* **168** 21-8 (2005)

[30] T.J. Keating et al. Microtubule release from the centrosome. *PNAS* **94** 5078-83 (1997)

[31] A.L. Jolly, H. Kim, D. Srinivasan, M. Lakonishok, A.G. Larson, V.I. Gelfand. Kinesin-1 heavy chain mediates microtubule sliding to drive changes in cell shape. *PNAS* **107** 12151-6 (2010)

[32] Bicek et al. Anterograde microtubule transport drives microtubule bending in LLC-PK1 epithelial cells. *MBoC* **20** 2943 (2009)

[33] J. Wu et al. Effects of dynein on microtubule mechanics and centrosome positioning. *Mol. Biol. Cell* **22** 4834-41 (2011)

[34] Burakove et al. Centrosome positioning in interphase cells. *J. Cell Biol.* **162** 963-9 (2003)